Synthesis and Characterisation of Zr-fumarate MOF – a Promising Candidate for Biomedical Applications

Von der Naturwissenschaftlichen Fakultät der

Gottfried Wilhelm Leibniz Universität Hannover

zur Erlangung des Grades

Doktorin der Naturwissenschaften

Dr. rer. nat.

genehmigte Dissertation von

Dipl.-Chem. Gesa Zahn, geb. Wißmann

geboren am 25. Mai 1986 in Celle

2015

Danksagung

Mein Dank gilt zunächst Herrn Prof. Dr. Peter Behrens, der mir die Möglichkeit gegeben hat in seiner Arbeitsgruppe ein interessantes, vielfältiges und interdisziplinäres Thema zu bearbeiten.

Prof. Dr. Jürgen Caro danke ich für die Übernahme des Korreferats und Prof. Dr. Franz Renz für die Übernahme des Prüfungsvorsitzes.

Den Mitgliedern des SFB 599 („Zukunftsfähige bioresorbierbare und permanente Implantate aus metallischen und keramischen Werkstoffen") sowie des SPP 1362 („Porous Metal-Organic Frameworks") danke ich für den wissenschaftlichen Austausch, unter anderem auf Tagungen, im Graduiertenkolleg und bei Projekttreffen.

Meinen HiWis Wing-Yin Tsang und insbesondere Hendrik A. Schulze danke ich für die Unterstützung bei zahlreichen Synthesen und Probenvorbereitungen.

Für die Durchführung von Sorptions- und TG/MS-Messungen danke ich unseren Kooperationspartnern Uta Sazama, Sandra König und Prof. Dr. Michael Fröba von der Universität Hamburg.

Unseren Kooperationspartnern Jörn Schaeske und Prof. Dr. Meike Stiesch (Medizinische Hochschule Hannover), Dominik Müller und Prof. Dr. Kirsten Haastert-Talini (Medizinische Hochschule Hannover), Deniz Ali Bölükbas und PD Dr. Silke Meiners (Ludwig-Maximilians-Universität München) sowie Katharina Ferkaljuk und Prof. Dr. Angelika Vollmar (Ludwig-Maximilians-Universität München) danke ich für die Zellkulturuntersuchungen.

Katharina Nolte und Sergej Springer danke ich für die vielen TG-Messungen.

Für die zahlreichen Sorptionsmessungen danke ich Georg Platz, Jann Lippke und Natalja Wendt.

Ein weiterer Dank geht an Dr. Britta Hering, Dr. Imke Bremer und Dr. Florian Waltz für die Aufnahme von REM-Bildern.

Bei Thomas Preuße und Prof. Dr. Adelheid Godt von der Universität Bielefeld möchte ich mich für die NMR-Messungen bedanken.

Gerne denke ich an die anstrengenden, aber auch lustigen DESY-Aufenthalte zurück, die ich mit Jann Lippke, Philip Zerner, Fabian L. Kempf, Dr. Christian A. Schröder

Abstract

In recent years, metal-organic frameworks (MOFs) have emerged as a novel class of porous materials with interesting properties. As an alternative to well-investigated zeolites, these materials feature a tunable design and therefore a tailorable porosity. Depending on the application of the resulting metal-organic framework, various metal ions acting as nodes can be combined with different organic molecules as bridging ligands. Thus, frameworks with different pore sizes, varying functionalities and morphologies can be established making this material interesting for catalysis, separation and gas storage as well as for biomedical applications like drug delivery systems.

In this work, a new and highly stable metal-organic framework was investigated thoroughly. Inspired by the possible future application as a biomaterial, Zr^{4+} as metal ion and the biologically occurring fumaric acid as linker were utilised. The first synthesis of Zr-fumarate MOF was successful from a DMF-based system by applying a so-called modulation approach, i.e. by adding a monocarboxylic acid to the reaction mixture which competes with the dicarboxylic fumaric acid for the coordination sites of the zirconium ions. Depending on the modulator concentration, the crystallinity, the degree of aggregation and the particle size can be influenced. Also, the general reproducibility of the syntheses is improved. Apart from the synthesis in DMF, Zr-fumarate MOF can also be synthesised from aqueous systems under benign reaction conditions. In both cases, the addition of formic acid as modulator opened the way to a highly crystalline, microporous material exhibiting an exceptional stability against various solvents and harsh pH conditions. *In situ* kinetic investigations using synchrotron radiation revealed a decelerating effect of the modulator in the water-based synthesis. The presence of a coordination-modulation mechanism could be confirmed. Furthermore, a strongly increased reaction rate was observed in a DMF-based synthesis when water was added to the synthesis. Surprisingly, even small amounts of water that are present in the commercially available formic acid revealed a crucial influence so that increasing the modulator concentration and thus concomitantly increasing the water content resulted in an accelerated reaction rate.

First investigations concerning the biocompatibility of Zr-fumarate MOF considering different cell lines show no significant toxicity of the MOF even at higher concentrations. Consequently, Zr-fumarate MOF might be a promising material with regard to biomedical applications.

The main part of this thesis consists of three original research articles dealing with the synthesis and properties of the Zr-fumarate MOFs. These parts are preceded by an introduction and the presentation of general principles pertinent to this work. Finally, conclusions and an outlook are given, containing also the results of the yet unpublished biological tests.

Keywords: metal-organic frameworks • Zr compounds • coordination modulation • nanoparticles • biomaterial

Inhaltsübersicht

Metall-organische Gerüstverbindungen (MOFs) rückten in den letzten Jahren als eine neue Klasse poröser Materialien in den Fokus der Forschung. Diese Materialklasse, die eine Alternative zu den bereits intensiv erforschten Zeolithen darstellt, zeichnet sich durch ihren modularen Aufbau und die damit verbundene einstellbare Porosität aus. Durch die Wahl geeigneter Metallionen als Verknüpfungspunkte in Kombination mit verschiedenen verbrückenden, organischen Linker-Molekülen kann das Metall-organische Gerüst entsprechend seiner Anwendung angepasst werden. So lassen sich Netzwerke mit unterschiedlichen Porengrößen, variierender Funktionalität und Morphologie generieren, so dass diese Materialien sowohl in der Katalyse, in Trennungsverfahren, als Gasspeicher wie auch in biomedizinischen Bereichen als Medikament-Abgabe-Systeme Verwendung finden können.

In dieser Arbeit wurde ein neuartiges, sehr stabiles Metall-organisches Gerüst sorgfältig untersucht. Inspiriert von der möglichen zukünftigen Anwendung als Biomaterial, wurde als Metallion Zr^{4+} und als verbrückender Ligand Fumarsäure, ein natürlich vorkommendes Molekül, gewählt. Die erste Synthese des Zr-fumarat-MOFs gelang aus Dimethylformamid (DMF) mithilfe des sogenannten Modulationsansatzes. Hierbei wird eine Monocarbonsäure als Modulator hinzugegeben, die mit der Dicarbonsäure Fumarsäure um die Koordinationsstellen an den Zirconiumionen konkurriert. Abhängig von der Menge an Modulator können so die Kristallinität, der Grad der Aggregation und die Partikelgröße beeinflusst werden. Auch die Reproduzierbarkeit der Synthesen wird verbessert. Neben der Synthese aus DMF konnte der Zr-fumarat-MOF zudem aus wässriger Lösung unter milden Reaktionsbedingungen synthetisiert werden. In beiden Fällen wird durch den Einsatz von Ameisensäure als Modulator ein hochkristallines, mikroporöses Material erhalten, welches eine herausragende Stabilität gegenüber organischen Lösungsmitteln sowie harschen pH-Bedingungen zeigt. Kinetische Untersuchungen, die *in situ* mittels Synchrotronstrahlung durchgeführt wurden, zeigten den verlangsamenden Einfluss des Modulators auf die Reaktionsgeschwindigkeit in der wasserbasierten Synthese. Es konnte bestätigt werden, dass in diesem Fall ein sogenannter Koordinations-Modulations-Mechanismus vorliegt. Außerdem wurde eine starke Erhöhung der Reaktionsgeschwindigkeit in der DMF-basierten Synthese bei Wasserzugabe beobachtet. Überraschenderweise zeigten bereits geringe Wasseranteile, die in der kommerziell erhältlichen Ameisensäure vorhanden sind, einen schnelleren Reaktionsverlauf, so dass hier eine Erhöhung der Modulatorkonzentration und die damit einhergehende Erhöhung des Wasseranteils in einer Beschleunigung der Reaktionsgeschwindigkeit resultierten.

Erste Untersuchungen bezüglich der Biokompatibilität des Zr-fumarat-MOFs zeigten, dass dieses Material gegenüber verschiedenen Zelltypen auch bei hohen Konzentrationen keine relevanten toxischen Effekte zeigt, so dass die Anwendung des Zr-fumarat-MOFs im biomedizinischen Bereich vielversprechend ist.

Der Hauptteil dieser Dissertation besteht aus drei Originalarbeiten, die sich mit der Synthese und den Eigenschaften des Zr-fumarat-MOFs beschäftigen. Diesem Teil vorangestellt sind eine Einleitung und die Darstellung allgemeiner Grundlagen, die für diese Arbeit wichtig sind. Abschließend werden die Ergebnisse zusammengefasst und ein Ausblick auf mögliche weitere Arbeiten gegeben. In diesem Abschnitt werden auch die Ergebnisse der bisher unveröffentlichten biologischen Untersuchungen dargestellt.

Stichwörter: Metall-organische Gerüste • Zr-Verbindungen • Koordinations-Modulation • Nanopartikel • Biomaterial

Table of Contents

1   Introduction

Nowadays, the research concerning the development of new materials that might be interesting for environmental or medical application gains a lot of interest, e.g. with regard to the separation of greenhouse gases, energy storage or the improvement of medical devices like drug delivery systems. The great challenge of the latter is the control of the drug administration. Therapeutic agents often suffer from a low cell membrane permeability and low physiological stability so that the drug degrades before the target is reached. For that purpose, usually high doses of drugs are necessary to observe a therapeutic effect. Such a high exposure can cause side effects and should be handled with care. One idea to circumvent these problems is the development of nanocarriers in which the therapeutic agent is encapsulated and thus prevents the drug from premature degradation.[1] Furthermore, the cellular uptake can be enhanced and the delivery of the active agent can take place at the required target. To develop a nanocarrier that exhibits the desired characteristics, several materials have been investigated like organic-based liposomes,[2] biodegradable polymeric nanoparticles[3] as well as inorganic mesoporous silica.[4–7] Although these materials offered the opportunity to encapsulate various drugs, an adjustment according to the desired drug release profile is limited. On the one hand organic-based nanocarriers can be functionalised easily to improve the polymer-drug interactions, but the release profile is often determined by the degradation or swelling process of the polymer as it does not show a regular, porous network. Mesoporous silica also allow surface modification to enhance the silica-drug interactions. By applying a surfactant-assisted synthesis route a rather robust and well-defined pore system is obtained after the removal of the templating agent. Thus, mesoporous silica are in general suitable for drug delivery systems and have been investigated for biomedical applications for years. Their porosity usually allows for much higher drug loadings as compared to polymer materials. Nevertheless, mesoporous silica also exhibits several limitations with regard to the chemical composition (which is fixed), pore size adjustment and functionalisation of the material. Another class of nanoporous materials, namely metal-organic frameworks (MOFs) or porous coordination polymers, hold great promise for biomedical applications. The further development of these hybrid materials built up from organic and inorganic components is in the focus of this work. One of the key advantages of metal-organic frameworks is their chemical versatility: combination of different metal ions with different organic linking

molecules allows to establish a large variety of highly porous, three-dimensional networks that can be tailored according to the envisaged application. Depending on the length of the organic linking molecule, the pore size can be adjusted and the organic parts of the material can be functionalised to improve host-guest interactions. With regard to the application as biomaterial, zirconium ions and the naturally occurring fumaric acid have been chosen as metal source and organic bridging molecule, respectively. Zr-based MOFs are well-known for their high thermal and chemical stability so that they might be promising candidates for biomedical application as they do not degrade rapidly when they get in contact with aqueous solutions.[8] Zirconium compounds like zirconium dioxide or zirconium phosphate are currently used as biomaterials, for example in dentistry.[9–12] These compounds are regarded as biocompatible and bioinert biomaterials, and as long as a zirconium compound does not degrade rapidly in a body environment, it may be considered as safe. Fumaric acid is part of the normal metabolism so that no toxic side effects are expected; also iron fumarate is used as a drug[13,14] and the iron-based fumarate MOF is also regarded as a biomaterial.[15] Due to the very short length of the fumaric acid, fumarate-based MOFs might also be applicable for gas storage and separation. One well-known example is the Al-fumarate MOF Basolite A520 that is synthesised industrially from water in a ton-scale production at BASF.[16]

In this work, a Zr-fumarate MOF has successfully been synthesised with the focus on characterising thoroughly the material. By applying the so-called modulation approach which was originally investigated by the group of KITAGAWA,[17,18] the synthesis control of the Zr-fumarate MOF could be enhanced resulting in a highly crystalline material. After having synthesised the Zr-fumarate MOF from DMF (see section 3.1),[19] we also succeeded to obtain this MOF from a water-based system (section 3.2)[20] making this material especially interesting for industrial applications as it is also highly stable against various chemical media. *In situ* investigations of the formation of Zr-fumarate MOF yielded information about the crystallisation behaviour in the DMF- as well as in the water-based system under the influence of various additives (section 3.3).[21] Finally, first cell culture tests were performed revealing that Zr-fumarate MOF does not cause any toxic effects even at high concentrations. Thus, further investigations might be promising to establish a new drug delivery system as various basic conditions seem to be favourable.

References

(1)   Cho, K.; Wang, X.; Nie, S.; Chen, Z. G.; Shin, D. M. *Clin. Cancer Res.* **2008**, *14*, 1310–1316.

(2)   Kaneda, Y. *Adv. Drug Deliv. Rev.* **2000**, *43*, 197–205.

(3)   Soppimath, K. S.; Aminabhavi, T. M.; Kulkarni, A. R.; Rudzinski, W. E. *J. Control. Release* **2001**, *70*, 1–20.

(4)   Vallet-Regí, M.; Balas, F.; Arcos, D. *Angew. Chem. Int. Ed.* **2007**, *46*, 7548–7558.

(5)   Mamaeva, V.; Sahlgren, C.; Lindén, M. *Adv. Drug Deliv. Rev.* **2013**, *65*, 689–702.

(6)   Popat, A.; Hartono, S. B.; Stahr, F.; Liu, J.; Qiao, S. Z.; Lu, G. Q. M. *Nanoscale* **2011**, *3*, 2801–2818.

(7)   Wu, S.-H.; Hung, Y.; Mou, C.-Y. *Chem. Commun.* **2011**, *47*, 9972–9985.

(8)   Cavka, J. H.; Jakobsen, S.; Olsbye, U.; Guillou, N.; Lamberti, C.; Bordiga, S.; Lillerud, K. P. *J. Am. Chem. Soc.* **2008**, *130*, 13850–13851.

(9)   Lee, D. B. N.; Roberts, M.; Bluchel, C. G.; Odell, R. A. *ASAIO J.* **2010**, *56*, 550–556.

(10)   Sollazzo, V.; Pezzetti, F.; Scarano, A.; Piattelli, A.; Bignozzi, C. A.; Massari, L.; Brunelli, G.; Carinci, F. *Dent. Mater.* **2008**, *24*, 357–361.

(11)   Nothdurft, F. P.; Merker, S.; Pospiech, P. R. *Clin. Oral Investig.* **2011**, *15*, 89–97.

(12)   Díaz, A.; David, A.; Pérez, R.; González, M. L.; Báez, A.; Wark, S. E.; Zhang, P.; Clearfield, A.; Colón, J. L. *Biomacromolecules* **2010**, *11*, 2465–2470.

(13)   Zlotkin, S.; Arthur, P.; Antwi, K. Y.; Yeung, G. *Am. Soc. Clin. Nutr.* **2001**, *74*, 791–795.

(14)   Erichsen, K.; Ulvik, R. J.; Nysaeter, G.; Johansen, J.; Ostborg, J.; Berstad, A.; Berge, R. K.; Hausken, T. *Scand. J. Gastroenterol.* **2005**, *40*, 1058–1065.

(15)   Baati, T.; Njim, L.; Neffati, F.; Kerkeni, A.; Bouttemi, M.; Gref, R.; Najjar, M. F.; Zakhama, A.; Couvreur, P.; Serre, C.; Horcajada, P. *Chem. Sci.* **2013**, *4*, 1597–1607.

(16)   Gaab, M.; Trukhan, N.; Maurer, S.; Gummaraju, R.; Müller, U. *Microporous Mesoporous Mater.* **2012**, *157*, 131–136.

(17)   Diring, S.; Furukawa, S.; Takashima, Y.; Tsuruoka, T.; Kitagawa, S. *Chem. Mater.* **2010**, *22*, 4531–4538.

(18)   Tsuruoka, T.; Furukawa, S.; Takashima, Y.; Yoshida, K.; Isoda, S.; Kitagawa,
        S. *Angew. Chem. Int. Ed.* **2009**, *48*, 4739–4743.

(19)   Wißmann, G.; Schaate, A.; Lilienthal, S.; Bremer, I.; Schneider, A. M.;
        Behrens, P. *Microporous Mesoporous Mater.* **2012**, *152*, 64–70.

(20)   Zahn, G.; Schulze, H. A.; Lippke, J.; König, S.; Sazama, U.; Fröba, M.;
        Behrens, P. *Microporous Mesoporous Mater.* **2015**, *203*, 186–194.

(21)   Zahn, G.; Zerner, P.; Lippke, J.; Kempf, F. L.; Lilienthal, S.; Schröder, C. A.;
        Schneider, A. M.; Behrens, P. *CrystEngComm* **2014**, *16*, 9198–9207.

2   Metal-organic frameworks

2.1   General principles of the formation of metal-organic frameworks

Metal-organic frameworks (MOFs) emerged as a new class of material in 1995 when the group of YAGHI reported the first synthesis of a microporous metal-organic framework.[22] Similar to zeolites, MOFs exhibit a porous network making these materials interesting for gas separation,[23] catalysis,[24] gas storage[25] or biomedical applications like drug delivery.[26–28] Metal-organic frameworks, often also named porous coordination polymers (PCPs), consist of metal nodes that are linked by an organic bridging molecule. The general principle of the formation of metal-organic frameworks is illustrated in Figure 1.

metal/
metal cluster

+

organic linker

3D metal-organic framework
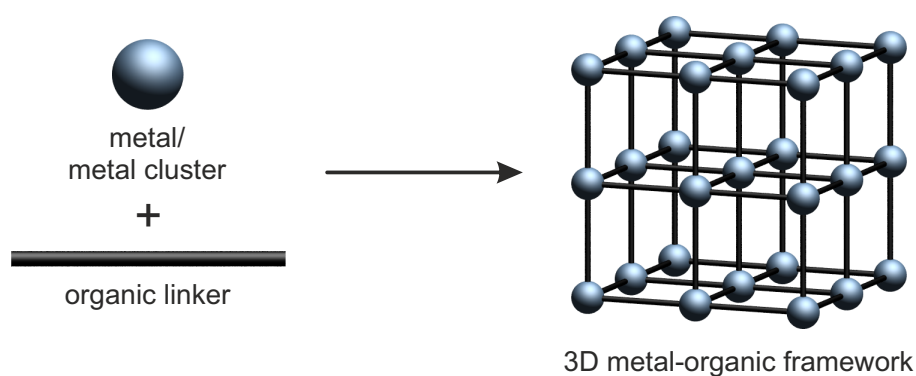
Figure 1. Principle of MOF formation. The combination of a metal or a metal cluster with a bridging organic linker results in the establishment of a three-dimensional, porous network.

Depending on the nature of the metal clusters and the number of functional groups of the bridging linker molecules, a variety of three-dimensional networks can be prepared. Metal clusters or inorganic building units (IBUs) with various points of extensions and multitopic linkers are shown exemplarily in Figure 2 and Figure 3, respectively.
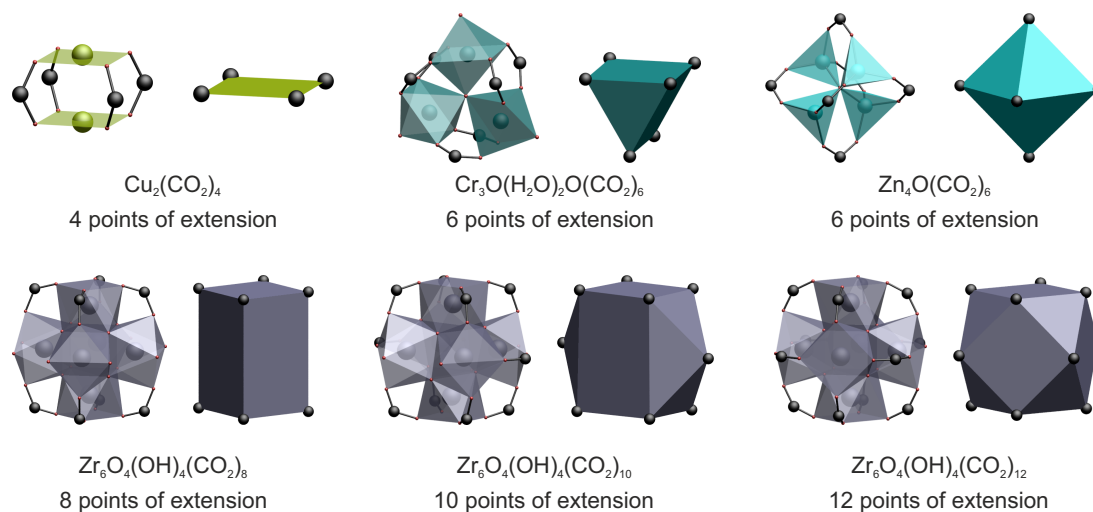
Figure 2. Metal clusters/IBUs with various points of extension as they occur in MOFs, e.g. HKUST-1,[29] MIL-88,[30] MOF-5,[31] DUT-67,[32] MOF-802,[33] and UiO-66.[8]
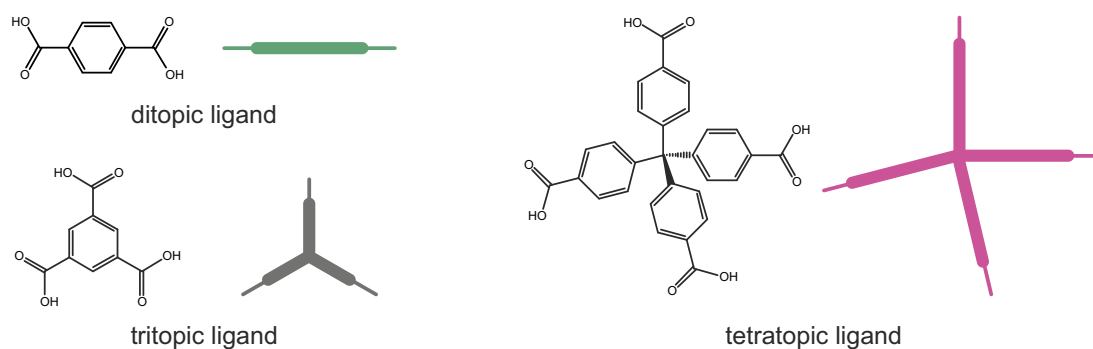
Figure 3. Variety of multitopic linking molecules that are used for the synthesis of metal-organic frameworks.

The combination of an inorganic building unit with eight points of extension, for example, with a tetratopic or ditopic ligand, respectively, leads to different network topologies as shown in Figure 4.

$Zr_6O_4(OH)_4(CO_2)_8$
8 points of extension

MOF-841
flu topology

DUT-67
reo topology

Figure 4. Reaction of a metal cluster/Zr-IBU with different multitopic ligands results in different network topologies. Crystal structures depicted are from references 32, 33.

According to the type of the IBU and the bridging linker, various pore geometries can be generated. The longer the linker, the larger the pores can be. However, the size of the pores is limited as the utilisation of very long linkers often results in an interpenetration of the framework. The great variety of linking molecules that can be associated to the metal centres opens a wide field of new materials; correspondingly, these materials captivate the imagination due to the diverse possibilities in structural modifications. Especially functionalised linking molecules offer the opportunity to establish specific host-guest interactions or for postsynthetic modifications. Appropriately, MOF research has gained a lot of interest in the last 20 years resulting in numerous different structures.[34–36] To rationalise structural complexity and to foresee possible new structures the concept of isoreticular structures was developed. This concept was firstly reported by the YAGHI group and is described as a part of section 2.2.[37]

2.2   Synthesis of metal-organic frameworks

2.2.1   Isoreticular structures of metal-organic frameworks

The most investigated MOF until now is MOF-5, which was synthesised by the group of YAGHI in 1999.[31] In this structure zinc cluster nodes are linked by the dicarboxylic terephthalate so that a cubic network is established (Figure 5). The zinc cluster nodes are built up from a central oxygen atom that is coordinated tetrahedrally to four zinc ions resulting in a ZnO_4 tetrahedron. Each zinc ion is further bonded to oxygen originating from the carboxylate groups of the linking

terephthalate forming the $(Zn)_4O(CO_2)_6$ cluster. Due to different orientations of the zinc clusters, alternating small and large pores with a diameter of 11.0 Å and 15.1 Å are present, respectively.[31]
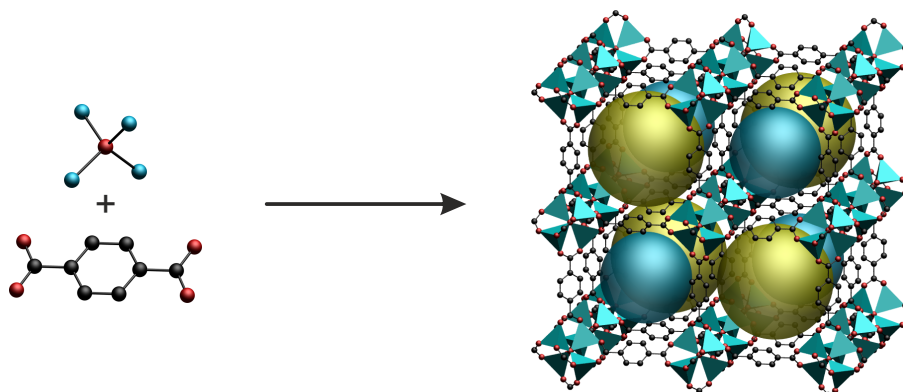
Figure 5. Generation of the structure of MOF-5 according to reference 31. The small and large pores are highlighted in blue and yellow, respectively.

Dependent on the linker length, the pore size can be adjusted with regard to the desired application. By choosing longer linker molecules, the pore system can be extended resulting in MOFs with larger pores. As these structures exhibit the same framework topology, they are isoreticular to MOF-5 are therefore named IRMOFs[37] (isoreticular metal-organic frameworks, Figure 6).
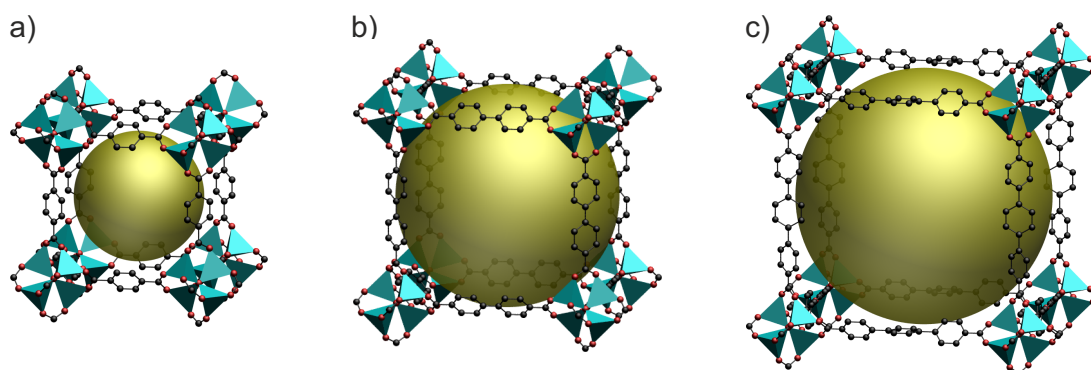
Figure 6. Members of the IRMOF series: IRMOF-1 (a), IRMOF-10 (b) and IRMOF-16 (c), according to reference 37.

Unfortunately, MOF-5 and the corresponding IRMOFs are rather unstable and prone to hydrolysis so that they are not really promising for industrial applications. On the contrary, MOFs based on tetravalent cations like Zr^{4+} are regarded as robust materials and are discussed in section 2.3 in detail.

2.2.2 Modulated synthesis of metal-organic frameworks

The synthesis of crystalline MOFs is in many cases not straightforward as many attempts of combining metal ions with organic linkers only result in amorphous products. In 2009, the group of KITAGAWA dealt with the problem of fabricating MOF nanoparticles with certain size and shape and high crystallinity in comparison to the less crystalline bulk material obtained using conventional solvothermal synthesis.[17,18] By applying acetic acid as capping reagent in the synthesis of the three-dimensional porous coordination framework [{$Cu_2(ndc)_2(dabco)$}$_n$] (ndc = 1,4-naphthalene dicarboxylate; $dabco$ = 1,4-diazabicyclo[2.2.2]octane), a competition between the monocarboxylic and the dicarboxylic acid obviously leads to anisotropic growth by oriented attachment. As acetic acid, the so-called modulator, exhibits the same chemical functionality as the linking naphthalene dicarboxylate, it can coordinate to the metal ion without acting as bridging molecule and thus "modulates" the three-dimensional expansion of the framework. As a result, [{$Cu_2(ndc)_2(dabco)$}$_n$] was not obtained as bulk material, but as nanorods, because the acetic acid hampers the ndc-copper interaction and thus leads to crystal growth in the [001] direction.[18] The influence of the modulator on the nucleation was observed qualitatively during the synthesis of HKUST-1 ($Cu_3(btc)_2$; btc = benzene-1,3,5-tricarboxylate) with dodecanoic acid as modulator. The more modulator was added to the synthesis mixture, the larger the particles grew. DIRING et $al.$ assigned this effect to slower nucleation due to the competition of added modulator and the present linker molecules that both can coordinate to the copper ions. Thus, the oversaturation of the metal precursors is decreased so that fewer nuclei grow to larger particles.[17] The competition of the modulator and the bridging ligand is schematically illustrated in Figure 7.

conventional synthesis
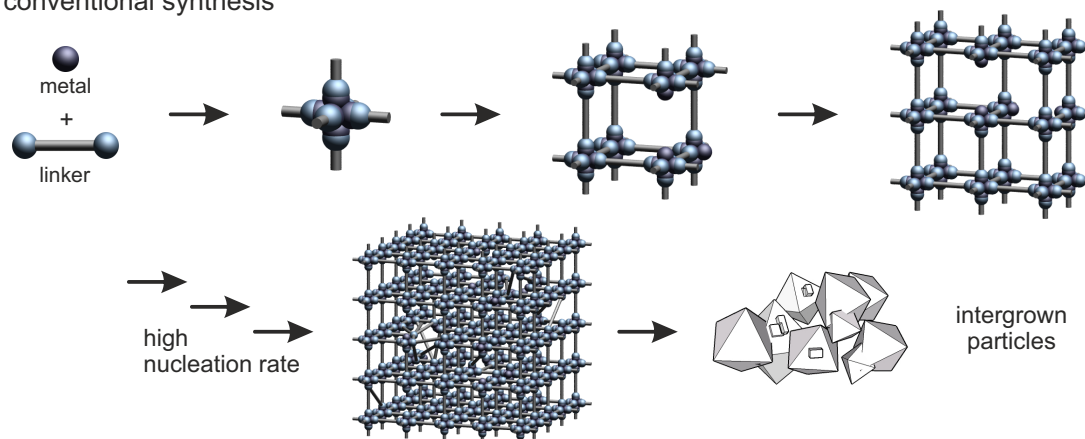
coordination modulation approach
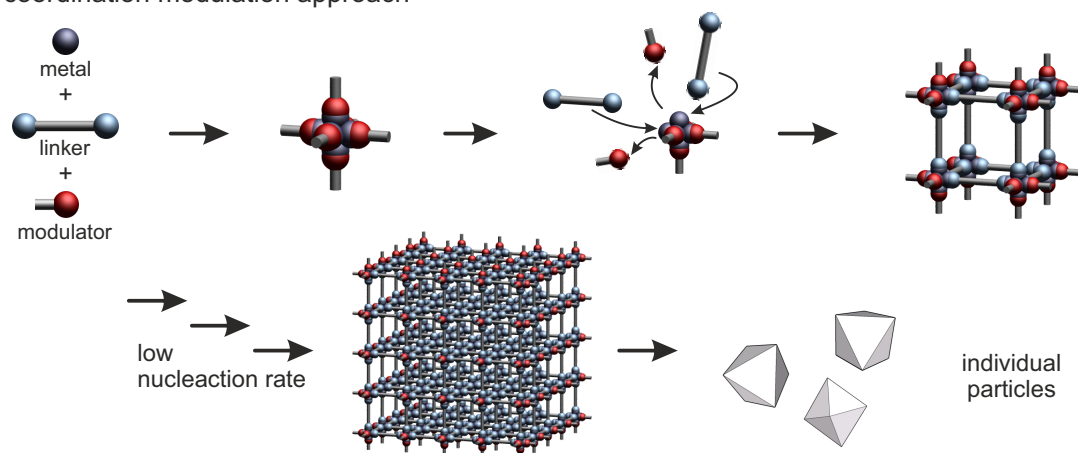
Figure 7. Schematic illustration of the coordination modulation mechanism according to references 17, 18. During the conventional synthesis (top) the framework is built up rapidly so that a disordered network may be formed. In the modulated synthesis (bottom), a modulator molecule coordinates to the metal cluster and has to be exchanged against the linker in order to establish further growth of the network.

Without any modulator, the growth of a three-dimensional network often occurs very fast. As a consequence, defects or disorder can occur in the framework; often very small and intergrown particles are formed. In contrast to that, the modulation agent decreases the nucleation and thus the reaction rate leading to a highly crystalline, non-aggregated material as the modulating molecules act as capping agents so that the intergrowth of nuclei is inhibited. Furthermore, the application of a modulating agent allows the control of the particle size and shape as well as the control of the nucleation rate which favours the reproducibility of the synthesis.

Apart from the coordination modulation mechanism, a modulator can also act as deprotonating agent. CRAVILLON *et al.* investigated the synthesis of ZIF-8 by adding sodium formate as modulator. In this case, the modulator does not act as a

competitive coordinating ligand, but as a base and enhances the deprotonation of the bridging 2-methylimadazole linking molecule.[38] This deprotonation modulation mechanism further leads to an acceleration of the reaction rate and shows another possibility how a modulator can influence the crystallisation behaviour. Furthermore, in DMF-based synthesis systems the modulator might undergo side reactions, like the formation of amides or anhydrides. The formation of water is also possible which can play a crucial role as water influences dramatically the kinetics of MOF formation (see section 3.3).

Additionally, the application of modulating agents can also promote defect formation in the resulting samples. Missing linkers in the framework give rise to larger pore volumes and BET surface areas making such materials interesting for sorption applications as well as for catalysis due to the generation of open metal sites.[39,40] Concerning Zr- and Hf-based metal-organic frameworks, it was reported recently by the KASKEL group that it is also possible to incorporate the modulator molecules regularly into the framework. Here, the modulator molecules do not only act as crystal growth inhibitors, but are part of the resulting MOF structure. Consequently, the connectivity of the IBU and thus the resulting framework topology are influenced (see section 2.3.5).[32,41,42]

The exchange of coordinating carboxylic acids, as it was proposed by KITAGAWA[17,18] for metal-organic frameworks, has already been reported earlier for Zr clusters. The first two crystalline Zr cluster with methacrylate,[43] benzoate and acrylate[44] were published by the group of SCHUBERT in the 1990s. The inner structure of these clusters correspond to the $Zr_6O_4(OH)_4$ core present in the UiO structure. The Zr atoms are arranged octahedrally and the triangular faces are capped by either μ_3-O or μ_3-OH groups. The coordination of the carboxylic acids occurs in a different way. Three of the 12 acids are coordinated to three Zr ions of one triangular face while the remaining nine acids bridge the other edges (Figure 8).
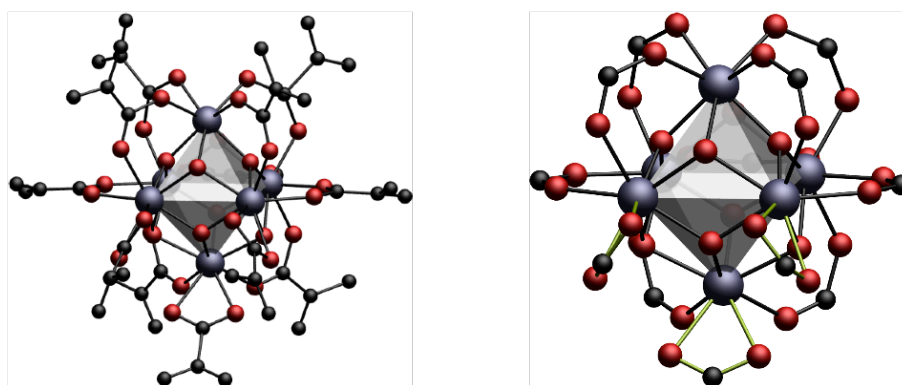
Figure 8. Structure of the oxozirconium methacrylate cluster saturated with methacrylate (left) according to reference 43. Right: Methacrylate residues omitted for clarity of the structure.

These $Zr_6O_4(OH)_4(methacrylate)_{12}$ clusters can undergo partial or complete exchange with other carboxylic acids present, like, for example, propionic acid or isobutyric acid resulting in mixed-carboxylate clusters while the arrangement of the coordinating acids changes.[45] Apart from these Zr6 clusters, Zr12 clusters can also be obtained with acrylate. By exchange reactions mixed Zr12 clusters are also possible, although a Zr6 cluster cannot be converted into a Zr12 cluster.[46] Based on these observations, we assume a similar cluster formation during a modulated synthesis of Zr-based MOFs.

The influence of a modulator with regard to the Zr-fumarate MOF synthesis is topic of section 3.1 and 3.2. Furthermore, the kinetic evaluation of the Zr-fumarate MOF formation under the influence of a modulator will be discussed particularly in section 3.3.

2.3   Zr-based metal-organic frameworks

Zr-based MOFs have gained an enormous attention due to their exceptional high thermal, chemical and mechanical[47] stability as well as to the opportunity to introduce a variety of functional groups. These advantages make Zr-based MOFs interesting for gas storage,[48–51] water adsorption,[33,52,53] separation,[54–56] catalysis,[40,57-62] and biomedical applications.[63,64] A selection of possible linkers suitable which have been used for the synthesis of Zr-based MOFs is given in Table 1. Among others, UiO-66 and UiO-67 with terephthalate and biphenylene dicarboxylate, respectively, as linker as well as their derivatives are the most popular candidates.

Table 1. Overview of linkers successfully used in the syntheses of Zr-based MOFs.

MOF	linker	ref.	MOF	linker	ref.
Zr-*fum* MOF		19	UiO-68-NH₂		65
Zr-*muconate* MOF		67	Zr-*anthracene* MOF		66
Zr-*squ* MOF		68	Zr-*sal* MOF		69
UiO-66		8	Zr-*BINAP* MOF		78
UiO-66-X	X=NH₂, NO₂, Br, CH₃, CF₃, OH, Cl, F, OCH₃, SO₃H, N₃, I, COOH, CN	61, 70–77	PIZOFs		83
UiO-66-(X)₂	X=OH, CH₃, CF₃, NH₂, COOH, F, Cl, Br, OCH₃	13, 30, 37, 38, 42–45	MOF-812 MOF-841		33
UiO-66-1,4-*naph*		70	MOF-535		84
MOF-808		33	MOF-525 MOF-545 PCN-222		84,85
MOF-802		33	NU-1000		88
DUT-67, DUT-68 DUT-69		41			
DUT-52 DUT-84		42			
MOF-805		33			
UiO-67		8			
Zr-MOF-bipy		62,86			
MOF-806		33			
Zr-*abdc* MOF		87			
DUT-51		32			
UiO-68		8			

2.3.1   Zr-based metal-organic frameworks with UiO-type structure

The first Zr-MOFs were reported by the group of LILLERUD in 2008. They published the isoreticular UiO (UiO = Universitet i Oslo) series consisting of UiO-66, UiO-67 and UiO-68 with terephthalate, biphenylene dicarboxylate and terphenylene dicarboxylate, respectively, as linking molecules (Figure 9).[8] However, the synthesis of UiO-68 with an unsubstituted terphenylene dicarboxylate linker has never been described. The original paper does not give any data on the compound.[8] In our laboratory, all synthesis attempts failed due to the extreme insolubility of the terphenylene dicarboxylic acid. However, derivatives of UiO-68 containing linkers carrying additional functional groups which lend them better solubility have been described.[65]
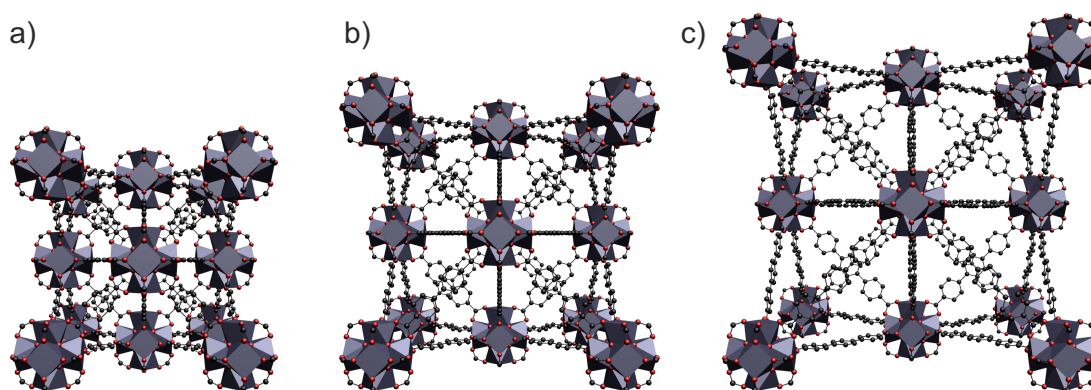
Figure 9. Central view on the structures of UiO-66 (a), UiO-67 (b), and UiO-68 (c) according to reference 8.

All these UiOs consist of a Zr-inorganic building unit (IBU; often also called secondary-building unit, SBU) that is twelvefold connected by the corresponding dicarboxylate. Each IBU is constructed from six zirconium atoms arranged in an octahedron. The triangular faces of the octahedra are capped with oxygen or hydroxo groups resulting in a $Zr_6O_4(OH)_4$ metal node (Figure 10). Free coordination sites at this node can be bridged by dicarboxylate groups of the linkers. Twelve such sites are available per linker. When all are used, the twelvefold coordination leads to a cubic close packing (*ccp*) which contains four octahedral and eight tetrahedral cavities (Figure 11).
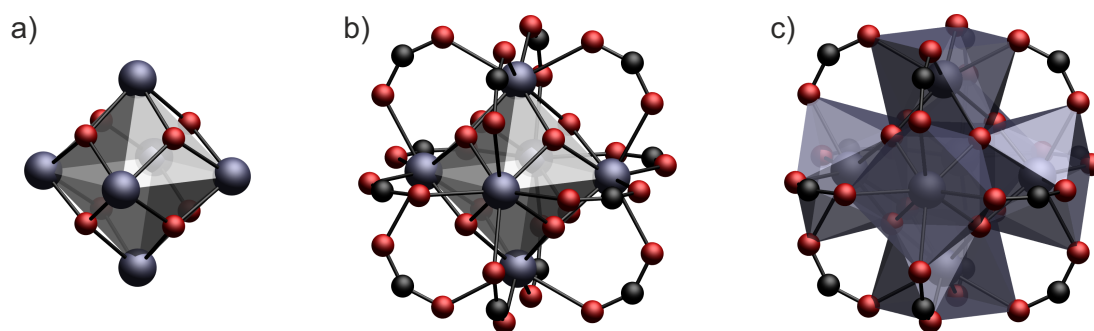
Figure 10. Design of the Zr-based IBU. Six zirconium atoms form an octahedron whose faces are capped with oxo or hydroxo groups, respectively (a). Twelve carboxylate groups of the linker coordinate to the zirconium atoms (b) leading to a square antiprismatic coordination of the zirconium atom (c).
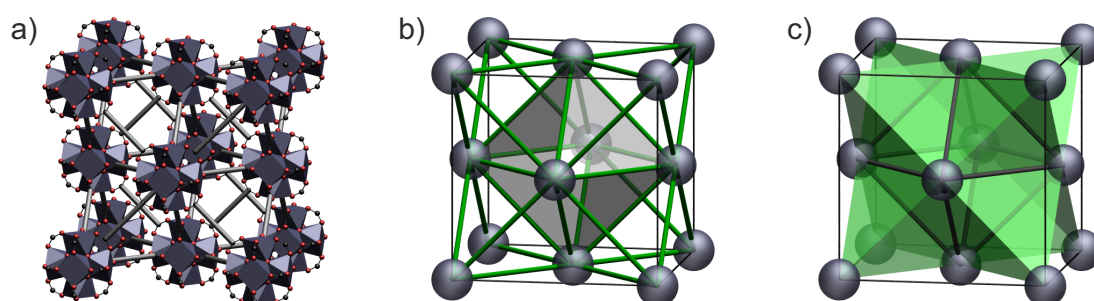
Figure 11. Schematic illustration of the UiO topology (a) and its relation to the cubic close packing (*ccp*). The octahedral and tetrahedral voids of the *ccp* structure are highlighted in grey (b) and green (c).

The strong interaction of Zr^{4+} with oxygen ligand functions and the remarkably high degree of interlinking (twelvefold connectivity) cause exceptional high thermal stability of the UiO-66 and its analogues compared to other MOF systems. Upon heating of UiO-66, one might expect that the destruction of the framework starts with the bond cleavage between the linker and the inorganic brick. Surprisingly, instead the carbon-carbon bond between the benzene ring of the terephthalate and the neighbouring carboxylate group emerged as the weakest points in the structure.[8] Nonetheless, the conclusion that changing the ligand should not affect the thermal or chemical stability was disproved later, as reports mention the exchange of the linker terephthalate in aqueous media[74] or the replacement of the metal zirconium to titanium.[89] Regarding the chemical stability against various solvents, UiO-66 shows indeed remarkable stability against water, 0.1 M hydrochloric acid and various organic solvents like chloroform, pyridine, acetone, isopropanol and methanol. Only

after exposure to alkaline 0.1 M NaOH the structure collapses. In contrast to that, UiO-67 shows a decreased stability in aqueous media. After stirring in water, hydrochloric acid or sodium hydroxide solution, respectively, the crystalline structure of the MOF is destroyed. Even upon prolonged storage in humid air, degradation is observed.[86] While the treatment with NaOH results in an amorphous product, transformation to monoclinic zirconia occurs in water and hydrochloric acid, respectively. WALTON *et al.* ascribe this instability of the framework to steric and rotational effects of the double ring structure. The possibility that water molecules reach the IBU is enhanced due to the longer linker so that the destruction of the framework is simplified compared to MOFs containing only a single organic ring like UiO-66.[86] In contrast, MONDLOCH *et al.* recently proposed that the destruction of UiO-67 after water exposure can be traced back to capillary forces. If water is exchanged with acetone before the sample is activated under high vacuum, the crystalline structure is retained.[90] Comparing the chemical stability of UiO-67 with its nitrogen containing analogue Zr-MOF-*bipy* (*bipy* = 2,2-bipyridine-5,5'-dicarboxylate) the latter suffers from destruction of the framework in protic solvents like water, methanol and isopropanol. Due to the fact that the nitrogen atoms of the bipyridine linker can act as base, these solvents are deprotonated resulting in the strong nucleophiles hydroxide, methoxy and isopropoxy, respectively, that cause a structural breakdown. Also the thermal stability of Zr-MOF-*bipy* is smaller than UiO-67. This is explained by the electron withdrawing effect of the nitrogen atoms, thus weakening the neighbouring carbon-carbon bond, so that the destruction of the framework starts at lower temperatures (approx. 480 °C) compared to pristine UiO-67 or UiO-66 (approx. 520 °C).[86] The thermal stability of several UiO-66 derivatives and the corresponding surface areas are given in Table 2. In literature, sometimes deviations concerning the thermal stability of the same UiO material become obvious and were investigated recently by SHEARER *et. al.* They found out that the thermal stability of UiO-66 is dependent on the synthesis temperature, the linker to zirconium ratio and the washing procedure. Synthesis performed at lower temperatures, for example, resulted in poorly stable UiO-66 which was assigned to an increased number of linker vacancies in the framework.[91] Comparing the thermal stability of various functionalised UiO-66 derivatives the amino-modified UiO-66-$(NH_2)_2$ as well as the UiO-66-N_3 show by far the lowest thermal stability compared to all others functionalised UiO-66 materials.

Table 2. BET surface areas and thermal stabilities of various functionalised UiO-66 derivatives.

	surface area $[m^2\,g^{-1}]$	thermal stability [°C]	ref.		surface area $[m^2\,g^{-1}]$	thermal stability [°C]	ref.
UiO-66	1110	500	92				
UiO-66-NH$_2$	1112	350	70	UiO-66-(NH$_2$)$_2$	540	200	81
UiO-66-NO$_2$	756	400	70				
UiO-66-Br	851	500	70	UiO-66-Br$_2$	339[1)]	390	73
UiO-66-CH$_3$	1065	450	72	UiO-66-(CH$_3$)$_2$	868	480	79
UiO-66-CF$_3$	739[1)]	380	73	UiO-66-(CF$_3$)$_2$	540	-[3)]	80
UiO-66-OH	1131[2)]	450	74	UiO-66-(OH)$_2$	755	250	64
UiO-66-N$_3$	872[2)]	200	74				
UiO-66-COOH	842[1)]	340	76	UiO-66-(COOH)$_2$	428	300	49
UiO-66-I	799[1)]	360	76				
UiO-66-SO$_3$H	769[1)]	260	76				
UiO-66-Cl	-[3)]	400	61	UiO-66-Cl$_2$	609[1)]	390	73
UiO-66-F	-[3)]	400	61	UiO-66-F$_2$	836[1)]	350	73
UiO-66-OCH$_3$	-[3)]	300	61	UiO-66-(OCH$_3$)$_2$	868	-[3)]	82
UiO-66-CN	661	400	77				
UiO-66-1,4-*naph*	615	450	70				

1) Langmuir surface area
2) product obtained via post-synthetic modification; 50 % conversion of UiO-66-NH$_2$
3) no values available

Upon thermal heating in vacuum the inorganic building unit Zr$_6$O$_4$(OH)$_4$ undergoes a dehydroxylation process. Above a temperature of 250 °C the Zr$_6$O$_4$(OH)$_4$ cluster releases two water molecules so that the coordination number of the zirconium atoms is reduced from 8 to 7. If the dehydroxylated UiO-66 is exposed to air and moisture, the fully conversion to the hydroxylated form occurs (Figure 12).[39,93]
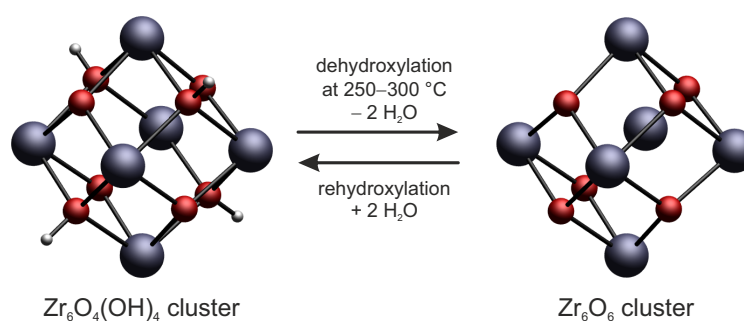

Figure 12. Hydroxylation/dehydroxylation process of the zirconium IBU according to references 8, 92.

The dehydroxylation results in a distorted Zr_6O_6 inner core with one open metal site per zirconium. VERMOORTELE et al. have shown that dehydroxylated forms of UiO-66 and UiO-66-NH$_2$ act as catalysts for the cross-aldol condensation in the synthesis of jasminaldehyde.[60] Dehydroxylated UiO-66-NH$_2$ is even more advantageous compared to unfunctionalised UiO-66, because apart from open zirconium sites that can activate benzaldehyde, the amino groups are additionally able to activate the methylenic group in the aliphatic aldehyde which results in higher yields and exceptional good selectivity. After grafting with lithium *tert*-butoxide, dehydroxylated UiO-66 offers further potential by revealing good ionic conductivity at room temperature and showing the possibility of UiO-66 for applications in Li battery technology.[94] Apart from the original UiOs, many UiO-MOF derivatives are accessible by introducing functional groups at the phenylene ring by simply using a functionalised linker instead of the non-functionalised one. Thus, sorption properties can strongly be influenced. On the one hand, functionalisation with methyl groups leads to a higher CO_2 uptake compared to the unfunctionalised analogue which was explained by the more intense interactions between the framework and the carbon dioxide due to smaller pores.[79,72] On the other hand, introduction of small, polar groups like amino, nitro and methoxy groups improve the CO_2/CH_4 and CO_2/N_2 selectivity which is interesting for gas separation.[82]

Nevertheless, some functionalised linkers are thermally unstable and cannot be used in the solvothermal syntheses of metal-organic frameworks. To circumvent this reaction process, COHEN et al. demonstrated that azide groups which are interesting for their photoreactivity and their use in "click-chemistry" can be introduced by the utilisation of postsynthetic exchange functionalisation (PSE). In this case, UiO-66 was suspended in an aqueous solution containing 2-azido-1,4-benzenedicarboxylate (N$_3$-*bdc*) under ambient conditions. Dependent on the reaction time, the degree of PSE was determined to approximately 50% after 5 days of reaction.[74] A similar ligand exchange is also obvious when two different functionalised MOFs like UiO-66-NH$_2$ and UiO-66-Br are mixed in water and stored for five days. Then, aerosol time-of-flight mass spectrometry (ATOFMS) studies revealed that most particles exhibit both *bdc*-NH$_2$ and *bdc*-Br linking molecules in the same MOF particles. Nevertheless, no ligand exchange could be detected when the particles were mixed physically in the absence of any solvent.[74] Further postsynthetic modification (PSM) was again done by COHEN et al. with UiO-66-NH$_2$ as reactant or by the group of TILSET, who used aliphatic and cyclic anhydrides to yield the

corresponding UiO-66 amides.[70,95] Another example is the synthesis of UiO-66-CN which cannot directly be obtained from a zirconium source and H$_2$bdc-CN as linker using microwaves. In this case, a solvothermal approach via a 4-step-synthesis is necessary. To avoid such a time-consuming progress, microwave-assisted PSM with UiO-66-Br and CuCN is a faster alternative and delivers higher yield of the desired UiO-66-CN.[77] Another post-synthetic modification is proposed by the COHEN group regarding cationic exchange in UiO-66(Zr). Herein, they assert the successful synthesis of UiO-66(Zr/Ti) materials via post-synthetic cation exchange (PSE) using a solution containing titanium ions. Depending on the titanium salt used in the reaction, the degree of cation exchange is influenced. The best results were obtained using TiCl$_4$(THF)$_4$ leading to around 38 wt% titanium ions in the sample.[89] The circumstance that the titanium-based version of UiO-66 is not accessible applying the traditional solvothermal synthesis, this method might provide a new route in synthesising new MOF materials. A summary of these post-synthetic modifications is schematically shown in Figure 13.
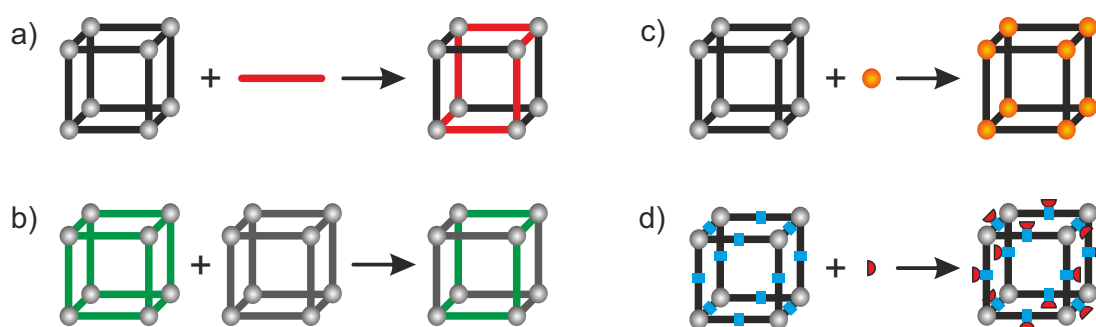
Figure 13. Post-synthetic modifications of metal-organic frameworks. a) Post-synthetic exchange of a linker molecule; b) mixed-linker MOF synthesis; c) post-synthetic cation exchange; d) post-synthetic functionalisation of the linker molecules.

In the case of isostructural frameworks concerning the UiO-67, functionalisation turned out to be interesting using the sulfone-modified biphenylene dicarboxylic acid. Compared to unfunctionalised UiO-67, this MOF exhibits a 120 % increase in CO$_2$ uptake and thus an enhanced CO$_2$/CH$_4$ selectivity.[96] WALTON et al. as well as the COHEN group report the synthesis of a Zr-MOF with 2,2'-bipyridine-5,5'-dicarboxylate (bipy) as linker. It can either be obtained in a direct synthesis or via a PSE reaction of UiO-67.[62,86] UiO-67-bipy is an interesting candidate as catalyst as it can act as chelating agent. Post-synthetic metalation with PdCl$_2$ produces active palladium sites so that a solid-state catalyst can be achieved. The successful catalytic activity was investigated considering the SUZUKI-MIYAURA cross-coupling reaction

between aryl halides and arylboronic acids that shows enhanced yields compared to commercially available Pd loaded on carbon.[62]

In our group, we have also focused on Zr-based MOFs. Unfortunately, we were not able yet to reproduce the synthesis of highly crystalline UiO-67 and UiO-68 according to the synthesis procedure published by LILLERUD et al. Nonetheless, we were successful in synthesising highly crystalline UiO-66, UiO-66-NH$_2$ and UiO-67 nanoparticles and to tune the particle sizes from nanometer to micrometer sizes as well as to even obtain single crystals by applying the coordination modulation approach.[65] However, as described above, in our laboratory UiO-68 was not accessible at all, but the amino-functionalised terphenylene dicarboxylate gave rise to the UiO-68-NH$_2$ by applying a monocarboxylic acid as modulator.[65]

Apart from acetic and benzoic acid used as modulators by SCHAATE et al.,[65] other monocarboxylic acids are also promising as modulating agents. VAN DER VOORT et al. synthesised functionalised UiO-66 frameworks like UiO-66-CF$_3$, -F$_2$, -Cl$_2$, -Br$_2$ and -SO$_3$H by applying formic acid among others. All structures remained stable after a solvent exchange with methanol and an activation process at 65 °C under vacuum.[73] However, the addition of a modulating agent does not only increase the crystallinity and allows the preparation of individual nanoparticles, but may also promote defect formation.[39,68,97] Neutron diffraction measurements on UiO-66 revealed that one out of 12 linkers is missing when acetic acid is applied in the synthesis. This offers many advantages as the linker vacancies can be adjusted by varying the concentration of the modulator. As a result, the pore volume can be increased from 0.4 cm^3·g^{-1} to 0.65 cm^3·g^{-1} and the BET surface area was enhanced from 1000 to 1620 m^2·g^{-1}. For a hypothetical structure that is built up from only 11 linkers the pore volume and the BET surface area could be calculated to 0.502 cm^3·g^{-1} and 1433 m^2·g^{-1}, respectively. These values are approximately 20% and 50% higher than the theoretically calculated values for a UiO-66 crystal without any defects (0.426 cm^3·g^{-1} pore volume and BET surface area of 954 m^2·g^{-1}), respectively. This control over the defect concentration is quite interesting with regard to sorption properties as the gas uptake of, for example, carbon dioxide could be drastically enhanced.[39] With regard to Zr-*squ* MOF (*squ* = squarate) a theoretical, defect-free material does not exhibit any porosity, but accessible microporosity can be achieved when formic acid is used as modulator in the reaction synthesis.[68] A similar defect formation was investigated by the group of DE VOS who used

trifluoroacetic acid as modulator in the UiO-66 synthesis. Here again, the modulator partially substitutes linker molecules and after its removal open metal sites are generated acting as LEWIS acid, although the modulator does not affect the crystal size. The catalytic activity of dehydroxylated UiO-66 was proved following the cyclisation of citronellal to isopulegol.[40]

2.3.2 Zr-fumarate MOF

Inspired by the robustness of the UiO-type MOFs, we have focussed on the synthesis of Zr-based MOFs with regard to biomedical applications, e.g. for implant coatings or oral composites to establish a drug delivery system. For that purpose, we have been interested in Zr-based MOFs with linkers that will not cause any defence reaction in the human body. Fumaric acid, a biologically occurring molecule in the KREBS cycle, seemed to be a promising candidate to synthesise a biofriendly metal-organic framework that might be suitable for a drug delivery system or as an implant coating.

The synthesis of the Zr-fumarate MOF (Zr-*fum* MOF) proved to be possible by applying the already mentioned coordination modulation approach, originally investigated by KITAGAWA *et al.*[17,18] As modulator we used mainly the monocarboxylic acid formic acid which was added to DMF- as well as to water-based synthesis systems (see section 3.1 and 3.2, respectively).[19,20] Without any modulator only broad reflections in XRD studies were present indicating an amorphous or highly disordered material. In all cases, the formic acid influenced the crystallinity, the particle size, the degree of aggregation, and the kinetics. The kinetic influence of the modulator as well as the influence of additional water present in the reaction mixture is presented in section 3.3.[21] Unfortunately, we were not able to slow down the reaction rate so strongly by further increasing the amount of modulator that we could obtain Zr-fumarate MOF single crystals. Thus, the crystal structure was simulated using quenched dynamic simulations in "Materials Studio". The simulated powder pattern was in good agreement with the experimental one so that Zr-fumarate MOF obviously crystallises in a cubic primitive crystal structure (space group *Pn*−3). These results were confirmed recently by the group of YAGHI who were able to perform single crystal analysis on Zr-fumarate MOF (renamed by YAGHI to MOF-801) using synchrotron radiation.[33] The crystal structure of the Zr-fumarate MOF is depicted in Figure 15. The framework topology is the same as that

of the UiO MOFs. Each Zr IBU is twelvefold connected via the fumarate linker molecules. Due to the very short linker fumarate, the microporous cavities show diameters of 5−7 Å which are smaller compared to those of UiO-66 (8−11 Å).
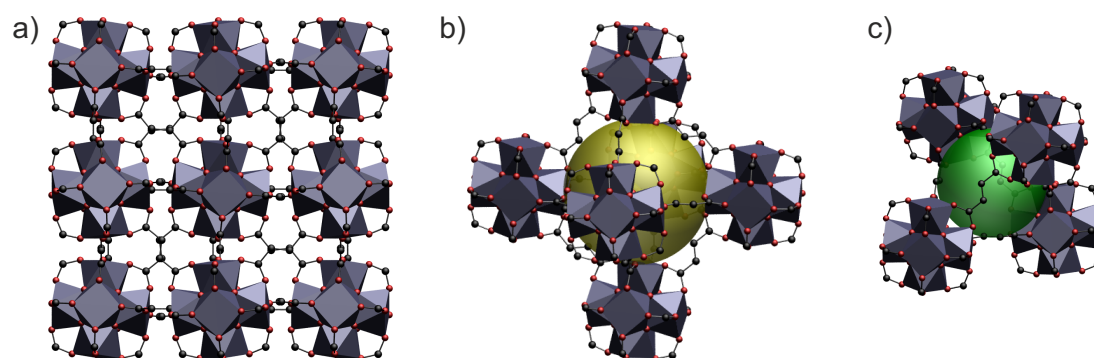
Figure 14. Structure of Zr-fumarate MOF along the *a*-axis (a); octahedral (b), and tetrahedral (c) cavity.

As linker, fumarate is not a linear molecule as terephthalate, but has a kink. The arrangement in the structure demands a tilting of the IBUs. If all the IBUs were oriented to the same direction, a connection of the IBUs would result in a shift of the IBUs that destroys the cubic symmetry (Figure 15, left). Tilting of the IBUs can also compensate for the asymmetry of the linker (Figure 15, right). This tilting leads to two crystallographically distinct IBUs and is also accompanied by a decrease in symmetry, which occurs, however, within the cubic symmetry class from the face-centred cubic space group *Fm−3m* (LAUE class *m−3m*) to the cubic primitive space group *Pn−3* (LAUE class *m−3*).
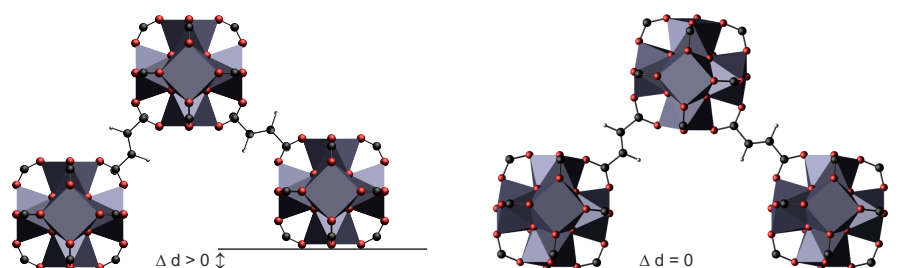
Figure 15. Connection of IBUs of the Zr-fumarate MOF with uniformly oriented, but shifted (left) and with tilted IBUs (right).

Other UiO-type structures with such a kink in the linking molecules were described at about the same time for azobenzene-MOFs like Zr-*abdc* MOF (*abdc* = 4,4'-azobenzenedicarboxylate) synthesised in our group by SCHAATE *et al.*[87] and the Zr-*Cl₂abdc* MOF (*Cl₂abdc* = 3,3'-dichloro-4,4'-azobenzenedicarboxylate) reported

by the group of MAURIN.[98] Single crystal analysis of the Zr-*abdc* MOF revealed a high disorder of the linker molecules maybe due to the staggered structure of the azobenzenedicarboxylate which prevents a concrete determination of the crystal structure. Nevertheless, the face-centred structure *Fm−3m* was considered as the most suitable space group as the reflections of the powder XRD pattern could be indexed within a face-centred cubic cell.[87]

2.3.3 Porous interpenetrated zirconium-organic frameworks (PIZOFs)

Apart from the UiO series the PIZOF (PIZOF = porous interpenetrated zirconium-organic framework) family shows a high chemical versatility as well. These PIZOFs which were invented in our group by SCHAATE *et al.* in 2011 exhibit rod-like linkers consisting of alternating phenylene (P) and ethynylene (E) units (HOOC[PE-P(R^1,R^2)-EP]COOH).[83] The central phenylene ring offers the opportunity to introduce functionalities by the variation of the residues R^1 and R^2 (Figure 16).
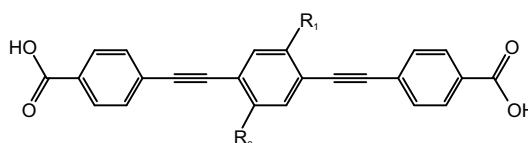
Figure 16. Structural formula of the PIZOF linker.

Until today, 23 different PIZOFs could be synthesised ranging from very hydrophobic to very hydrophilic ones. Furthermore, the tuning of the linker also allows further post-synthetic modifications like a 1,3-dipolar cycloaddition with an alkyne-functionalised residue and azide groups or a DIELS ALDER cycloaddition using a furan-functionalised residue and maleimide.[99] In comparison to the UiO series the PIZOF linkers are very long (6.8 Å in UiO-66 to 15.4 Å in UiO-68 derivatives compared to 20.4 Å in the PIZOF) and allow interpenetration of the framework. Single-crystal structure analysis of PIZOF-2 (R^1, R^2 = OMe) revealed two independent networks, each comparable to the UiO topology with the same Zr IBU as described in section 2.3.1. For clarity, one individual framework is presented in Figure 17.
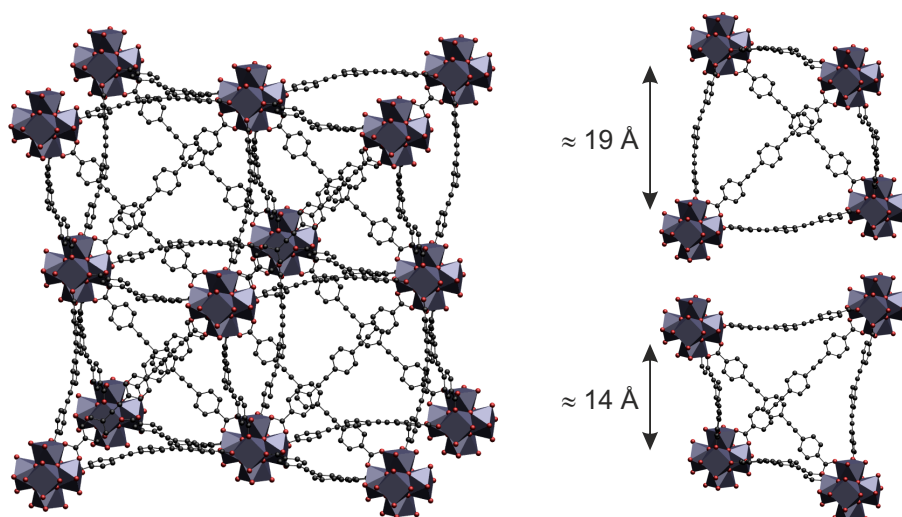
Figure 17. Individual framework within the PIZOF according to reference 83. The bended linkers result in convex and concave cavities with a diameter of 19 Å and 14 Å, respectively.

One half of the tetrahedral cavities in one framework is occupied by IBUs of the second one so that the IBU positions of both are comparable with the zinc and sulphur positions in the cubic zincblende structure. Due to the bending of the linkers concave as well as convex tetrahedral voids are present with a diameter of 14 Å and 19 Å, respectively, whereas all convex voids are free of IBUs of the interpenetrating network and all concave voids are occupied (Figure 18).
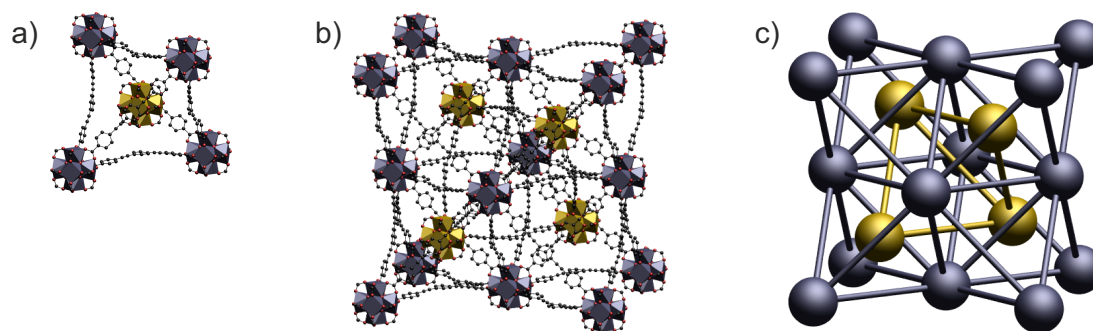
Figure 18. PIZOF structure showing the interpenetration of one framework with a second one (highlighted in yellow). All concave voids are occupied (a) by an IBU of the other framework so that in the PIZOF framework (b) all IBUs are arranged analogously to the atoms in ZnS as shown simplified in c).

Although the PIZOFs consist of very long linkers, they are highly stable against aqueous solutions. Due to the interpenetration of the framework, the IBUs are protected by the linkers of the interpenetrating framework, so that they are not accessible for water molecules.

2.3.4   MIL-140

In 2012, SERRE *et al*. described zirconium-organic frameworks that consist of subunits built up from zirconium oxide chains.[100] In this case, the zirconium ions are sevenfold coordinated by oxygen atoms and the resulting zirconium polyhedra are connected to 1D chains which can either be considered as the linkage of two parallel corner-sharing chains or of edge-sharing dimers of the zirconium polyhedra. These are in turn linked to six other chains by organic dicarboxylates leading to a 1D pore system. Depending on the linker, four different MIL-140 structures (MIL = Matériaux Institut Lavoisier), namely MIL-140A, MIL-140B, MIL-140C, and MIL-140D consisting of 1,4-benzene dicarboxylate, 2,6-naphthalene dicarboxylate, 4,4'-diphenylene dicarboxylate, and 3,3'-dichloro-4,4'-azobenzene dicarboxylate, respectively, were synthesised (Figure 19).
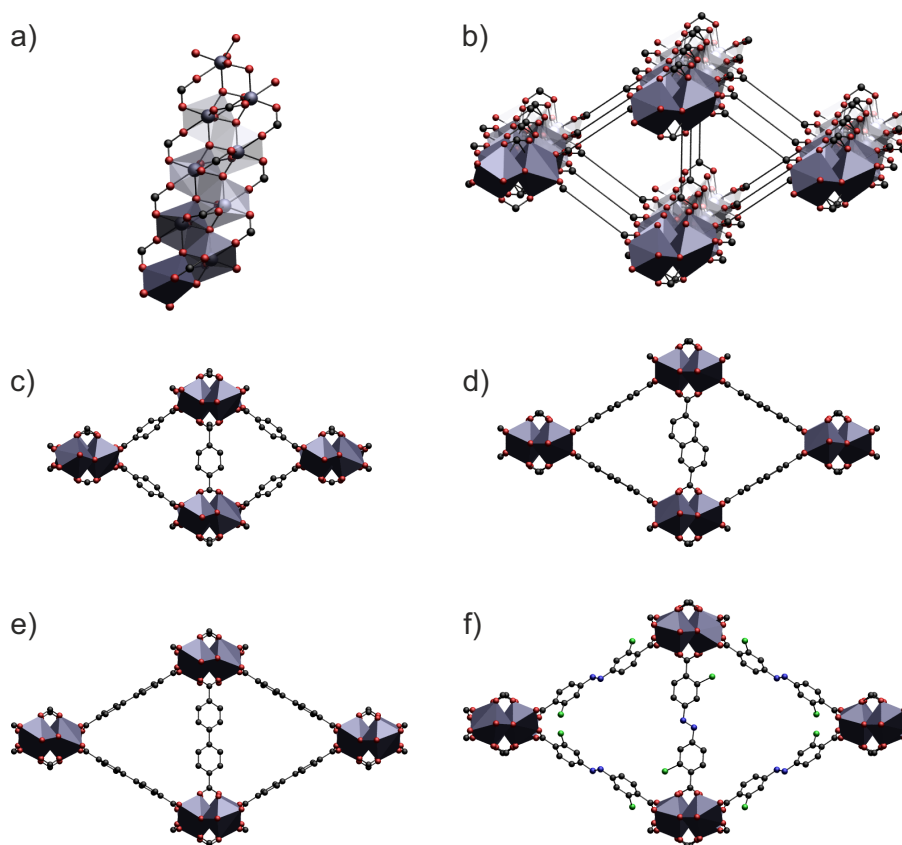
Figure 19. The MIL series consists of a chain-like IBU (a) that is connected to six other parallel IBU chains forming a three dimensional network with channel-like pores (b). Depending on the linker length, different pore sizes are obtained. The porous structures of MIL-140A (c), MIL-140B (d), MIL-140C (e) and MIL-140D (f) are presented along the *c*-axis. The crystal data were obtained from reference 100.

These MIL-140 series can be obtained at reaction temperatures above 180 °C. By applying lower reaction temperatures (150 °C – 160 °C) the corresponding UiO

structures crystallise. Thus, the MIL-140s might be the thermodynamically stable phases of polymorphous UiOs. Furthermore, they show less porosity $(400 - 700 \text{ m}^2 \cdot \text{g}^{-1})$ and are less stable when combusted in air ($\approx 500 °C$), but all of them retain their crystallinity after treatment with water and exhibit a better mechanical stability.

2.3.5   Zr-based MOF with decreased coordination numbers

Apart from the twelvefold coordination of the Zr-IBU as present in the UiO-type MOFs, the Zr-fumarate MOF and the PIZOFs, the modulating approach allowed the synthesis of a lot of new Zr-based MOFs with decreased coordination numbers. In recent years, the KASKEL group investigated the synthesis of several DUT structures (DUT = Dresden University of Technology) with dithienothiophene dicarboxylate (DUT-51) and 2,5-thiophenedicarboxylate (DUT-67, DUT-68 and DUT-69, respectively) as linking molecules. By applying benzoic acid as modulator in the synthesis of DUT-51, the connectivity of the Zr-IBU can be decreased to eight resulting in a reo topology while the other coordination sites are occupied by the modulating agents. This material is less stable compared to other Zr-based MOFs as the structural breakdown of the framework occurs with the removal of the modulator benzoic acid at 150 °C.[32] Regarding the synthesis of DUT-67, DUT-68 and DUT-69, respectively, these structures can be obtained by adjusting the modulator concentration. While DUT-69, which contains a 10-connected IBU, is obtained with low concentration of acetic acid as modulator, the increase of the modulator concentration leads to eightfold connected Zr-IBUs and the formation of DUT-68 (space group *Im−3m*) and DUT-67 (space group *Fm−3m*).[41] A similar approach using 2,6-naphthalene dicarboxylate as linking molecule and a low concentration of acetic acid as modulator resulted in the formation of DUT-52 which is isoreticular to UiO-66. By increasing the modulator concentration five times DUT-84 was obtained. It contains a sixfold connected IBU which was observed for the first time for Zr-based metal-organic frameworks.[42] Apart from the DUT structures various Zr-MOFs with decreased coordination numbers have also been investigated, for example PCN-222,[85] NU-1000,[88] MOF-545,[84] MOF-802,[33] MOF-808,[33] and MOF-841.[33]

2.4   *In situ* investigations using synchrotron radiation

Until today, a lot of MOF structures have been reported. However, only few publications deal with *in situ* investigations concerning the crystallisation mechanisms. Often, such experiments are difficult to realise with standard laboratory equipment. To record even the earlier stages of the crystallisation process, a high intensity of radiation is necessary to detect even small amounts of diffraction solid in the reaction vessel in a short period of time. Synchrotrons offer a lot of advantages to monitor such reactions. In comparison to conventional X-ray diffraction, synchrotron radiation exhibits a broad electromagnetic spectrum extended from the infrared to hard X-rays (Figure 20).
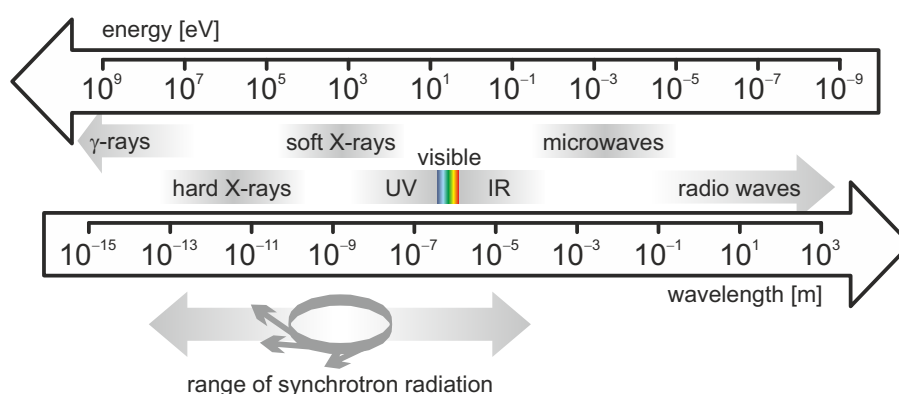
Figure 20. Electromagnetic spectrum (modelled according to reference 101).

With the help of synchrotron radiation and applying energy-dispersive X-ray diffraction (EDXRD) the crystallisation behaviour of Zr-fumarate MOF, especially under the influence of a modulator in water-based as well as in DMF-based synthesis systems could be investigated. For that purpose, all corresponding experiments (section 3.3) were performed at the synchrotron radiation source DORIS III at Deutsches Elektronen-Synchrotron, DESY, in Hamburg, Germany.

Synchrotron radiation originally occurred as a by-product when charged particles with high relativistic velocities moved on circular orbits and was observed for the first time in 1946. Only in the 1980s, investigations using synchrotron radiation appeared as a novel opportunity to, for example, diffraction techniques. The wide spectral range, high parallel and narrow beams as well as exceptional intensity result in rapid data collection and better signal to noise ratios. A schematic of a modern synchrotron radiation source is given in Figure 21.
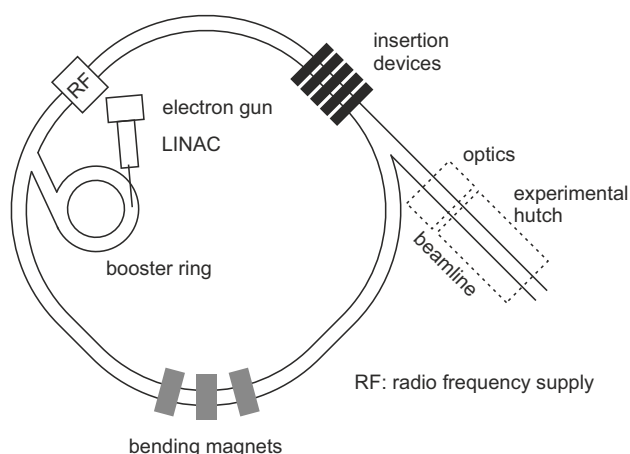
Figure 21. Schematic illustration of a synchrotron radiation source (according to reference 102).

Electrons provided from an electron gun are accelerated to about 100 MeV using a linear accelerator (LINAC). At DORIS III positrons are accelerated. Before the charged particles are injected periodically in bunches to the main storage ring, they are further accelerated in the booster ring. Although the whole system is operated under high vacuum, collisions between charged particles and gaseous impurities lead to a decay of the electron beam current so that the storage ring has to be refilled after several hours. After injection into the storage ring, bending magnets in the arced section of the ring force the electrons to change their path. In the straight sections of the ring insertion devices like wigglers and undulators enhance the brilliance of the synchrotron radiation further, although even without these magnets the radiation would still be more intense by orders of magnitude than the radiation provided for example by sealed tubes in the laboratory. If the charged particles exhibit a velocity that is close to the velocity of light, synchrotron radiation is emitted tangentially from the electron orbit. The emission of a white beam offers the possibility to perform energy-dispersive diffraction (EDXRD, Figure 22).
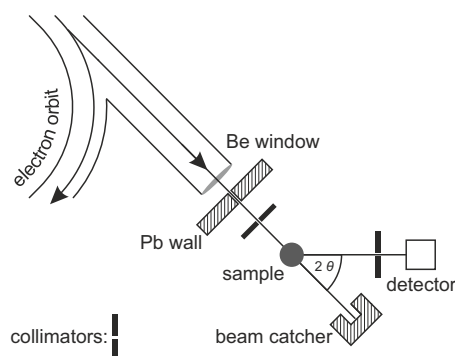
Figure 22. Schematic illustration of the principle of energy-dispersive diffraction (EDXRD) (modelled according to reference 103).

Due to the emission of synchrotron radiation, the storage ring suffers from an energy loss that has to be compensated by a radio frequency supply (RF). During the measurement the full white beam hits the sample while the scattering angle 2θ remains fixed. The photon energy that fulfils the BRAGG condition is analysed by the detector. This method is really beneficial, because the whole diffraction pattern is recorded simultaneously including the element-specific fluorescence radiation. Thus, the data collection times are quite short compared to angle-dispersive diffractometry so that time-dependent processes like crystallisation including phase transitions can be studied. As a result, the scattered intensity in dependence of the photon energy is monitored and the crystallisation behaviour can be investigated *in situ*.[101–104]

2.5   Biological applications of metal-organic frameworks

Since their discovery, the application of metal-organic frameworks has mainly focussed on separation, storage and catalysis. Nowadays, their utilisation for biomedical purposes gains more interest, because in this research field, metal-organic frameworks seem to be a promising material as well.[105] However, in every case, the stability of the material in body fluids and the metabolism of its degradation products, in general metal cations and linkers, have to be taken into account in order to avoid cytotoxicity effects. Great efforts have been devoted to the incorporation of small gaseous molecules, for example nitrogen oxide,[106–109] and the incorporation and release of cosmetic, anti-inflammatory, antiviral and anticancer drugs.[27,28,110–120] Furthermore, metal-organic frameworks might be promising candidates for optical imaging, magnetic-resonance imaging (MRI) and X-ray computed tomography (CT).[26,63,121–125]

Active gases like nitrogen oxide can adsorb at unsaturated metal sites of the framework and can afterwards be released again.[106–109] NO is antibacterial, anti-thrombotic, muscle relaxing, attractive for wound healing and is involved in the balance of hypotension and hypertension. Especially CPO-27-Ni and CPO-27-Co[107,108] showed exceptionally high NO storage capacity and favourable delivery properties compared to Cu-based HKUST-1.[106] Whereas the adsorption capacity of HKUST-1 for NO is quite large (9 mmol·g^{-1}), unfortunately its release is by two orders of magnitude less (2 μmol·g^{-1}). Despite this behaviour, the NO release of HKUST-1 was sufficient to inhibit platelet aggregation *in vitro*; however, copper

ions were liberated which would cause toxic side effects in the human body. CPO-27 also showed promising results in *in vitro* tests as the release of NO lead to 100% relaxation of precontracted pig coronary arteries. As in the study of compounds for NO release, also for other applications, often MOFs are considered which contain toxic metals which might cause side effects in the human body. To circumvent these disadvantages, MOFs comprised of non-toxic components gained more interest. Until now, four different so-called "Bio"-MOFs have been reported which are based on biocompatible metal cations and biomolecules as linkers.[126–129] BioMOF-1 and BioMOF-100 consist of zinc ions and adenine (a purine nucleobase) as well as biphenylene dicarboxylate as linker. BioMOF-1 remains stable for several weeks in various solvents, water and phosphate-buffered saline (PBS) solution. The anionic nature of BioMOF-1 offers the opportunity to incorporate cationic drugs like the antiarythmia drug procainamide·HCl. The drug release is enhanced in PBS solution due to cation-triggered drug release mediated by drug exchange with the PBS buffer cations.[126] BioMOF-100, which is constructed similarly, features an exceptionally high BET surface area ($4300 \, \mathrm{m^2 \cdot g^{-1}}$) and the largest pore volume ($4.3 \, \mathrm{cm^3 \cdot g^{-1}}$) reported concerning MOFs until now. The combination of biphenylene dicarboxylate as linker and a quite large zinc-adeninate building unit (ZABU, 14.2 Å) compared to the more common zinc-carboxylate building unit (10.5 Å) results in very large pores making this material interesting for drug incorporation[130] as it might serve as drug reservoir for molecules with high steric demands. As no interpenetration occurs, channels with a diameter of 28 Å are generated in mesoporous BioMOF-100. Thermogravimetric measurements of BioMOF-100 revealed a mass loss of 60% up to 200 °C which is assigned to the removal of guest molecules. No further mass loss occurred until the material decomposes at 350 °C.[127]

Another task is to construct MOFs that release bioactive components after destruction of the framework. The first therapeutically active MOF was published by the group of SERRE in 2010; it is built up from iron ions and nicotinate molecules. The so-called Bio-MIL-1 is not stable in physiological solvents and degrades after one hour in PBS delivering the linking nicotinic acid (niacin, vitamin B3).[128] In the case of Bio-MIL-2 that consists of calcium and glutarate, both metal ions and linkers are bioactive after a rapid degradation of the framework in aqueous media. The release of calcium as therapeutic agent can prevent osteoporosis and osteomalacia

whereas glutaric acid plays a crucial role in the catabolism of essential amino acids.[129]

Nevertheless, the incorporation of drugs into metal-organic frameworks and the release is still a great challenge but also offers a lot of advantages. Lower doses of drugs may be necessary, because of local instead of systemic application. Moreover, the high tunability of the surface, variation of pore sizes or functionalisation of the metal-organic framework allow a good adjustment of MOF-drug interaction. Thus, biomedical research on MOFs focuses increasingly on the application as nanocarriers.[131]

Between others, MIL structures have gained interest with regard to drug encapsulation, drug release and cytotoxicity of the material. On the one hand, the variety of MILs (Figure 23) offers a wide range of applicable pore sizes and on the other hand functionalisation of the linkers is possible to enhance the drug loading capacity.
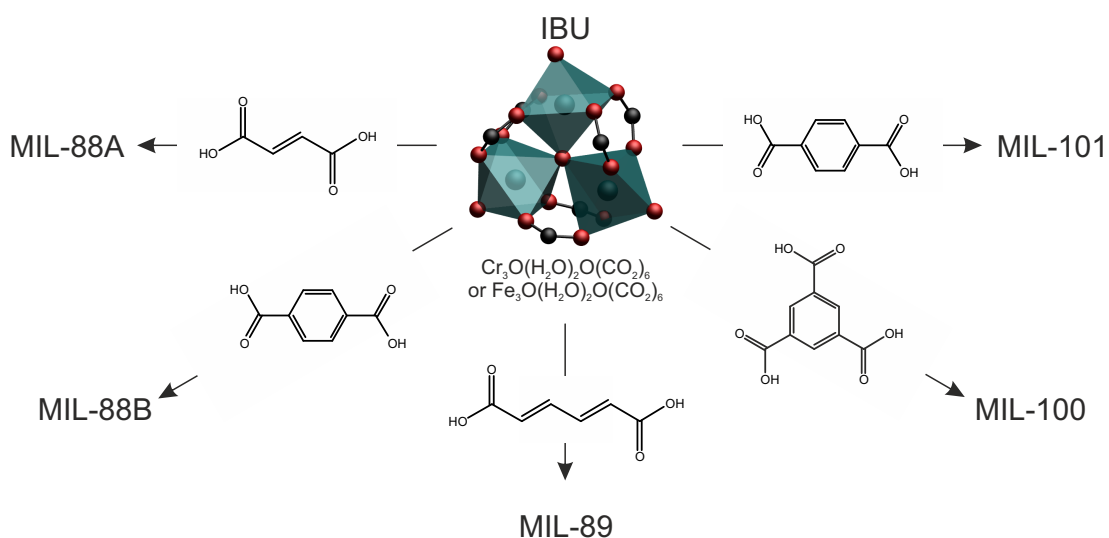
Figure 23. Combination of iron- or chromium-based IBUs with different organic linkers leads to the formation of various MIL structures that might be interesting for drug incorporation.

Especially the incorporation of ibuprofen, an anti-inflammatory drug, was thoroughly investigated as a model drug both experimentally and by using computational simulations,[130,132] because of its simple structure and the presence of a carboxylic group that is also often part of other drug molecules. The influence of the pore size becomes obvious considering the much higher ibuprofen loading in the Cr-based MIL-101 compared to MIL-100 (1.4 g ibuprofen per gram MIL-101 and 0.35 g

ibuprofen per gram MIL-100, respectively); MIL-100 exhibits smaller pore windows than the former.[28] The application of a "breathing MOF" like MIL-53(Cr,Fe) is one idea to circumvent this disadvantage. Actually, the breathing effect can be seen upon hydration/dehydration of the material (Figure 24). In the dehydrated form, MIL-53 has a pore opening of 13.04 Å. Upon hydration or adsorption of molecules the pore opening can reach 7.85 Å. Thus, the pore size of the MOF might also be adjusted according to the size of a drug.
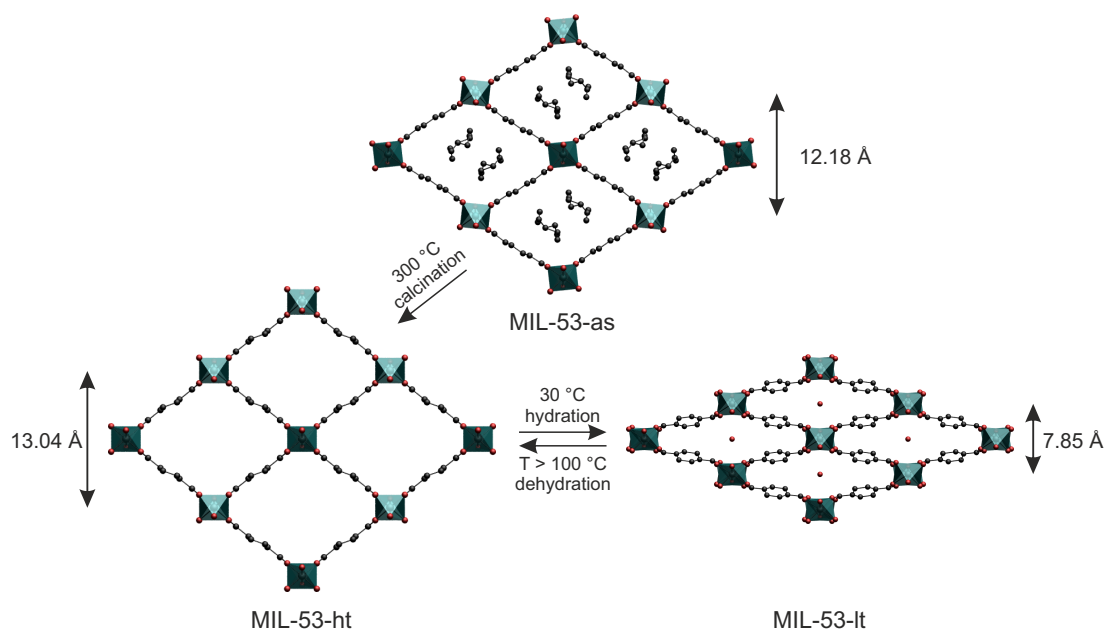
Figure 24. "Breathing" behaviour of MIL-53(Cr,Fe) according to reference 133. After calcination of the as-synthesised MIL-53-as large pores are generated in the MIL-53-ht (high temperature). Upon hydration the pore diameter is decreased resulting in the MIL-53-lt (low temperature).

HORCAJADA *et al*. reported such a successful incorporation of ibuprofen in MIL-53 and a subsequent slow delivery over three weeks in simulated body fluid (SBF). X-ray powder diffraction of the drug loaded MIL-53 confirmed a partial pore opening of 11.34 Å (Figure 25).[27]
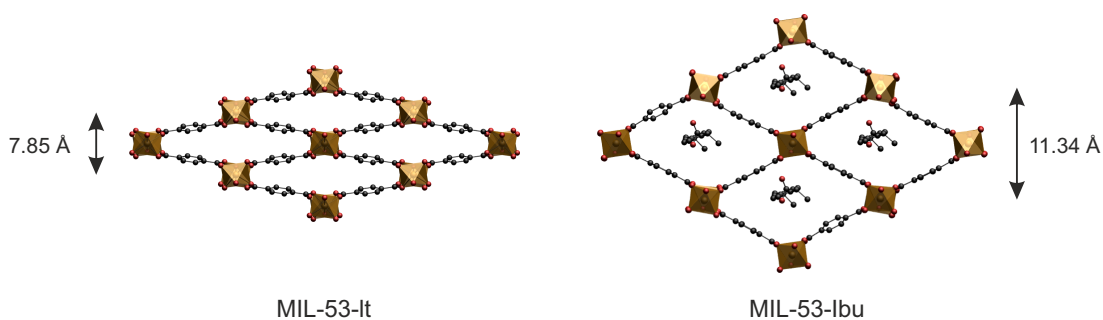
Figure 25. Partial pore opening of MIL-53(Fe) (left) after incorporation of ibuprofen (right) according to reference 27.

Apart from the pore sizes, the interior nature of the pores is also important. For that purpose, the encapsulation of a cosmetic molecule, the amphiphilic caffeine, was investigated in flexible, functionalised MIL-88B(Fe).[110] A functionalisation of the linking terephthalate with polar, hydrophilic or H-donor groups leads to an enhanced drug uptake because of the formation of hydrogen bonds between the functional groups and the carbonyl function present in the caffeine molecule.

The incorporation of other drugs which are applied in HIV or anticancer therapy is also possible in MOFs. Some of these drugs, especially the antiviral azidothymidine triphosphate (AZT-TP, phosphorylated zidovudin) which protects cells from HIV infection, and the anticancer drug busulfan, both suffer from low stability in biological media. AZT-TP further shows a low cellular uptake and cannot penetrate the cell membrane. A successful incorporation of this drug into MIL-100(Fe) particles enabled the delivery of AZT-TP into the cells thus resulting in 90% inhibition of the viral replication of infected human PBMCs (Peripheral Blood Mononuclear Cells).[111] Similarly, busulfan was entrapped in several MILs like MIL-53, MIL-100, MIL-88B and MIL-89 by simple impregnation methods.[112] Within the investigated MILs, MIL-100 showed the highest busulfan loading of 26 wt%. *In vitro* cytotoxicity tests of empty MIL-100 nanoparticles with different cell lines (human leukemia CCRF-CEM, human macrophages J774 and human multiple myeloma RPMI-8226) revealed no toxicity up to 50 $\mu g \cdot mL^{-1}$. In contrast to that, the busulfan-loaded nanoparticles showed similar toxicity as the free drug under preservation of the pharmacological activity. MIL-100 as well as MIL-101 were also considered for the encapsulation of other anticancer drugs like topotectan (TPT) and ethoxysuccinato-cisplatin (ESCP). The *in vitro* tests concerning encapsulated TPT in MIL-100 were carried out with three different cell lines (human alveolar

adenocarcinoma A549, human pancreatic cancer cell line MiaPaCa2 and human pancreatic cell line PANC1), all of which showed an efficient antitumoral activity of these particles.[134] ESCP-loaded particles of amino-functionalised MIL-101(Fe) also exhibited appreciable cytotoxicity with regard to the HT-29 cell line (human colon adenocarcinoma cells).[117] Concerning the drug incorporation and release of anticancer drug, several other drug like SN-38,[113] camptothecin (CPT),[113,114] daunomycin (DAU),[113] and doxorubicin (DOX),[113,135] as well as nimesulfide,[115] and 5-fluoruracil (5-FU)[119] were released from Zn-*bix* MOF (*bix*: 1,4-bis(imidazol-1-ylmethyl)benzene),[113] ZIF-8,[114,119,135] and HKUST-1,[115] respectively. Especially ZIF-8 might be an interesting candidate for a triggered drug release, because it decomposes under acidic conditions. Hence, a low release is reported under neutral conditions (in PBS at pH = 7.4), but a strong release appeared under deconstruction of the framework at pH = 5.[119] With regard to HKUST-1 even a targeted drug release is possible. A magnetic nanocomposite Fe_3O_4/HKUST-1 loaded with the anticancer drug nimesulfide can be influenced by an external magnetic field so that the drug incorporated into the magnetic composite can be targeted to the desired treatment location. This strategy offers many advantages, because particle circulation in the body and common side effects in chemotherapy can be omitted.[115]

For optical imaging TAYLOR-PASHOW *et al.* showed that the contrast agent BODIPY (BODIPY = 1,3,5,7-tetramethyl-4,4-difluoro-8-bromomethyl-4-bora-3*a*,4*a*-diaza-*s*-indacene) can be attached covalently to the amino group of a functionalised MIL-101. As MIL-101 undergoes degradation when getting in contact with PBS, a silica covering enhanced the stability of the particles and slowed down the drug release. Further *in vitro* investigations also revealed that free BODIPY is not able to penetrate the cell membrane, but BODIPY loaded and silica covered MIL-101 allowed the delivery of the imaging contrast reagent resulting in fluorescent labelling of HT-29 cells.[117] Metal organic frameworks that are based on paramagnetic metal ions might find application as contrast agents in magnetic resonance imaging (MRI). For that purpose, MOFs based on gadolinium[122,136–138] or manganese[123] are mainly considered. Contrast agents with high electron density and therefore high atomic numbers are applicable for X-ray computed tomography (CT) which is based on differences in X-ray attenuation. For that purpose, iodinated Cu- and Zn-MOFs as well as UiO-66 and its Hf-analogue have been tested as potential contrast agents for X-ray computed tomography (CT) imaging.[124,63] Regarding UiO-66(Zr) and

UiO-66(Hf), both MOFs seem to be applicable, although UiO-66(Hf) with the heavier Hf atoms revealed more encouraging results. To provide the MOF from degradation it is feasible to coat the particles with an amorphous silica layer, in this way making them also more biocompatible. Further functionalisation by grafting the surface with poly(ethylene glycol) (PEG) prevents protein adsorption and aggregation. In *in vivo* studies performed with this Hf-MOF@SiO$_2$@PEG accumulation occurred in liver and spleen, so that imaging of these organs is possible.[63]

Apart from the potential application for CT imaging, Zr-based MOFs were also investigated regarding the encapsulation of drugs like caffeine and ibuprofen in UiO-66 derivatives.[64] Thus, Zr-based MOFs have only rarely been investigated with regard to biomedical applications and only few examples were reported until today.

In the course of our research, first *in vitro* cell cytotoxicity tests were performed with the Zr-fumarate MOF. For this purpose, we have provided Zr-*fum* MOF particles of different sizes. The deep knowledge we had gained on different Zr-*fum* MOF synthesis systems during the course of this work (as described in sections 3.1, 3.2 and 3.3) allowed us the synthesis of nanoparticles of various sizes, a feat which has so far been proven possible for only few MOFs. The size of nanoparticles is, however, a crucial factor for biomedical applications, for example with regard to passage through cell layers as blood vessel walls or cellular uptake. To the best of our knowledge, no investigation concerning the cytotoxicity of MOFs dependent on their particle size has been reported.

In a recent investigation, fumaric acid was evaluated as a rather toxic linker (IC$_{50}$ = 0.03 mg·mL^{-1} concerning HeLa cells and IC$_{50}$ = 0.40 mg·mL^{-1} concerning J774 macrophages) in a study of several MOFs containing different metals and linkers.[139] However, these results are in contrast to *in vivo* studies of the fumarate-based MIL-88A[15,26] and are thus questionable. Besides, the combination of Zr^{4+} as metal ions and fumarate as linker has to be evaluated to figure out how the viability of different cells is influenced by the material. Due to the fact that we were able to synthesise the Zr-*fum* MOF with different particles sizes from DMF as well as from water-based systems, it was possible to consider the influence of the reaction conditions as well as the influence of the particle size. The cell culture tests were carried out in collaboration with JÖRN SCHAESKE (AG Prof. Dr. MEIKE STIESCH,

Clinic for Dental Prosthetics, Hannover Medical School), DOMINIK MÜLLER (AG Prof. Dr. KIRSTEN HAASTERT-TALINI, Institute of Neuroanatomy, Hannover Medical School), DENIZ ALI BÖLÜKBAS (AG PD Dr. SILKE MEINERS, Comprehensive Pneumology Center, Ludwig-Maximilians-Universität München) and KATHARINA FERKALJUK (AG Prof. Dr. ANGELIKA VOLLMAR, Faculty of Chemistry and Pharmacy, Pharmaceutical Biology, Ludwig-Maximilians-Universität München). First studies concerning the choice of solvent in the synthesis revealed good viability of the cells (gingival fibroblasts) over a wide range of concentration. The viability of the cells was examined by applying a MTT assay (MTT: 3-(4,5-dimethylthiazol-2-yl)-2,5-diphenyltetrazolium bromide).[140] Active mitochondria of living cells can convert the pale yellow cyclic molecule in the dark blue formazan. The colour change can be detected by UV/Vis spectroscopy. 100% metabolic activity corresponds to fibroblasts without any MOF contact. Surprisingly, none of the samples indicated any cytotoxicity effects, not even Zr-*fum* MOF synthesised from DMF. Thus, a standard washing procedure with ethanol seems to be sufficient to get rid of almost all DMF molecules. Particles that were synthesised in DMF and SOXHLET-extracted with ethanol after the synthesis revealed good results as well. In summary, the choice of solvent has no influence on the viability of gingiva fibroblasts. However, toxic solvents like DMF should generally be avoided in the preparation of biomedical devices.

In a further study, Zr-fumarate MOF was synthesised from aqueous systems under benign reaction conditions. With the help of the coordination modulation approach and by adjusting the reaction temperature, three different particle sizes of Zr-*fum* MOF were obtained (Figure 26).
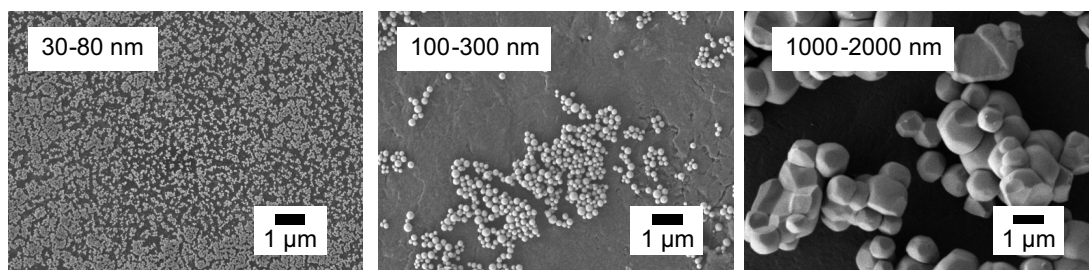

Figure 26. SEM micrographs of Zr-fumarate MOF synthesised from aqueous systems. By adjusting the reaction conditions small (left), medium (center) and large (right) particles could be obtained.

All *Zr-fum* MOF syntheses were carried out in water in Teflon-capped glass vials without stirring. For the standard synthesis, $ZrCl_4$ (0.517 mmol, 1 eq) was dissolved in 10 mL water and various amounts of modulator formic acid (70 or 90 eq, respectively, with regard to $ZrCl_4$) as well as fumaric acid (1.550 mmol, 3 eq) as linker molecule were added. All chemicals were obtained commercially from Sigma-Aldrich and were used without further purification. To synthesise small particles (Figure 26, left), 70 eq of formic acid were used and the synthesis mixture was heated for 2 h at 100 °C. By decreasing the reaction temperature to room temperature (varying between 19 °C and 25 °C during the synthesis) medium and large particles were obtained with 70 eq and 90 eq of formic, respectively, with a prolonged reaction time of one week. After the reaction, the precipitates were collected by centrifugation and washed with sterile water (Ampuwa® Spüllösung, Plastipur) and ethanol. After the washing procedure, the purified samples were suspended immediately in sterile water using sonification (Branson S-450D digital ultrasonic processor for 2 min with approx. 20% power) to avoid particle agglomeration. After the determination of the particle concentration by drying 5 ml of the suspension, the suspensions were diluted with sterile water for cell culture studies.

The *in vitro* cell tests with *Zr-fum* MOF samples started simultaneously in all collaborating groups. The metabolic activity of the cells was assessed by applying the MTT,[140] WST-1,[141] or LDH assay.[142] All these assays are based on the reduction of a tetrazolium ring to formazan induced by enzymatic reaction of active mitochondria. The conversion of (3-(4,5-dimethylethiazol-2-yl)-2,5-diphenyl tetrazolium bromide (MTT) to formazan causes a colour change that can be detected photometrically. In comparison to the MTT assay, the WST assay is performed with a water soluble tetrazolium salt (WST, 4-[3-(4-iodophenyl)-2-(4-nitrophenyl)-2*H*-5-tetrazolio]-1,3-benzene disulfonate). Another approach to evaluate the viability of cells is to measure the lactate dehydrogenase (LDH) content that is released from damaged cell membranes of dead cells. Several induced oxidation and reduction processes lead to an electron transfer so that finally the tetrazolium ring of iodonitrotetrazolium is converted into formazan. Fortunately, all cell culture test that were performed with different cell lines (MLE12 mouse lung epithelial cells, MHS mouse lung macrophages, SCHWANN cells and gingival fibroblasts) showed very good viability in a wide concentration range of 12.5–100 µg·mL⁻¹, independent of the particle size. Only very high concentrations of MOFs of 200 µg·mL⁻¹ exhibited a

decreased metabolic activity of 20–60% except for gingiva fibroblasts that also show a good viability at such a high concentration (Figure 27).
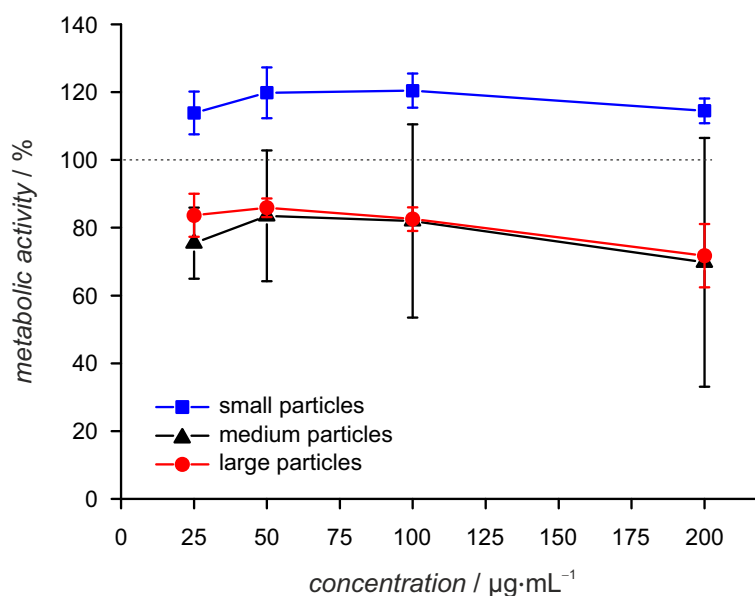
Figure 27. Metabolic activity of gingival fibroblasts as a function of Zr-fumarate MOF concentration. Zr-*fum* MOFs were provided with different particle sizes. Cell culture tests were performed by JÖRN SCHAESKE (Hannover Medical School).

Further tests carried out with HMECs and HUVECs revealed neither damages of the cytoskeleton nor inflammations reactions caused by the MOFs, respectively.

These results are currently being compiled into a manuscript which will describe cytotoxicity evaluations of the Zr-*fum* MOF compound with a variety of different cell lines.

References

(1)   Cho, K.; Wang, X.; Nie, S.; Chen, Z. G.; Shin, D. M. *Clin. Cancer Res.* **2008**, *14*, 1310–1316.

(2)   Kaneda, Y. *Adv. Drug Deliv. Rev.* **2000**, *43*, 197–205.

(3)   Soppimath, K. S.; Aminabhavi, T. M.; Kulkarni, A. R.; Rudzinski, W. E. *J. Control. Release* **2001**, *70*, 1–20.

(4)   Vallet-Regí, M.; Balas, F.; Arcos, D. *Angew. Chem. Int. Ed.* **2007**, *46*, 7548–7558.

(5)   Mamaeva, V.; Sahlgren, C.; Lindén, M. *Adv. Drug Deliv. Rev.* **2013**, *65*, 689–702.

(6)   Popat, A.; Hartono, S. B.; Stahr, F.; Liu, J.; Qiao, S. Z.; Lu, G. Q. M. *Nanoscale* **2011**, *3*, 2801–2818.

(7)   Wu, S.-H.; Hung, Y.; Mou, C.-Y. *Chem. Commun.* **2011**, *47*, 9972–9985.

(8)   Cavka, J. H.; Jakobsen, S.; Olsbye, U.; Guillou, N.; Lamberti, C.; Bordiga, S.; Lillerud, K. P. *J. Am. Chem. Soc.* **2008**, *130*, 13850–13851.

(9)   Lee, D. B. N.; Roberts, M.; Bluchel, C. G.; Odell, R. A. *ASAIO J.* **2010**, *56*, 550–556.

(10)   Sollazzo, V.; Pezzetti, F.; Scarano, A.; Piattelli, A.; Bignozzi, C. A.; Massari, L.; Brunelli, G.; Carinci, F. *Dent. Mater.* **2008**, *24*, 357–361.

(11)   Nothdurft, F. P.; Merker, S.; Pospiech, P. R. *Clin. Oral Investig.* **2011**, *15*, 89–97.

(12)   Díaz, A.; David, A.; Pérez, R.; González, M. L.; Báez, A.; Wark, S. E.; Zhang, P.; Clearfield, A.; Colón, J. L. *Biomacromolecules* **2010**, *11*, 2465–2470.

(13)   Zlotkin, S.; Arthur, P.; Antwi, K. Y.; Yeung, G. *Am. Soc. Clin. Nutr.* **2001**, *74*, 791–795.

(14)   Erichsen, K.; Ulvik, R. J.; Nysaeter, G.; Johansen, J.; Ostborg, J.; Berstad, A.; Berge, R. K.; Hausken, T. *Scand. J. Gastroenterol.* **2005**, *40*, 1058–1065.

(15)   Baati, T.; Njim, L.; Neffati, F.; Kerkeni, A.; Bouttemi, M.; Gref, R.; Najjar, M. F.; Zakhama, A.; Couvreur, P.; Serre, C.; Horcajada, P. *Chem. Sci.* **2013**, *4*, 1597–1607.

(16)   Gaab, M.; Trukhan, N.; Maurer, S.; Gummaraju, R.; Müller, U. *Microporous Mesoporous Mater.* **2012**, *157*, 131–136.

(17)   Diring, S.; Furukawa, S.; Takashima, Y.; Tsuruoka, T.; Kitagawa, S. *Chem. Mater.* **2010**, *22*, 4531–4538.

(18) Tsuruoka, T.; Furukawa, S.; Takashima, Y.; Yoshida, K.; Isoda, S.; Kitagawa, S. *Angew. Chem. Int. Ed.* **2009**, *48*, 4739–4743.

(19) Wißmann, G.; Schaate, A.; Lilienthal, S.; Bremer, I.; Schneider, A. M.; Behrens, P. *Microporous Mesoporous Mater.* **2012**, *152*, 64–70.

(20) Zahn, G.; Schulze, H. A.; Lippke, J.; König, S.; Sazama, U.; Fröba, M.; Behrens, P. *Microporous Mesoporous Mater.* **2015**, *203*, 186–194.

(21) Zahn, G.; Zerner, P.; Lippke, J.; Kempf, F. L.; Lilienthal, S.; Schröder, C. A.; Schneider, A. M.; Behrens, P. *CrystEngComm* **2014**, *16*, 9198–9207.

(22) Yaghi, O. M.; Li, H. *J. Am. Chem. Soc.* **1995**, *117*, 10401–10402.

(23) Li, J.-R.; Kuppler, R. J.; Zhou, H.-C. *Chem. Soc. Rev.* **2009**, *38*, 1477–1504.

(24) Liu, J.; Chen, L.; Cui, H.; Zhang, J.; Zhang, L.; Su, C.-Y. *Chem. Soc. Rev.* **2014**, 6011–6061.

(25) Mason, J. A.; Veenstra, M.; Long, J. R. *Chem. Sci.* **2014**, *5*, 32–51.

(26) Horcajada, P.; Chalati, T.; Serre, C.; Gillet, B.; Sebrie, C.; Baati, T.; Eubank, J. F.; Heurtaux, D.; Clayette, P.; Kreuz, C.; Chang, J.-S.; Hwang, Y. K.; Marsaud, V.; Bories, P.-N.; Cynober, L.; Gil, S.; Férey, G.; Couvreur, P.; Gref, R. *Nat. Mater.* **2010**, *9*, 172–178.

(27) Horcajada, P.; Serre, C.; Maurin, G.; Ramsahye, N. A.; Balas, F.; Vallet-Regí, M.; Sebban, M.; Taulelle, F.; Férey, G. *J. Am. Chem. Soc.* **2008**, *130*, 6774–6780.

(28) Horcajada, P.; Serre, C.; Vallet-Regí, M.; Sebban, M.; Taulelle, F.; Férey, G. *Angew. Chem. Int. Ed.* **2006**, *45*, 5974–5978.

(29) Chui, S. S. *Science* **1999**, *283*, 1148–1150.

(30) Surblé, S.; Serre, C.; Mellot-Draznieks, C.; Millange, F.; Férey, G. *Chem. Commun.* **2006**, 284–286.

(31) Li, H.; Eddaoudi, M.; O'Keeffe, M.; Yaghi, O. M. *Nature* **1999**, *402*, 276–279.

(32) Bon, V.; Senkovskyy, V.; Senkovska, I.; Kaskel, S. *Chem. Commun.* **2012**, *48*, 8407–8409.

(33) Furukawa, H.; Gándara, F.; Zhang, Y.-B.; Jiang, J.; Queen, W. L.; Hudson, M. R.; Yaghi, O. M. *J. Am. Chem. Soc.* **2014**, *136*, 4369–4381.

(34) Furukawa, H.; Cordova, K. E.; O'Keeffe, M.; Yaghi, O. M. *Science* **2013**, *341*, 1230444.

(35) Lu, W.; Wei, Z.; Gu, Z.-Y.; Liu, T.-F.; Park, J.; Park, J.; Tian, J.; Zhang, M.; Zhang, Q.; Gentle Iii, T.; Bosch, M.; Zhou, H.-C. *Chem. Soc. Rev.* **2014**, 5561–5593.

(36) O'Keeffe, M.; Yaghi, O. M. *Chem. Rev.* **2012**, *112*, 675–702.

(37) Eddaoudi, M.; Kim, J.; Rosi, N.; Vodak, D.; Wachter, J.; O'Keeffe, M.; Yaghi, O. M. *Science* **2002**, *295*, 469–472.

(38) Cravillon, J.; Schröder, C. A.; Bux, H.; Rothkirch, A.; Caro, J.; Wiebcke, M. *CrystEngComm* **2012**, *14*, 492–498.

(39) Wu, H.; Chua, Y. S.; Krungleviciute, V.; Tyagi, M.; Chen, P.; Yildirim, T.; Zhou, W. *J. Am. Chem. Soc.* **2013**, *135*, 10525–10532.

(40) Vermoortele, F.; Bueken, B.; Le Bars, G.; Van de Voorde, B.; Vandichel, M.; Houthoofd, K.; Vimont, A.; Daturi, M.; Waroquier, M.; Van Speybroeck, V.; Kirschhock, C.; De Vos, D. E. *J. Am. Chem. Soc.* **2013**, *135*, 11465–11468.

(41) Bon, V.; Senkovska, I.; Baburin, I. A.; Kaskel, S. *Cryst. Growth Des.* **2013**, *13*, 1231–1237.

(42) Bon, V.; Senkovska, I.; Weiss, M. S.; Kaskel, S. *CrystEngComm* **2013**, *15*, 9572.

(43) Kickelbick, G.; Schubert, U. *Chem. Ber.* **1997**, *130*, 473–478.

(44) Kickelbick, G.; Wiede, P.; Schubert, U. *Inorg. Chim. Acta* **1999**, *284*, 1–7.

(45) Kogler, F. R.; Jupa, M.; Puchberger, M.; Schubert, U. *J. Mater. Chem.* **2004**, *14*, 3133.

(46) Puchberger, M.; Kogler, F. R.; Jupa, M.; Gross, S.; Fric, H.; Kickelbick, G.; Schubert, U. *Eur. J. Inorg. Chem.* **2006**, 3283–3293.

(47) Wu, H.; Yildirim, T.; Zhou, W. *J. Phys. Chem. Lett.* **2013**, *4*, 925–930.

(48) Abid, H. R.; Tian, H.; Ang, H.-M.; Tade, M. O.; Buckley, C. E.; Wang, S. *Chem. Eng. J.* **2012**, *187*, 415–420.

(49) Yang, Q.; Vaesen, S.; Ragon, F.; Wiersum, A. D.; Wu, D.; Lago, A.; Devic, T.; Martineau, C.; Taulelle, F.; Llewellyn, P. L.; Jobic, H.; Zhong, C.; Serre, C.; De Weireld, G.; Maurin, G. *Angew. Chem. Int. Ed.* **2013**, *52*, 10316–10320.

(50) Chavan, S.; Vitillo, J. G.; Gianolio, D.; Zavorotynska, O.; Civalleri, B.; Jakobsen, S.; Nilsen, M. H.; Valenzano, L.; Lamberti, C.; Lillerud, K. P.; Bordiga, S. *Phys. Chem. Chem. Phys.* **2012**, *14*, 1614–1626.

(51) Ren, J.; Langmi, H. W.; North, B. C.; Mathe, M.; Bessarabov, D. *Int. J. Hydrogen Energy* **2014**, *39*, 890–895.

(52)   Jeremias, F.; Lozan, V.; Henninger, S. K.; Janiak, C. *Dalton Trans.* **2013**, *42*, 15967–15973.

(53)   Schoenecker, P. M.; Carson, C. G.; Jasuja, H.; Flemming, C. J. J.; Walton, K. S. *Ind. Eng. Chem. Res.* **2012**, *51*, 6513–6519.

(54)   Yang, Q.; Wiersum, A. D.; Jobic, H.; Guillerm, V.; Serre, C.; Llewellyn, P. L.; Maurin, G. *J. Phys. Chem. C* **2011**, *115*, 13768–13774.

(55)   Bárcia, P. S.; Guimarães, D.; Mendes, P. A. P.; Silva, J. A. C.; Guillerm, V.; Chevreau, H.; Serre, C.; Rodrigues, A. E. *Microporous Mesoporous Mater.* **2011**, *139*, 67–73.

(56)   Duerinck, T.; Denayer, J. F. M. *Adsorption* **2013**, *20*, 251–259.

(57)   Katz, M. J.; Mondloch, J. E.; Totten, R. K.; Park, J. K.; Nguyen, S. T.; Farha, O. K.; Hupp, J. T. *Angew. Chem. Int. Ed.* **2014**, *53*, 497–501.

(58)   Gomes Silva, C.; Luz, I.; Llabrés i Xamena, F. X.; Corma, A.; García, H. *Chemistry* **2010**, *16*, 11133–11138.

(59)   Shen, L.; Wu, W.; Liang, R.; Lin, R.; Wu, L. *Nanoscale* **2013**, *5*, 9374–9382.

(60)   Vermoortele, F.; Ameloot, R.; Vimont, A.; Serre, C.; De Vos, D. *Chem. Commun.* **2011**, *47*, 1521–1523.

(61)   Vermoortele, F.; Vandichel, M.; Van de Voorde, B.; Ameloot, R.; Waroquier, M.; Van Speybroeck, V.; De Vos, D. E. *Angew. Chem. Int. Ed.* **2012**, *51*, 4887–4890.

(62)   Fei, H.; Cohen, S. M. *Chem. Commun.* **2014**, *50*, 4810–4812.

(63)   deKrafft, K. E.; Boyle, W. S.; Burk, L. M.; Zhou, O. Z.; Lin, W. *J. Mater. Chem.* **2012**, *22*, 18139–18144.

(64)   Cunha, D.; Gaudin, C.; Colinet, I.; Horcajada, P.; Maurin, G.; Serre, C. *J. Mater. Chem. B* **2013**, *1*, 1101–1108.

(65)   Schaate, A.; Roy, P.; Godt, A.; Lippke, J.; Waltz, F.; Wiebcke, M.; Behrens, P. *Chem. Eur. J.* **2011**, *17*, 6643–6651.

(66)   Wang, C.; Volotskova, O.; Lu, K.; Ahmad, M.; Sun, C.; Xing, L.; Lin, W. *J. Am. Chem. Soc.* **2014**, *136*, 6171–6174.

(67)   Guillerm, V.; Gross, S.; Serre, C.; Devic, T.; Bauer, M.; Férey, G. *Chem. Commun.* **2010**, *46*, 767–769.

(68)   Bueken, B.; Reinsch, H.; Reimer, N.; Stassen, I.; Vermoortele, F.; Ameloot, R.; Stock, N.; Kirschhock, C. E. A.; De Vos, D. E. *Chem. Commun.* **2014**, *50*, 10055–10058.

(69)   Manna, K.; Zhang, T.; Carboni, M.; Abney, C. W.; Lin, W. *J. Am. Chem. Soc.*
       2014, *136*, 13182–13185.

(70)   Garibay, S. J.; Cohen, S. M. *Chem. Commun.* **2010**, *46*, 7700–7702.

(71)   Kandiah, M.; Nilsen, M. H.; Usseglio, S.; Jakobsen, S.; Olsbye, U.; Tilset, M.;
       Larabi, C.; Quadrelli, E. A.; Bonino, F.; Lillerud, K. P. *Chem. Mater.* **2010**,
       22, 6632–6640.

(72)   Jasuja, H.; Zang, J.; Sholl, D. S.; Walton, K. S. *J. Phys. Chem. C* **2012**, *116*,
       23526–23532.

(73)   Biswas, S.; Van Der Voort, P. *Eur. J. Inorg. Chem.* **2013**, 2154–2160.

(74)   Kim, M.; Cahill, J. F.; Su, Y.; Prather, K. A.; Cohen, S. M. *Chem. Sci.* **2012**,
       3, 126–130.

(75)   Lin Foo, M.; Horike, S.; Fukushima, T.; Hijikata, Y.; Kubota, Y.; Takata, M.;
       Kitagawa, S. *Dalton Trans.* **2012**, *41*, 13791–13794.

(76)   Biswas, S.; Zhang, J.; Li, Z.; Liu, Y.-Y.; Grzywa, M.; Sun, L.; Volkmer, D.;
       Van Der Voort, P. *Dalton Trans.* **2013**, *42*, 4730–4737.

(77)   Kim, M.; Garibay, S. J.; Cohen, S. M. *Inorg. Chem.* **2011**, *50*, 729–731.

(78)   Falkowski, J. M.; Sawano, T.; Zhang, T.; Tsun, G.; Chen, Y.; Lockard, J. V;
       Lin, W. *J. Am. Chem. Soc.* **2014**, *136*, 5213–5216.

(79)   Huang, Y.; Qin, W.; Li, Z.; Li, Y. *Dalton Trans.* **2012**, *41*, 9283–9285.

(80)   Zlotea, C.; Phanon, D.; Mazaj, M.; Heurtaux, D.; Guillerm, V.; Serre, C.;
       Horcajada, P.; Devic, T.; Magnier, E.; Cuevas, F.; Férey, G.; Llewellyn, P. L.;
       Latroche, M. *Dalton Trans.* **2011**, *40*, 4879–4881.

(81)   Katz, M. J.; Brown, Z. J.; Colón, Y. J.; Siu, P. W.; Scheidt, K. A.; Snurr, R.
       Q.; Hupp, J. T.; Farha, O. K. *Chem. Commun.* **2013**, *49*, 9449–9451.

(82)   Cmarik, G. E.; Kim, M.; Cohen, S. M.; Walton, K. S. *Langmuir* **2012**, *28*,
       15606–15613.

(83)   Schaate, A.; Roy, P.; Preusse, T.; Lohmeier, S. J.; Godt, A.; Behrens, P. *Chem.
       Eur. J.* **2011**, *17*, 9320–9325.

(84)   Morris, W.; Volosskiy, B.; Demir, S.; Gándara, F.; McGrier, P. L.; Furukawa,
       H.; Cascio, D.; Stoddart, J. F.; Yaghi, O. M. *Inorg. Chem.* **2012**, *51*, 6443–
       6445.

(85)   Feng, D.; Gu, Z.-Y.; Li, J.-R.; Jiang, H.-L.; Wei, Z.; Zhou, H.-C. *Angew.
       Chem. Int. Ed.* **2012**, *51*, 10307–10310.

(86)   DeCoste, J. B.; Peterson, G. W.; Jasuja, H.; Glover, T. G.; Huang, Y.; Walton,
       K. S. *J. Mater. Chem. A* **2013**, *1*, 5642–5650.

(87)   Schaate, A.; Dühnen, S.; Platz, G.; Lilienthal, S.; Schneider, A. M.; Behrens, P. *Eur. J. Inorg. Chem.* **2012**, *2012*, 790–796.

(88)   Mondloch, J. E.; Bury, W.; Fairen-Jimenez, D.; Kwon, S.; DeMarco, E. J.; Weston, M. H.; Sarjeant, A. A.; Nguyen, S. T.; Stair, P. C.; Snurr, R. Q.; Farha, O. K.; Hupp, J. T. *J. Am. Chem. Soc.* **2013**, *135*, 10294–10297.

(89)   Kim, M.; Cahill, J. F.; Fei, H.; Prather, K. A.; Cohen, S. M. *J. Am. Chem. Soc.* **2012**, *134*, 18082–18088.

(90)   Mondloch, J. E.; Katz, M. J.; Planas, N.; Semrouni, D.; Gagliardi, L.; Hupp, J. T.; Farha, O. K. *Chem. Commun.* **2014**, *50*, 8944–8946.

(91)   Shearer, G. C.; Chavan, S.; Ethiraj, J.; Vitillo, J. G.; Svelle, S.; Olsbye, U.; Lamberti, C.; Bordiga, S.; Lillerud, K. P. *Chem. Mater.* **2014**, *26*, 4068–4071.

(92)   Valenzano, L.; Civalleri, B.; Chavan, S.; Bordiga, S.; Nilsen, M. H.; Jakobsen, S.; Lillerud, K. P.; Lamberti, C. *Chem. Mater.* **2011**, *23*, 1700–1718.

(93)   Wiersum, A. D.; Soubeyrand-Lenoir, E.; Yang, Q.; Moulin, B.; Guillerm, V.; Yahia, M. Ben; Bourrelly, S.; Vimont, A.; Miller, S.; Vagner, C.; Daturi, M.; Clet, G.; Serre, C.; Maurin, G.; Llewellyn, P. L. *Chem. Asian J.* **2011**, *6*, 3270–3280.

(94)   Ameloot, R.; Aubrey, M.; Wiers, B. M.; Gómora-Figueroa, A. P.; Patel, S. N.; Balsara, N. P.; Long, J. R. *Chemistry* **2013**, *19*, 5533–5536.

(95)   Kandiah, M.; Usseglio, S.; Svelle, S.; Olsbye, U.; Lillerud, K. P.; Tilset, M. *J. Mater. Chem.* **2010**, *20*, 9848–9851.

(96)   Xydias, P.; Spanopoulos, I.; Klontzas, E.; Froudakis, G. E.; Trikalitis, P. N. *Inorg. Chem.* **2014**, *53*, 679–681.

(97)   Øien, S.; Wragg, D.; Reinsch, H.; Svelle, S.; Bordiga, S.; Lamberti, C.; Lillerud, K. P. *Cryst. Growth Des.* **2014**, 141003125543007.

(98)   Yang, Q.; Guillerm, V.; Ragon, F.; Wiersum, A. D.; Llewellyn, P. L.; Zhong, C.; Devic, T.; Serre, C.; Maurin, G. *Chem. Commun.* **2012**, *48*, 9831–9833.

(99)   Roy, P.; Schaate, A.; Behrens, P.; Godt, A. *Chem. Eur. J.* **2012**, *18*, 6979–6985.

(100) Guillerm, V.; Ragon, F.; Dan-Hardi, M.; Devic, T.; Vishnuvarthan, M.; Campo, B.; Vimont, A.; Clet, G.; Yang, Q.; Maurin, G.; Férey, G.; Vittadini, A.; Gross, S.; Serre, C. *Angew. Chem. Int. Ed.* **2012**, *51*, 9267–9271.

(101) Ezquerra, T. A.; García-Gutiérrez, M.; Nogales, A.; Gómez, M. *Applications of Synchrotron Light to Scattering and Diffraction in Materials and Life Science*; Springer-Verlag: Berlin Heidelberg, 2009.

(102) Willmott, P. *An Introduction to Synchrotron Radiation - Techniques and Applications*; John Wiley and Sons, Ldt: Chichester, West Sussex, 2011.

(103) Kunz, C. *Synchrotron Radiation - Techniques and Applications*; Springer-Verlag: Berlin Heidelberg New York, 1979.

(104) Catlow, C. R. A.; Greaves, G. N. *Applications of Synchrotron Radiation*; Blackie and Son Ltd: Glasgow London, 1990.

(105) Horcajada, P.; Gref, R.; Baati, T.; Allan, P. K.; Maurin, G.; Couvreur, P.; Férey, G.; Morris, R. E.; Serre, C. *Chem. Rev.* **2012**, *112*, 1232–1268.

(106) Xiao, B.; Wheatley, P. S.; Zhao, X.; Fletcher, A. J.; Fox, S.; Rossi, A. G.; Megson, I. L.; Bordiga, S.; Regli, L.; Thomas, K. M.; Morris, R. E. *J. Am. Chem. Soc.* **2007**, *129*, 1203–1209.

(107) McKinlay, A. C.; Xiao, B.; Wragg, D. S.; Wheatley, P. S.; Megson, I. L.; Morris, R. E. *J. Am. Chem. Soc.* **2008**, *130*, 10440–10444.

(108) Hinks, N. J.; McKinlay, A. C.; Xiao, B.; Wheatley, P. S.; Morris, R. E. *Microporous Mesoporous Mater.* **2010**, *129*, 330–334.

(109) Nguyen, J. G.; Tanabe, K. K.; Cohen, S. M. *CrystEngComm* **2010**, *12*, 2335–2338.

(110) Gaudin, C.; Cunha, D.; Ivanoff, E.; Horcajada, P.; Chevé, G.; Yasri, A.; Loget, O.; Serre, C.; Maurin, G. *Microporous Mesoporous Mater.* **2012**, *157*, 124–130.

(111) Agostoni, V.; Chalati, T.; Horcajada, P.; Willaime, H.; Anand, R.; Semiramoth, N.; Baati, T.; Hall, S.; Maurin, G.; Chacun, H.; Bouchemal, K.; Martineau, C.; Taulelle, F.; Couvreur, P.; Rogez-Kreuz, C.; Clayette, P.; Monti, S.; Serre, C.; Gref, R. *Adv. Healthc. Mater.* **2013**, *2*, 1630–1637.

(112) Chalati, T.; Horcajada, P.; Couvreur, P.; Serre, C.; Ben Yahia, M.; Maurin, G.; Gref, R. *Nanomedicine* **2011**, *6*, 1683–1695.

(113) Imaz, I.; Rubio-Martínez, M.; García-Fernández, L.; García, F.; Ruiz-Molina, D.; Hernando, J.; Puntes, V.; Maspoch, D. *Chem. Commun.* **2010**, *46*, 4737–4739.

(114) Zhuang, J.; Kuo, C.-H.; Chou, L.-Y.; Liu, D.-Y.; Weerapana, E.; Tsung, C.-K. *ACS Nano* **2014**, *8*, 2812–2819.

(115) Ke, F.; Yuan, Y.-P.; Qiu, L.-G.; Shen, Y.-H.; Xie, A.-J.; Zhu, J.-F.; Tian, X.-Y.; Zhang, L.-D. *J. Mater. Chem.* **2011**, *21*, 3843–3848.

(116) Di Nunzio, M. R.; Agostoni, V.; Cohen, B.; Gref, R.; Douhal, A. *J. Med. Chem.* **2014**, *57*, 411–420.

(117) Taylor-Pashow, K. M. L.; Della Rocca, J.; Xie, Z.; Tran, S.; Lin, W. *J. Am. Chem. Soc.* **2009**, *131*, 14261–14263.

(118) Rieter, W. J.; Pott, K. M.; Taylor, K. M. L.; Lin, W. *J. Am. Chem. Soc.* **2008**, *130*, 11584–11585.

(119)   Sun, C.-Y.; Qin, C.; Wang, X.-L.; Yang, G.-S.; Shao, K.-Z.; Lan, Y.-Q.; Su,
        Z.-M.; Huang, P.; Wang, C.-G.; Wang, E.-B. *Dalton Trans.* **2012**, *41*, 6906–
        6909.

(120)   Kundu, T.; Mitra, S.; Patra, P.; Goswami, A.; Díaz Díaz, D.; Banerjee, R.
        Chemistry **2014**, *20*, 10514–10518.

(121)   Liu, D.; Lu, K.; Poon, C.; Lin, W. *Inorg. Chem.* **2014**, *53*, 1916–1924.

(122)   Taylor, K. M. L.; Jin, A.; Lin, W. *Angew. Chem. Int. Ed.* **2008**, *47*, 7722–
        7725.

(123)   Taylor, K. M. L.; Rieter, W. J.; Lin, W. *J. Am. Chem. Soc.* **2008**, *130*, 14358–
        14359.

(124)   deKrafft, K. E.; Xie, Z.; Cao, G.; Tran, S.; Ma, L.; Zhou, O. Z.; Lin, W.
        Angew. Chem. Int. Ed. **2009**, *48*, 9901–9904.

(125)   Liu, D.; Huxford, R. C.; Lin, W. *Angew. Chem. Int. Ed.* **2011**, *50*, 3696–3700.

(126)   An, J.; Geib, S. J.; Rosi, N. L. *J. Am. Chem. Soc.* **2009**, *131*, 8376–8377.

(127)   An, J.; Farha, O. K.; Hupp, J. T.; Pohl, E.; Yeh, J. I.; Rosi, N. L. *Nat. commun.*
        2012, *3*, 1–6.

(128)   Miller, S. R.; Heurtaux, D.; Baati, T.; Horcajada, P.; Grenèche, J.-M.; Serre,
        C. *Chem. Commun.* **2010**, *46*, 4526–4528.

(129)   Miller, S. R.; Horcajada, P.; Serre, C. *CrystEngComm* **2011**, *13*, 1894–1898.

(130)   Bernini, M. C.; Fairen-Jimenez, D.; Pasinetti, M.; Ramirez-Pastor, A. J.;
        Snurr, R. Q. *J. Mater. Chem. B* **2014**, *2*, 766–774.

(131)   Horcajada, P.; Serre, C.; Férey, G.; Couvreur, P.; Gref, R. *Médecine Sci.* **2010**,
        26, 761–767.

(132)   Babarao, R.; Jiang, J. *J. Phys. Chem. C* **2009**, *113*, 18287–18291.

(133)   Serre, C.; Millange, F.; Thouvenot, C.; Noguès, M.; Marsolier, G.; Louër, D.;
        Férey, G. *J. Am. Chem. Soc.* **2002**, *124*, 13519–13526.

(134)   Di Nunzio, M. R.; Agostoni, V.; Cohen, B.; Gref, R.; Douhal, A. *J. Med.
        Chem.* **2014**, *57*, 411–420.

(135)   Vasconcelos, I. B.; da Silva, T. G.; Militão, G. C. G.; Soares, T. A.;
        Rodrigues, N. M.; Rodrigues, M. O.; da Costa, N. B.; Freire, R. O.; Junior, S.
        A. *RSC Adv.* **2012**, *2*, 9437–9442.

(136)   Rieter, W. J.; Taylor, K. M. L.; An, H.; Lin, W.; Lin, W. *J. Am. Chem. Soc.*
        2006, *128*, 9024–9025.

(137) Rowe, M. D.; Thamm, D. H.; Kraft, S. L.; Boyes, S. G. *Biomacromolec.* **2009**, *10*, 983–993.

(138) Rieter, W. J.; Taylor, K. M. L.; Lin, W. *J. Am. Chem. Soc.* **2007**, *129*, 9852–9853.

(139) Tamames-Tabar, C.; Cunha, D.; Imbuluzqueta, E.; Ragon, F.; Serre, C.; Blanco-Prieto, M. J.; Horcajada, P. *J. Mater. Chem. B* **2014**, *2*, 262–271.

(140) Mosmann, T. *J. Immunol. Methods* **1983**, *65*, 55–63.

(141) Ishiyama, M.; Shiga, M.; Sasamoto, K.; Mizoguchi, M.; He, P. *Chem. Pharm. Bull.* **1993**, *41*, 1118–1122.

(142) Decker, T.; Lohmann-Matthes, M. L. *J. Immunol. Methods* **1988**, *115*, 61–69.

3   Results and Discussion

3.1   Modulated Synthesis of Zr-fumarate MOF

Gesa Wißmann, Andreas Schaate, Sebastian Lilienthal, Imke Bremer, Andreas M. Schneider, Peter Behrens

The final publication is available at
http://www.sciencedirect.com/science/article/pii/S1387181111005956

Preface

The following work "Modulated synthesis of Zr-fumarate MOF" was published as full paper in the Journal *Microporous and Mesoporous Materials* in 2012. In this publication, the synthesis and the properties of a new Zr-based MOF from a DMF-based system are given. By choosing fumarate as organic bridging ligand, a biologically occurring molecule is introduced making this material interesting for biomedical applications. Basis of the success in the synthesis of the novel Zr-fumarate MOF was the application of the so called modulation approach, originally investigated by the group of KITAGAWA.[1,2] By adding only small amounts of formic acid as modulator, the crystallinity was enhanced and even the particle size could be adjusted. An increase of formic acid entailed a higher crystallinity as well as larger, less aggregated particles. Whereas Dr. ANDREAS SCHAATE provided the material first, the author of this thesis investigated the synthesis of this material in detail, especially with regard to the influence of formic acid on the crystallinity and the particle size, and tested with regard to thermal stability and chemical stability towards various solvents. The corresponding SEM images were obtained with the help of Dr. IMKE BREMER, Dr. BRITTA HERING und Dr. FLORIAN WALTZ. Sorption measurements performed by GEORG PLATZ revealed a micropore system that can be activated via SOXHLET-extraction and drying under reduced pressure. Unfortunately, we did not obtain single crystals for a structure refinement. Thus, the structure was obtained based on powder diffraction data and computational modelling by SEBASTIAN LILIENTHAL under the guidance of Dr. ANDREAS M. SCHNEIDER. Prof. Dr. PETER BEHRENS initiated and guided this study. The author of this thesis wrote the initial manuscript and refined it together with Prof. Dr. PETER BEHRENS.

[1] Diring, S.; Furukawa, S.; Takashima, Y.; Tsuruoka, T.; Kitagawa, S. *Chem. Mater.* **2010**, *22*, 4531−4538.

[2] Tsuruoka, T.; Furukawa, S.; Takashima, Y.; Yoshida, K.; Isoda, S.; Kitagawa, S. *Angew. Chem. Int. Ed.* **2009**, *48*, 4739−4743.
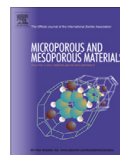
Modulated synthesis of Zr-fumarate MOF

Gesa Wißmann [1], Andreas Schaate [1], Sebastian Lilienthal [1], Imke Bremer [1], Andreas M. Schneider [1], Peter Behrens *,[1]

Leibniz Universität Hannover, Institut für Anorganische Chemie, Callinstr. 9, 30167 Hannover, Germany

ARTICLE INFO

ABSTRACT

We present the synthesis and characterization of a novel Zr-based metal–organic framework (MOF) which contains fumarate (*fum*) dianions as linkers: $^-OOC–CH=CH–COO^-$. The synthesis of this MOF is possible only via modulation, i.e. by the addition of a monocarboxylic acid to the synthesis mixture. We have used formic acid as a modulator and have investigated its influence on the synthesis of the Zr-fumarate MOF in detail. The modulator improves the crystallinity of the material; varying its amounts, the crystal size and the degree of aggregation can be influenced. The novel MOF probably has a topology which is similar to that of UiO-66, but has a primitive cubic lattice instead of a face-centered one. A structural model in line with the experimental data is proposed. The Zr-*fum* MOF is further characterized by thermogravimetric analysis (TGA) and Ar sorption, showing that it can be activated and exhibits microporosity. The linker fumarate as well as the modulator formic acid used in the synthesis of Zr-*fum* MOF are both naturally occurring molecules; possible applications of the MOF may thus lie in the field of biomaterials. Therefore, the stability of Zr-*fum* MOF was tested in water-based salt solutions commonly used in biomedical research.

© 2011 Elsevier Inc. All rights reserved.

1. Introduction

Metal–organic frameworks (MOFs) or porous coordination polymers have emerged as a new class of crystalline porous materials [1]. These compounds are constructed from metal ions or metal ion clusters and bridging organic linkers and often have very high surface areas [2,3]. The pore size can be engineered via the length of the linkers [4,5] and the chemistry of the pore interior can be designed by the functionalities these linkers carry [6]. Potential applications of porous MOFs cover a broad range from adsorption and catalysis to biomaterials [7–10]. A major disadvantage of many MOFs is their limited stability with regard to water, oxygen, other chemicals and temperature. For example, some Zn^{2+}-based MOFs, including the archetype MOF-5, are prone to hydrolysis when stored in air at ambient temperature [11–16].

More stable MOFs have been described with the Zr^{4+} cation [17]. The first members of this class consisted of the series UiO-66 (with terephthalate as linker) [17,18], UiO-67 (with biphenyl dicarboxylate) and UiO-68 (with terphenyl dicarboxylate) [17]. These compounds are isostructural and feature an arrangement of secondary building units (SBUs) which is topologically equivalent to a cubic close-packing. Correspondingly, the SBUs are twelvefold connected with each other by the dicarboxylic acids.

An SBU itself is constructed of six zirconium cations forming an octahedron. Each Zr ion is coordinated in a square–antiprismatic geometry by bridging $\mu_3–O$, $\mu_3–OH$ and carboxylate groups. Such Zr-oxo-hydroxo clusters, saturated by monocarboxylate ligands in their periphery, had been described before as isolated molecules [19,20]. In fact, Guillerm et al. used the methacrylate-terminated cluster $Zr_6O_4(OH)_4(maa)_{12}$ (*maa*: $CH_2=CH(CH_3)COO^-$) as a reagent for the synthesis of UiO-66 and an isostructural MOF possessing the muconic acid dianion as linker [21]. Recently, we have described a novel family of Zr-based MOFs containing very long linkers [22]. The structure of this family corresponds to a twofold interpenetrated version of the UiO-type topology. This can be understood with respect to the very long linkers used in their construction. In spite of the interpenetration, these compounds possess high surface areas and large pore volumes, and have therefore been named "porous interpenetrated Zr-organic frameworks" (PIZOFs) [22].

UiO-66 and the PIZOFs are highly temperature resistant and can be handled at atmospheric moisture [17,18]. The enhanced stability of Zr-based MOFs can be traced back to strong Zr–O bonds within the characteristic SBU which is present in all the described Zr-MOFs and to the high degree of interlinking of these SBUs. Further research in this class of MOFs thus appears worthwhile, and reports on the utility of some Zr-MOFs with the UiO-66 topology have recently appeared [23–26].

We have experienced difficulties in the synthesis of some of these MOFs. However, the modulation approach, originally

---

introduced by the group of Kitagawa [27,28], helped us tremendously. This approach consists in the addition of monovalent modulator molecules, in this case monocarboxylic acids, to the reaction mixture. It enhances the reproducibility of the synthesis procedures, allows to increase the crystallinity of the product and in certain cases to control the crystal size and morphology as well as the degree of agglomeration/aggregation of the crystals [27–29]. In case of the synthesis of UiO-66, we were able to vary the size of individual nanocrystals by the addition of benzoic acid as a modulator [29]. In the case of UiO-67, we were not able to reproduce the original synthesis procedure [17]; with the addition of a modulator, the synthesis proved to be highly reproducible and individual micrometer-sized crystals were obtained [29]. Whereas we have never been able to synthesize UiO-68 due to the persistent insolubility of terphenylene dicarboxylic acid in common solvents, we were able to produce an analogous compound, UiO-68-NH_2, with an amino-substituted terphenylene dicarboxylic acid as linker. In fact, in this case the modulator approach even led to the first single crystals of a Zr-based MOF [29]. All members of the PIZOF family could only be obtained using the modulation approach [22]. It is also worth noting that in the low-temperature synthesis of the Zr-muconic acid MOF, where the $Zr_6O_4(OH)_4(maa)_{12}$ complex was used as a precursor, the methacrylic acid anions of the starting complex can act as modulators [21].

It is assumed that the molecules of the modulating agent strongly influence crystal nucleation and growth by competing with the linker molecules for the coordination sites at the Zr atoms or Zr clusters, which become the SBUs of the framework [27–29]. However, there have only been few systematic studies on the application of the modulator approach. Here, we present such a study on a Zr-based MOF with fumarate dianions as linkers. Fumaric acid (trans-butene-1,4-dicarboxylic acid: $HO_2C–CH{=}CH–CO_2H$; H_2-fum) is an unbranched unsaturated dicarboxylic acid. This linker was chosen for its simple constitution and due to the fact that it is a biologically occurring molecule and used as a food additive (E297) so that MOFs constructed from it might find applications in medicine [10,30]. As a modulating agent we used the – also naturally occurring – formic acid, the simplest monocarboxylic acid. Steric effects of the modulating agent, which is presumed to coordinate to Zr atoms or Zr-based clusters during the synthesis reaction, are thus minimized.

2. Experimental

2.1. Zr-fumarate MOF

All chemicals were obtained commercially (Sigma Aldrich) and used without further purification.

The standard synthesis of the Zr-fum MOF was performed by dissolving $ZrCl_4$ (0.517 mmol, 1 eq) and fumaric acid (1.550 mmol, 3 eq) in 20 mL N,N-dimethylformamide (DMF) in a 100 mL glass flask at room temperature. To investigate the influence of the modulator, 0–100 eq of formic acid were added. The glass flasks were Teflon-capped and heated in an oven at 120 °C for 24 h. Furthermore, the influence of the modulator concentration on the yield at different reaction times was examined for 5 and 30 eq of modulator by sampling the reaction after 2, 4, 8, 24, and 48 h. After cooling, the white precipitate was washed with 10 mL DMF and 10 mL ethanol, respectively. The washing process was carried out by centrifugation and redispersion of the white powder, which was then dried at room temperature over night.

Further purification of the samples was carried out by Soxhlet extraction in ethanol for 24 h and drying over night at room temperature. Activation before porosity, powder X-ray diffraction and

thermal analysis was performed by heating the sample at 120 °C in vacuum for at least 8 h.

2.2. Characterization

Powder X-ray diffraction (PXRD) patterns were measured using a Stoe StadiP diffractometer operated with Ge(1 1 1)-monochromatized Cu$K\alpha_1$ radiation with a wavelength of λ = 1.54060 Å in transmission. The reflections observed were indexed by using the Werner Algorithm implemented in the WinXPow software [31] and were refined by least squares method. The particle size was calculated by applying Scherrer's equation to the first reflection at 8.5° 2θ. To determine the reflection broadening caused by the measurement equipment, a silicon standard was measured under the same experimental conditions.

Dynamic light scattering (DLS) measurements were performed on a Zetasizer Nano ZS from Malvern Instruments. The solid materials were redispersed in ethanol by sonification with a Sonorex Digitec ultrasonic bath with 640 W for 5 min. Afterward the suspensions were transferred to a polystyrene cuvette.

Scanning electron microscope (SEM) images were taken on a JEOL JESM-6700F field emission SEM with a semi in-lens detector using a working distance of 3 mm and an acceleration voltage of 2 kV. For the sample preparation the solid material was dispersed in ethanol and dropped onto a polished carbon block which was then dried under reduced pressure.

Thermogravimetric analysis (TGA) measurements were carried out using a Netzsch STA 429 thermoanalyser. The samples were heated with a rate of 5 °C/min in alumina crucibles. Air was used as a flushing gas and the measurements were terminated at 1000 °C.

Ar sorption isotherms were measured on a Quantachrome Autosorb-1 instrument. The samples were outgassed in vacuum at 120 °C for 74 h prior to the sorption measurement. The pore size distribution was calculated using non-linear density-functional theory (NLDFT) fitting of the Quantachrome Kernel "Ar at 87 K_zeolites/silica" to the experimental data.

For solution ^1H NMR spectroscopy, the Zr-fum was digested in DMSO-d6 through the addition of CsF and a drop of aqueous DCl (35 wt%). Then K_2CO_3 was added [32].

2.3. Structural simulations

Simulations of the structure of the Zr-fum MOF were performed within Accelrys' modeling environment 'Materials Studio 5.0' [33]. For the simulations, we chose the Universal forcefield [34]. In order to find low energy conformations, a quenched dynamics simulation was performed in the NpT ensemble (constant number of particles, pressure and temperature). All simulations were carried out in space group P1. The temperature of T = 900 K was controlled by scaling the velocities to hold the temperature in the desired region ($\Delta T = \pm 10$ K). The dynamics runs lasted 25 ps with a time step of 0.1 fs. Structures were saved and energy-minimized after every 250th step using the Smart algorithm implemented in the Forcite Module of Materials Studio. The algorithm employs a cascade of minimization algorithms starting with the robust steepest descent [35] method, after which an Adjusted Basis Set Newton–Raphson (ABNR) [36] minimization follows. The last step is the Quasi-Newton method in the Broyden–Fletcher–Goldfarb–Shanno (BFGS) variant [37]. The simulations were performed on a workstation system (AMD Athlon 64 X2 Dual Core 4800+, 2 × 2.4 GHz, 2 GB RAM). The simulated powder diffraction patterns were calculated using Powder Cell for Windows Version 2.4.

3. Results and discussion

3.1. Modulated synthesis of Zr-fumarate MOF

In the following, we state the amount of modulator added to a synthesis batch in relation to the amount of $ZrCl_4$ used and give this value as equivalents (eq). For example, in a synthesis designated as "5 eq", the molar ratio between the modulating agent formic acid and $ZrCl_4$ is 5:1. In the investigations presented here, the amount of formic acid was varied between 0 and 100 eq.

In Fig. 1, the PXRD patterns of the products of these syntheses are shown. Without the addition of a modulator (0 eq), an amorphous phase is obtained under the reaction conditions used here. Already with the addition of only 0.5 eq of the modulator, two broadened reflections can be discerned on the amorphous background. The product prepared with 1 eq of formic acid already shows the full set of reflections of a crystalline phase, although amorphous material is still present. When more than 5 eq of the modulator were present during the synthesis, a fully crystalline material was obtained as judged from the PXRD pattern. The characterization of this novel compound, the Zr-fumarate MOF (Zr-*fum* MOF), will further be described in Section 3.2.

The PXRD patterns in Fig. 1 reveal further changes due to the influence of the modulating agent. When smaller amounts of formic acids are used, the reflections are broadened. From Scherrer's equation, crystallite sizes can be calculated and are given in Table 1. In those cases where this method can be reasonably applied, the crystallite size increases with the amount of modulator present during the synthesis.

The samples were further investigated by SEM in order to ascertain the particle size and morphology as well as the state of agglomeration. Fig. 2 shows a selection of characteristic images, Table 1 summarizes characteristic findings (size ranges of particles and particle aggregates, morphological characteristics). Products obtained at small modulator concentrations (from 0 to 10 eq) show strongly intergrown small crystallites. No specific shape of the individual crystals can be discerned. When more than 30 eq of

modulator were used, the crystals attain an octahedral shape. The degree of agglomeration decreases on increasing the amount of formic acid from 30 to 100 eq. At the highest modulator concentration investigated, individual crystals were obtained. For the samples prepared at 5 and 10 eq, the sizes of the particles are around the values determined by evaluating the X-ray line broadening, as far as can be recognized. For modulator concentrations higher than 30 eq, the crystal sizes are outside the range of the application of Scherrer's equation.

Below 10 eq of modulator the SEM images show strongly aggregated particles. This results in broad size distributions in the DLS measurements. Larger aggregates observed in the SEM images cannot be detected by DLS, because they cannot be stabilized in suspensions and sediment during the measurement. Correspondingly, only smaller aggregates are measured. Samples prepared with high modulator concentrations (30–100 eq) show comparable values with regard to the size determination from SEM images and by DLS. This good agreement can be explained by the low agglomeration of octahedral crystals which remain suspended in aqueous media. The size distribution is rather broad, the sizes are in the range of 150–200 nm.

According to these observations the application of formic acid as a modulator on the synthesis of Zr-*fum* MOF has several effects which have in part already been discussed in preceding publications of our group [22,29]. At low concentrations of modulator, its presence inhibits the formation of an amorphous precipitate (which we observe when the concentration of the modulator is too small) and slows down the growth rate, yielding more crystalline products. This can possibly be ascribed to the formation of intermediate complexes between formate ions and Zr cations. With increasing concentration of formic acid, the competition between deprotonated linker molecules and formate ions for the coordination of the Zr cations reduces the number of nuclei of the crystalline Zr-*fum* framework; fewer nuclei then grow to larger crystals. Furthermore, with increasing amount of modulator, the aggregation of the product particles is reduced and more and more isolated MOF particles are obtained. This effect is only observed at modulator amounts higher than 10 eq, i.e. when a large excess of modulator is deployed.

Similar effects had been observed in the synthesis of UiO-66 and UiO-67 when benzoic acid or acetic acid were used as modulators [29]. However, in those cases we observed that precipitation of the product took longer and longer times as the concentration of modulating agent was increased, a behavior which is in accord with a coordination modulation mechanism as described above. When formic acid is used as a modulator, the situation is different: The higher the amount of modulator, the earlier the formation of a white precipitate starts. XRD measurements showed that in all cases, even after a reaction time of only 2 h, a crystalline product was obtained. So, formic acid obviously accelerates the formation of the crystalline Zr-*fum* MOF and thus appears to play a special role as a modulator. A possible reason for this could be that formic acid is a direct product of the decomposition of the solvent DMF with water:

The presence of formic acid added as a modulator could displace this equilibrium to the left side so that more water is available in the reaction system. Water is essential for the hydrolysis of the Zr precursor and for the supply of oxygen atoms for the
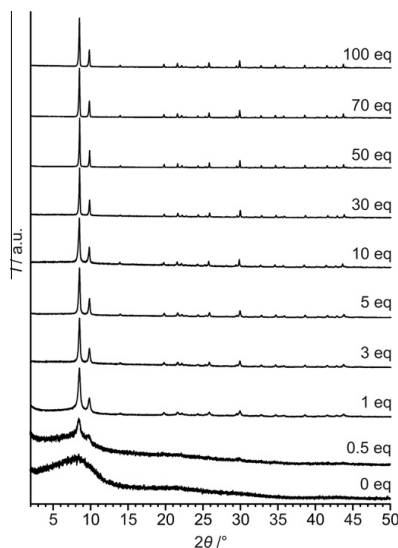

Fig. 1. PXRD patterns of the products of syntheses of Zr-*fum* MOFs performed in the presence of different equivalents (with respect to $ZrCl_4$) of formic acid as modulator.

Table 1
Characterization of the products of syntheses performed in the presence of different equivalents of formic acid (with respect to $ZrCl_4$) as modulator. Crystallite size d_{XRD} from X-ray diffraction line broadening, size range of agglomerates d_{SEM} and characterization of sample morphology from SEM images, hydrodynamic diameters d_{DLS} from dynamic light scattering measurements.

Eq of formic acid	d_{XRD} (nm)	d_{SEM} (nm)	Sample morphology	d_{DLS} (nm)[a]
0	_[b]	1600–6000	Strong agglomeration	360–740 (535)
0.5	_[c]	1000–4000	Strong agglomeration	410–860 (594)
1	39	1000–5000	Strong agglomeration	270–550 (386)
3	73	400–6000	Strong agglomeration, ill-defined crystal shape	170–480 (276)
5	86	700–6000	Strong agglomeration, ill-defined crystal shape	410–860 (627)
10	102	1000–4000	Strong agglomeration, ill-defined crystal shape	480–1150 (753)
30	_[d]	80–260	Medium agglomeration, indication of octahedral shape	130–310 (208)
50	_[d]	100–200	Weak agglomeration, octahedral shape with rounded edges	50–230 (166)
70	_[d]	80–280	Weak agglomeration, octahedral shape with rounded edges	100–200 (141)
100	_[d]	110–290	Individual octahedral	110–230 (156)

[a] Data for particle sizes from DLS measurements (the maximum of the distribution by using the Gauss fit is given in parentheses).
[b] Product is amorphous.
[c] Due to high background, no reasonable value for the peak width can be determined.
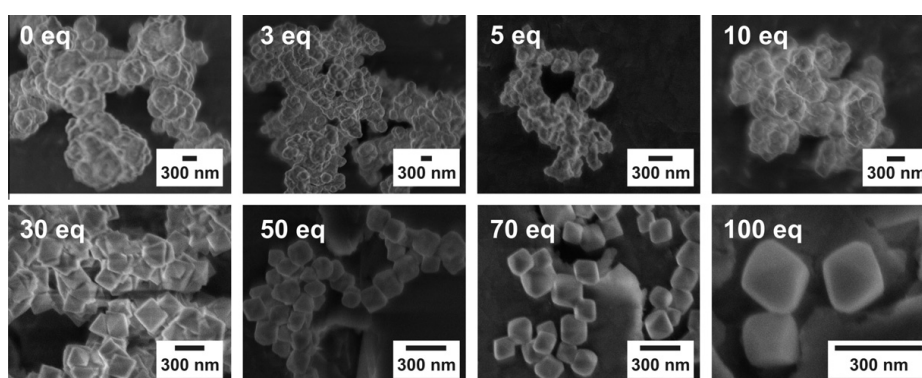[d] Crystallite sizes were out of scope for determination by Scherrer's equation.

Fig. 2. SEM images of the products of Zr-*fum* MOF syntheses carried out in the presence of different amounts of modulator (from 0 to 100 eq, as given in the images).

formation of the $Zr_6O_4(OH)_4(O_2C)_{12}$ SBU. Thus, formic acid could indirectly enhance the formation of the SBU and thus accelerate the formation of the Zr-*fum* MOF.

3.2. Characterization of Zr-fumarate MOF

All products synthesized in the presence of more than 30 eq of formic acid gave similar diffraction patterns which correspond to a fully crystalline material. An example is shown for the product obtained in the presence of 30 eq in Fig. 3, in comparison to a diffraction pattern of UiO-66.

The pattern of the novel Zr-*fum* MOF resembles that of UiO-66, taking into account that the reflections of the former are shifted to larger diffraction angles corresponding to a smaller lattice constant. For the new material we determined a cubic lattice constant of 17.9090 Å (the indexing of the PXRD pattern of Zr-*fum* MOF is given in the Supplementary material as Table A1). The lattice constant of UiO-66 has been given as 20.755 Å [17]. As the fumarate linker is shorter than the terephthalate linker in UiO-66, the smaller lattice constant for the Zr-fumarate MOF can be easily rationalized. On this basis it can be assumed that the novel material has a framework topology which is generally similar to that of UiO-66, i.e. similar SBUs are arranged in a packing similar to a cubic close-packing and are twelvefold connected by the linkers. However, a close inspection of the indexed diffraction pattern shows that, although an indexing based on a cubic lattice is possible,
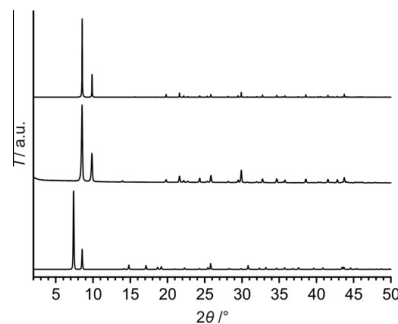
Fig. 3. Comparison of powder X-ray diffraction patterns. Top: simulated pattern based on the proposed structural model for the Zr-*fum* MOF (see text); middle: experimental pattern from a Zr-*fum* MOF synthesized with 30 eq of modulator; bottom: experimental pattern of UiO-66.

reflections are present in the PXRD of the Zr-*fum* MOF which break the face-centered symmetry of the *Fm-3m* space group of UiO-66. We ascribe this circumstance to the lower symmetry of the fumarate linker as compared to the terephthalate unit, as it is not strictly linear due to the *trans* configuration around the double bond (Fig. 4a). Any ordered distribution of the fumarate linkers

Fig. 4. (a) Structure of the non-linear linker fumarate; (b) and (c): structural model for the Zr-*fum* MOF as described in the text. In (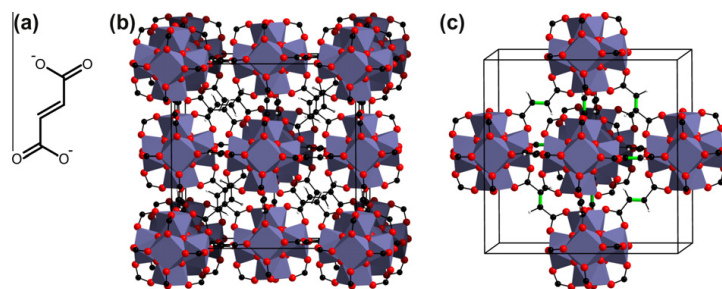b), the cubic unit cell is outlined. (c) Shows the central octahedron of a unit cell with the double bonds of the fumarate linkers depicted in green.

in the Zr-*fum* MOF should then lead to a lowering of the space group symmetry. Various models of a possible order of the orientation of the fumarate linkers were tested in order to derive a structure for the Zr-*fum* MOF. The best result was obtained by a symmetry reduction from space group *Fm-3m* (of UiO-66) to *P-3n*. This space group is in accordance with the indexing of the powder pattern. A PXRD pattern simulated on the basis of this model is compared to the experimentally obtained one in Fig. 3. There is a strong similarity between the two patterns so that we assume that the structural model as presented in Fig. 4b and c, which only contains the framework atoms, is correct (a list of the positional parameters for this structural model is given as Table A2 in the Supplementary material). In this model, the topology of the structure of UiO-66 is retained, i.e. $Zr_6O_4(OH)_4(O_2C)_{12}$ clusters are positioned at the corners and the faces of a cube and are interconnected to other SBUs by 12 linkers. However, due to the kinked geometry of the fumarate linkers, the Zr–O clusters are tilted into different directions; this destroys the face–centered symmetry present in UiO-66. Half of the SBUs (those at the corners and those in the front/back faces in Fig. 4b) are tilted in one direction, the other half (those at the left/right and bottom/top faces) in the other direction. When the structure of UiO-66 is seen as being related to the cubic close-packing of Cu metal, then the different tilting of the SBUs in the Zr-*fum* MOF leads to an analogy with the superstructure of the intermetallic phase CuAu.

The minor differences observed between the experimental PXRD pattern and the one simulated on the basis of this structural model can possibly be traced back to occluded guest molecules (see Supplementary material, Fig. A1). The low-resolution PXRD data do not allow for a full refinement of the structure including such guest species. We think that the structural model presented in Fig. 4b and c is basically correct, but as the focus of this publication lies on the modulated synthesis of the Zr-fumarate MOF, we refrain from further structural investigations.

The composition of the novel Zr-fumarate MOF material was investigated using thermogravimetric analysis (TGA, Fig. 5 and Table 2). The as-synthesized sample shows a nearly continuous mass loss up to 400 °C with no specific steps. This mass loss probably corresponds to the removal of all organic material, including the evaporation of guest molecules from the pores (like the solvents DMF and ethanol) and the combustion of the linker. A combined extraction–activation procedure was therefore applied to the material. The sample was Soxhlet-extracted for 24 h in ethanol, and after drying at room temperature, was heated to 140 °C for 8 h to remove the guest molecules. In fact, several investigations show that such a sample is essentially pure: IR spectra reveal, apart from the presence of carboxylate groups (symmetric and asymmetric stretching vibrations at ν_{sym}(C-O): 1410 cm^{-1} and at ν_{sym}(C-O): 1590 cm^{-1}, respectively), that a sample so treated does
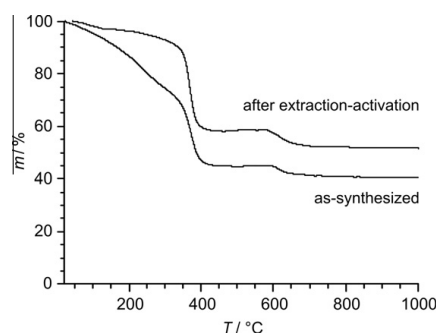

Fig. 5. Thermogravimetric analyses of Zr-*fum* MOFs (synthesized in the presence of 30 eq formic acid) in the as-synthesized state and after the Soxhlet extraction–activation procedure described in the text.

Table 2
Evaluation of thermogravimetric analyses. Mass losses measured in the given temperature ranges on a Zr-*fum* MOF synthesized in the presence of 30 eq of modulator after Soxhlet extraction and activation as described in the text.

Mass loss (%)	T (°C)	Calculated	Measured	Guest-free[a]
Guests	25–140	–	2.9	–
Linker	140–660	45.8	45.7	47.0
Residue	1000	54.2	51.5	53.0

[a] Experimental mass loss after correction for the removal of guest molecules.

not contain any DMF anymore, because the amide stretching vibration ν(C–O) at about 1660 cm^{-1} is lacking. Correspondingly, a CHN analysis also showed the absence of nitrogen. In addition, after dissolving such a sample, a ^{1}H NMR spectrum of the solution gives no signals for DMF or for formic acid [32]. The TG curve of a Soxhlet-extracted sample is much clearer and reveals two plateaus. The mass loss up to 140 °C is ascribed to the evaporation of residual guest molecules. The TGA then shows a plateau until at about 260 °C the decomposition of the linkers starts. This obviously occurs in two steps, one which is finished at 400 °C and another one which takes place at around 600 °C. The decomposition thus starts at a relatively low temperature as compared, for example, to UiO-66 which is stable in air up to a temperature of about 400 °C [29]. This is in line with the enhanced reactivity of an unsaturated linker as compared to an aromatic one. The decomposition of a sample of pure fumaric acid occurs between 200 and 400 °C. IR-spectroscopic investigation of a sample heated to 440 °C shows
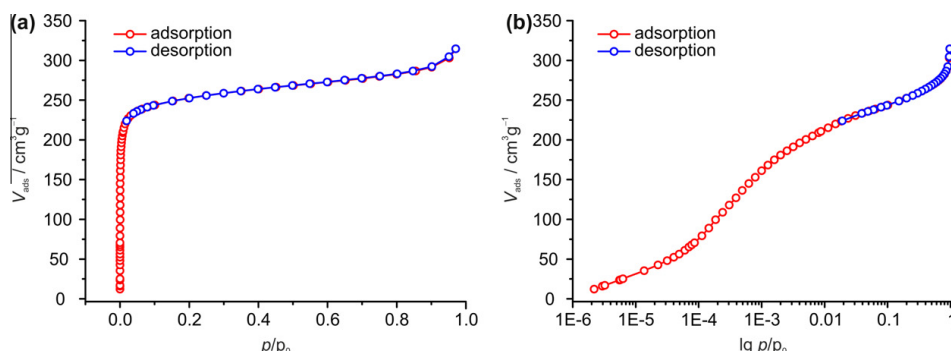
Fig. 6. Ar sorption isotherms of Zr-*fum* MOF synthesised with 30 eq of modulator.
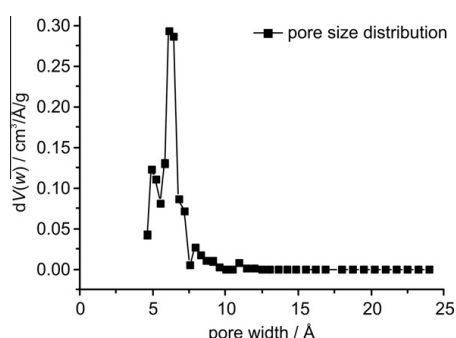

Fig. 7. Pore size distribution of Zr-*fum* MOF synthesized with 30 eq of modulator, calculated from the data given in Fig. 5.
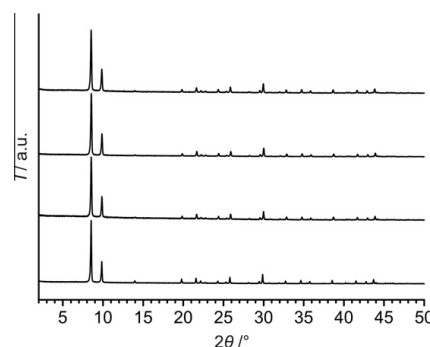

Fig. 8. Stability of Zr-*fum* MOFs in aqueous media: PXRD patterns measured after stirring for 1 week in comparison to the as-synthesized sample. From bottom to top: as-synthesized sample (synthesized with 50 eq of modulator); after stirring in water; after stirring in physiological NaCl solution; after stirring in PBS solution.

that any signs of the presence of C–H bonds have disappeared, but bands at 1410 cm^{-1} and at 1550 cm^{-1} still persist. We ascribe these signals to carbonate ions coordinated to Zr^{4+} ions, possibly to still intact Zr-oxo clusters. The last step in the TG curve at about 650 °C can then be assigned to the final decomposition where the carboxylate groups are released as CO$_2$. The residual sample was identified as monoclinic ZrO$_2$ using PXRD. When the mass loss between 260 and 700 °C is assumed to be due to release of the linker, and when this mass loss is compared to the residual mass, the ratio is near to the value expected for a Zr-*fum* MOF with a composition similar to that of UiO-66, i.e. Zr$_6$O$_4$(OH)$_4$(O$_2$C–(CH)$_2$–CO$_2$)$_6$ (Table 2). This finding further corroborates the assignment of the UiO-66 topology to the Zr-*fum* MOF.

To characterize the porosity of Zr-*fum* MOFs, Ar sorption measurements were performed on a sample of Zr-*fum* MOF prepared with 30 eq of modulator which was Soxhlet-extracted and activated. The linear and logarithmic depictions of the isotherms are shown in Fig. 6. They correspond to type I adsorption isotherms, as classified by IUPAC. When we calculate the pore size distribution (Fig. 7) using NLDFT fitting (see Fig. A2 in the Supplementary material for the fit). The corresponding plot shows the presence of micropores in the diameter range between 5 and 7 Å, peaking at 6 Å; the diameters of the cavities of UiO-66 were given as 8–11 Å [25]. The BET surface area determined from the sorption isotherm for the Zr-*fum* MOF is 856 m^2 g^{-1}. Due to the shorter linker it is not surprising that this value is smaller than that of UiO-66 for which a surface area of 1069 m^2 g^{-1} was given [18,25]. We note that the re-

sults from the sorption measurements agree with the assignment of a UiO-66-type topology to the Zr-*fum* MOF.

For several Zr-MOFs, a remarkably high stability versus high temperatures and various chemical agents has been reported [17,18,22,29]. From the thermogravimetric analyses described above, we estimate that Zr-*fum* MOF is stable up to a temperature of ca. 260 °C in air. In addition, we have investigated the stability of this novel Zr-MOF in water and in aqueous solutions. As we see possible applications of this MOF in the biomedical field we chose phosphate buffered saline (PBS) solution or physiological NaCl solution. For testing the stability, the solid material was dispersed in water or in one of the solutions and stirred at room temperature for 1 week. PXRD patterns of the re-isolated materials do not show any sign of destruction or disorder in comparison to the as-synthesized powder (Fig. 8).

4. Conclusions

This paper describes the modulated synthesis of a novel Zr-based metal-organic framework, namely the Zr-fumarate MOF. It is most interesting to note that whereas we have not been able to obtain this compound in the absence of a modulator, even very small amounts of the modulating agent formic acid induced the formation of this MOF. This gives rise to two speculations: (i) many MOFs which have been missed so far could possibly be synthesized

in the presence of a minor amount of a suitable "foreign" substance acting as a modulator; (ii) the fact that some syntheses of MOFs described in the literature are difficult to reproduce in other laboratories could be explained by the circumstance that obviously even small amounts of a "foreign" substance which acts as a modulator can decide about the success of a synthesis.

As in the case of the modulated synthesis of UiO-66 and UiO-67 [29], varying the concentration of the modulating agent allows for the preparation of samples with very different morphologies. However, formic acid is differentiated from other modulating agents by the fact that it accelerates the formation of a crystalline MOF, whereas usually the crystallization rate is decreased in the presence of a modulator.

Further characterization of the Zr-*fum* MOF using a variety of techniques gives results which all agree with the assumption that the structure of this novel MOF can be derived from the basic topology of the UiO-66 to -68 MOFs. A structural model which takes into account the kinked geometry of the linker molecule as well as the absence of face centering (deduced from the PXRD pattern) is proposed. Zr-*fum* MOF is porous, thermally stable up to a temperature of 260 °C in air and chemically stable in various aqueous media. As the organic components used in the synthesis of this MOF occur naturally, possible applications in the biomedical field are envisaged.

Acknowledgements

Appendix A. Supplementary data

Supplementary data associated with this article can be found, in the online version, at doi:10.1016/j.micromeso.2011.12.010.

References

[1] J.R. Long, O.M. Yaghi, Chem. Soc. Rev. 38 (2009) 1213–1214.
[2] S. Kitagawa, R. Kitaura, S. Noro, Angew. Chem. 116 (2004) 2388–2430. Angew. Chem. Int. Ed. 43 (2004) 2334–2375.
[3] G. Férey, Chem. Soc. Rev. 37 (2008) 191–214.
[4] O.M. Yaghi, M. O'Keeffe, N.W. Ockwig, H.K. Chae, M. Eddaoudi, J. Kim, Nature 423 (2003) 705–714.
[5] A. Robson, Dalton Trans. (2008) 5113–5131.
[6] Z. Wang, S.M. Cohen, Chem. Soc. Rev. 38 (2009) 1315–1329.
[7] S.T. Meek, J.A. Greathouse, M.D. Allendorf, Adv. Mater. 23 (2011) 249–267.
[8] H.-L. Jiang, Q. Xu, Chem. Commun. 47 (2011) 3351–3370.
[9] A.U. Czaja, N. Trukhan, U. Müller, Chem. Soc. Rev. 38 (2009) 1284–1293.
[10] S. Keskin, S. Kızılel, Ind. Eng. Chem. Res. 50 (2011) 1799–1812.
[11] J.L.C. Rowsell, O.M. Yaghi, J. Am. Chem. Soc. 128 (2006) 1304–1315.
[12] J. Hafizovic, M. Bjorgen, U. Olsbye, P.D.C. Dietzel, S. Bordiga, C. Prestipino, C. Lamberti, K.P. Lillerud, J. Am. Chem. Soc. 129 (2007) 3612–3620.
[13] S.S. Kaye, A. Dailly, O.M. Yaghi, J.R. Long, J. Am. Chem. Soc. 129 (2007) 14176–14177.
[14] C.A. Bauer, T.V. Timofeeva, T.B. Settersten, B.D. Patterson, V.H. Liu, B.A. Simmons, M.D. Allendorf, J. Am. Chem. Soc. 129 (2007) 7136–7144.
[15] Y.-S. Bae, D. Dubbeldam, A. Nelson, K.S. Walton, J.T. Hupp, R.Q. Snurr, Chem. Mater. 21 (2009) 4768–4777.
[16] P.L. Feng, J.J. Perry IV, S. Nikodemski, B.W. Jacobs, S.T. Meek, M.D. Allendorf, J. Am. Chem. Soc. 132 (2010) 15487–15489.
[17] J.H. Cavka, S. Jakobsen, U. Olsbye, N. Guillou, C. Lamberti, S. Bordiga, K.P. Lillerud, J. Am. Chem. Soc. 130 (2008) 13850–13851.
[18] L. Valenzano, B. Civalleri, S. Chavan, S. Bordiga, M.H. Nilsen, S. Jakobsen, K.P. Lillerud, C. Lamberti, Chem. Mater. 23 (2011) 1700–1718.
[19] G. Kickelbick, U. Schubert, Chem. Ber. 130 (1997) 473–477.
[20] P. Piszczek, A. Radtke, A. Grodzicki, A. Wojtczak, J. Chojnacki, Polyhedron 26 (2007) 679–685.
[21] V. Guillerm, S. Gross, C. Serre, T. Devic, M. Bauer, G. Férey, Chem. Commun. 46 (2010) 767–769.
[22] A. Schaate, P. Roy, T. Preuße, S.J. Lohmeier, A. Godt, P. Behrens, Chem. Eur. J. 17 (2011) 9320–9325.
[23] S.J. Garibay, S.M. Cohen, Chem. Commun. (2010) 7700–7702.
[24] M. Kandiah, S. Usseglio, S. Svelle, U. Olsbye, K.P. Lillerud, M. Tilset, J. Mater. Chem. 20 (2010) 9848–9851.
[25] P.S. Bárcia, D. Guimarães, P.A.P. Mendes, J.A.C. Silva, V. Guillerm, H. Chevreau, C. Serre, A.E. Rodrigues, Micropor. Mesopor. Mater. 139 (2011) 67–73.
[26] F. Vermoortele, R. Ameloot, A. Vimont, C. Serre, D. De Vos, Chem. Commun. 47 (2011) 1521–1523.
[27] T. Tsuruoka, S. Furukawa, Y. Takashima, K. Yoshida, S. Isoda, S. Kitagawa, Angew. Chem. 121 (2009) 4833–4837. Angew. Chem. Int. Ed. 48 (2009) 4739–4743.
[28] S. Diring, S. Furukawa, Y. Takashima, T. Tsuruoka, S. Kitagawa, Chem. Mater. 22 (2010) 4531–4538.
[29] A. Schaate, P. Roy, A. Godt, J. Lippke, F. Waltz, M. Wiebcke, P. Behrens, Chem. Eur. J. 17 (2011) 6643–6651.
[30] A.C. McKinlay, R.E. Morris, P. Horcajada, G. Férey, R. Gref, P. Couvreur, C. Serre, Angew. Chem. Int. Ed. 49 (2010) 6260–6266.
[31] WinXPOW, Version 1.08, STOE & Cie GmbH, Darmstadt, Germany, 2000.
[32] P. Roy, A. Schaate, P. Behrens, A. Godt, Chem. Eur. J. submitted for publication.
[33] Materials Studio, Version 5.0, Accelrys Software Inc., San Diego, CA, 2009.
[34] A.K. Rappe, C.J. Casewit, K.S. Colwell, W.A. Goddard, W.M. Skiff, J. Am. Chem. Soc. 114 (1992) 10024.
[35] K.B. Wiberg, J. Am. Chem. Soc. 87 (1965) 1070.
[36] B.R. Brooks, R.E. Bruccoleri, B.D. Olafson, D.J. States, S. Swaminathan, M. Karplus, J. Comput. Chem. 4 (1983) 187.
[37] D.F. Shanno, Math. Comput. 24 (1970) 647.

3.2   A Water-Born Zr-Based Porous Coordination Polymer: Modulated Synthesis of Zr-fumarate MOF

Gesa Zahn, Hendrik Albert Schulze, Jann Lippke, Sandra König, Uta Sazama, Michael Fröba, Peter Behrens

The final publication is available at

http://www.sciencedirect.com/science/article/pii/S1387181114006143

Preface

The present work deals with the synthesis of Zr-fumarate MOF from a water-based system. Often, metal-organic frameworks are prone to hydrolysis and cannot be precipitated from aqueous solution. As Zr-fumarate MOF synthesised from DMF exhibits exceptional stability against various aqueous media as reported in section 3.1, the synthesis from water seemed to be promising. Indeed, Zr-*fum* MOF can be successfully synthesised from aqueous solutions, even under very benign reaction conditions at room temperature. Again, the modulation approach had to be applied. Formic, acetic and propionic acid were applied as modulators. Using acetic or propionic acid, smaller particles were obtained as compared to Zr-fumarate MOF particles synthesised with equivalent concentrations of formic acid. The results of methane and carbon dioxide sorption measurements revealed a quite low methane and a comparably high carbon dioxide uptake making this material interesting for separation processes. Due to the exceptional small pores of the Zr-*fum* MOF with a pore limiting diameter of 3.48 Å, this material might also offer the opportunity of the adsorption or storage of small molecules like hydrogen. The manuscript was accepted for publication as a full article in *Microporous and Mesoporous Materials* during the evaluation of this thesis. Here, the paper is presented as it was published in the journal.

Many samples were synthesised with the help of HENDRIK A. SCHULZE. Argon and carbon dioxide sorption measurements were performed and evaluated by JANN LIPPKE and GEORG PLATZ. Methane and hydrogen sorption measurements as well as thermogravimetric analyses were carried out at the University of Hamburg in collaboration with SANDRA KÖNIG, UTA SAZAMA and Prof. Dr. MICHAEL FRÖBA. Prof. Dr. PETER BEHRENS initiated and guided this study. The author of this thesis wrote the initial manuscript and refined it together with Prof. Dr. PETER BEHRENS.

Contents lists available at ScienceDirect

Microporous and Mesoporous Materials

journal homepage: www.elsevier.com/locate/micromeso

CrossMark

A water-born Zr-based porous coordination polymer: Modulated synthesis of Zr-fumarate MOF

Gesa Zahn [a,b], Hendrik Albert Schulze [a,b], Jann Lippke [a,b], Sandra König [c], Uta Sazama [c], Michael Fröba [c], Peter Behrens [a,b,*]

[a] Leibniz Universität Hannover, Institut für Anorganische Chemie, Callinstr. 9, 30167 Hannover, Germany
[b] ZFM – Center for Solid-State Chemistry and New Materials, Germany
[c] Universität Hamburg, Institut für Anorganische und Angewandte Chemie, Martin-Luther-King-Platz 6, 20146 Hamburg, Germany

ABSTRACT

In this work, we present the water-based synthesis of the Zr-fumarate MOF (Zr-*fum* MOF) by applying a monocarboxylic acid as modulator. The original synthesis of Zr-*fum* MOF was performed in a DMF-based batch at 120 °C. The product showed exceptional stability against aqueous solutions. Thus, a water-based synthesis seemed to be promising. Indeed, by adding various amounts of formic acid, acetic acid or propionic acid as modulator, respectively, highly crystalline Zr-*fum* MOF can be obtained from water at 120 °C. The investigation of the influence of modulating molecules with different alkyl chain lengths showed that the particle size decreases when monocarboxylic acids with longer alkyl chains are used, e.g. acetic acid and propionic acid in comparison to formic acid. For the formation of the Zr-*fum* MOF synthesised with formic acid as modulator, the thermogravimetric and sorption behaviour as well as the stability against various solvents and pH values is discussed in detail. Furthermore, the Zr-*fum* MOF can also be obtained under very benign reaction conditions at room temperature from water, making this material interesting for various applications, for example as a biomaterial.

© 2014 Elsevier Inc. All rights reserved.

1. Introduction

Metal–organic frameworks (MOFs) or porous coordination polymers (PCPs) consist of metal cations or metal clusters which are connected via organic bridging molecules. The so-called linker molecules exhibit functional groups that coordinate to the metal centres building a porous three-dimensional network. The pore size of MOFs can be engineered via the length of the linker molecules and their chemical behaviour can be adjusted to the favoured application like adsorption, catalysis or biomaterials. Besides, the organic linkers might carry further functionalities or can be tailored through post-synthetic modification. One major disadvantage is the limited stability of numerous MOFs with regard to water, making these compounds unattractive for many industrial applications. One example of such an unstable framework is the famous Zn^{2+}-based MOF-5 which is prone to hydrolysis at ambient environment.

Zr-based MOFs were discovered by Lillerud and co-workers [1,2] and have been proven to exhibit a higher stability. The structure of the archetype framework UiO-66 features inorganic building units (IBUs) of formula $[Zr_6O_4(OH)_4)]^{12-}$ and dianions of terephthalic acid as linkers. Together, these form a framework with the topology of a cubic close packing [1], with the high degree of a twelvefold connectivity probably being one of the reasons for the increased stability, in addition to the strong coordination bonds formed at the Zr ions with a fourfold positive charge.

We have shown that the modulation approach, which was originally invented by the group of Kitagawa [3,4], can improve the reproducibility of the syntheses of Zr-based MOFs, enhances the crystallinity of the products and in some cases allows control over the particle size [5]. Certain Zr-based MOFs can in fact only be obtained using modulation [6–8]. The modulating agent is a coordinating molecule which exhibits only one functional group. When it is added to the synthesis, the modulator molecules will compete with the linkers for coordination sites at the metal centres, but cannot act as bridging molecules. However, it can coordinate to the zirconium ions so that the coordination sites are blocked with molecules of the modulating agent; for further MOF formation, they have to be exchanged by the linker molecules.

---

* Corresponding author at: Leibniz Universität Hannover, Institut für Anorganische Chemie, Callinstr. 9, 30167 Hannover, Germany. Tel.: +49 511 7623697.
E-mail address: Peter.Behrens@acb.uni-hannover.de (P. Behrens).

This competition reduces nucleation and growth rates, yielding a better control over the MOF formation reaction. Apart from this type of coordination modulation, other actions of the modulator may also play a role [9].

Novel Zr-based MOFs which were synthesised in our group employing the modulation approach usually show very robust characteristics. Porous interpenetrated Zr-organic frameworks (PIZOFs) were obtained by using very long linkers with tailored functionalities [7]. These compounds are usually water-stable. In addition, we also investigated Zr-based MOFs with very short linkers like fumaric acid [8]. From the solvent usually applied in MOF syntheses, namely dimethylformamide (DMF), the Zr-fumarate MOF (Zr-*fum* MOF) was only accessible when a modulating agent was used; in this case, very low concentrations of formic acid are sufficient (but necessary) to synthesise a highly crystalline material. The network topology of the Zr-*fum* MOF is the same as in UiO-66, with the IBUs arranged according to the metal atoms in a cubic close packing and with twelvefold connection of the IBUs through the linker molecules. However, the non-linear linker geometry causes a slight tilting of the IBUs and a lowering of the symmetry to the cubic primitive space group $Pn-3$ [8,10]. Caused by the short linker, the Zr-fumarate MOF exhibits small micropores with a diameter in the range of 5–7 Å, making this material interesting for sorption and separation applications involving small molecules. We also showed that the Zr-*fum* MOF has excellent stability in water and different aqueous solutions [8]. Furukawa et al. confirmed these results and investigated the water sorption behaviour of Zr-based MOFs, especially the Zr-*fum* MOF. They found out that the Zr-*fum* MOF exhibits an exceptionally high water uptake as well as good recyclability which makes this material interesting for use in advanced thermal batteries [10].

With regard to the high stability of the Zr-*fum* MOF in water and aqueous solutions, a water-based synthesis of this material appeared to be feasible. Omitting costly organic solvents in the synthesis is a prerequisite for large-scale industrial applications. A water-based synthesis is also used in the industrial production of Basolite A520, an Al-fumarate MOF which can be synthesised from water in a ton-scale production [11]. Apart from the fact that the synthesis can also be carried out successfully in DMF, the water-based system reaches higher space–time yields and the toxic solvent can be avoided, making the production environmentally reasonable. Such an uncomplicated change from one solvent to another is not granted, because often the change of the solvent from an organic one to water results in a non-crystalline product or a decreased porosity, for example due to uncoordinated water molecules like in DUT-4 (Al(OH)(*ndc*), *ndc* = 2,6-naphthalene dicarboxylate) [12]. Other well-known MOFs which can be synthesised in water-based systems were described by Férey and co-workers. They were able to synthesise Fe-MIL-53_NH₂ and Fe-MIL-102_NH₂ under solvothermal conditions in water [13], Al-based MOFs like MIL-69 in a hydrothermal reaction [14] or the Cr-based MOF MIL-101 from water using microwave irradiation [15].

Abstinence from solvents like DMF could also be of interest with regard to biomedical applications of MOFs, as such solvents are usually toxic and as it often proves difficult to totally remove the solvent from the pore system of a MOF. Accordingly, in a basic study on the biocompatibility of Fe-based MOFs, Horcajada et al. chose aqueous or ethanolic media for the syntheses of a variety of such substances, like for example, MIL-53 (Fe-terephthalate MOF) or MIL-88A (Fe-fumarate MOF) [16]. These and other Fe-MILs proved to be non-toxic and appear to be very promising as drug delivery systems as the release of several anticancer and antiviral drugs was successfully performed by either diffusion through the porous network or via degradation of the crystalline material. A Zr-*fum* MOF synthesised from water, containing fumarate, which is a central metabolite in living beings, as linker, and prepared

using a naturally occurring monocarboxylic acid (e.g. formic acid, acetic acid or propionic acid) as modulator should also be highly biocompatible.

In this paper, we present the synthesis of the Zr-fumarate MOF from a water-based system at 120 °C and also at room temperature by applying the modulation approach. The influence of three monocarboxylic acids, namely formic acid, acetic acid and propionic acid, respectively, on the crystallisation behaviour is discussed as well as the thermal and sorption behaviour of the prepared substances. Furthermore, the excellent chemical stability of the Zr-fumarate MOF over a wide pH range as well as against several solvents and solvent mixtures will be demonstrated.

2. Experimental

2.1. Synthesis of Zr-fumarate MOF

All chemicals were obtained commercially (Sigma Aldrich) and used without further purification. The standard synthesis for all samples was carried out as follows. ZrCl₄ (0.517 mmol, 1 eq) was dissolved in 10 mL water and various amounts of modulator (formic acid, acetic acid or propionic acid; amount of modulator: 0–100 eq with regard to ZrCl₄) as well as fumaric acid (1.550 mmol, 3 eq) as linker molecule were added. For reactions at 120 °C, the reaction mixture was transferred into Teflon-capped glass vials which were put into an oven pre-heated to 120 °C. The reaction time was 24 h. For reactions at room temperature, the reaction time was prolonged to one week. After the reaction, the white precipitate was collected by centrifugation and washed with 6 mL water and 6 mL ethanol, respectively. The white powders were dried at room temperature. Before sorption measurements and thermal analysis, the samples were in addition extracted with ethanol for 24 h in a Soxhlet apparatus and finally dried at room temperature.

2.2. Characterisation

Powder X-ray diffraction (XRD) patterns were measured in transmission using a Stoe StadiP diffractometer operated with Ge(111)-monochromatized Cu$K\alpha$1 radiation with a wavelength of λ = 1.54060 Å. The particle size was calculated by applying Scherrer's equation to the (111) reflection of the Zr-*fum* MOF at 8.5° 2θ. The reflection broadening caused by the measurement equipment was taken into account by measuring a silicon standard under the same experimental conditions.

Scanning electron microscope (SEM) images were registrated on a JEOL JESM-6700F field emission SEM with a semi in-lens detector applying a working distance of 8 mm or 3 mm and an acceleration voltage of 2 kV. The investigated solid material was dispersed in ethanol and dropped onto a polished carbon block which was afterwards dried under reduced pressure.

Dynamic light scattering (DLS) measurements were carried out on a Zetasizer Nano ZS from Malvern Instruments. Prior to the measurement, the powder was dispersed in water by sonification with a Branson S-450D digital ultrasonic processor for 2 min with approx. 20% power. The dispersions were filtered through a 0.8 μm syringe attachment filter after around 2 h and transferred to a polystyrene cuvette for the measurement. Data evaluation was performed using the Malvern Zetasizer software 7.02. The parameters chosen for the evaluation were those of a ZrO₂ material (refractive index of 2.13 and absorption of 0.01). The number of particles with a mean diameter was calculated.

Argon sorption isotherms were measured on a Quantachrome Autosorb-1 instrument. The samples were outgassed in vacuum for at least 24 h at 120 °C prior to the sorption measurement. The

"Micropore BET Assistant" implemented in the ASiQwin 2.0 software from Quantachrome was used to determine the maximum relative pressure for the BET (Brunauer, Emmett, Teller) plot. It determines the BET range according to the theory of Rouquerol, which was shown to be appropriate for different MOFs [17,18]. The pore size distribution was calculated by using non-linear density-functional theory (NLDFT) fitting of the Quantachrome Kernel "Ar at 87 K_zeolites/silica" to the experimental data. Pore volumes were determined from point of the isotherms before interparticular condensation occurs (p/p_0 = 0.92).

The thermogravimetric measurements were performed at a Netzsch STA 449 F3 Jupiter® simultaneous TG-FTIR-MS coupling. The samples were heated in an alumina crucible up to 800 °C under argon or under an argon/oxygen mixture (80% argon, 20% oxygen), respectively, as flushing gas.

Methane sorption isotherms were measured at a Quantachrome Autosorb-iQ-MP at 25 °C in a temperature-controlled water bath. Before the measurements were carried out, the samples were outgassed at 120 °C for 48 h at a Masterprep Degasser.

Carbon dioxide sorption isotherms were measured at a Quantachrome Autosorb-3 at 25 °C in a tempered ethylene glycol bath. Before the measurements were carried out, the samples were outgassed at 120 °C for 48 h.

Hydrogen sorption measurements were performed at a Quantachrome Autosorb 1-C at 77 K, 87 K and 97 K with an Optistat DN Cryostat. The samples were outgassed at 25 °C for 48 h at a Masterprep Degasser prior to the measurement.

Stability tests were carried out with approximately 20–30 mg of MOF in 3–3.5 mL solution. The dispersions were stirred for one week at room temperature or at 80 °C as mentioned in Section 3.4. The white powder was finally collected by centrifugation and the crystallinity was checked by XRD.

3. Results and discussion

As detailed in the introduction, we have formerly synthesised the Zr-fumarate MOF from DMF solution at 120 °C using formic acid as modulator [8]. In this work, we have employed water as a solvent and tested the three monocarboxylic acids formic acid, acetic acid and propionic acid as modulators, especially to evaluate the influence of different alkyl chain lengths of the modulating agent. The samples were characterised by various methods (XRD, SEM, sorption measurements and thermal analysis). A special focus was put on the stability of the Zr-*fum* MOF towards various solvents and solutions.

3.1. Zr-fumarate MOF synthesised from water at 120 °C

Highly crystalline Zr-*fum* MOF can be synthesised from a water-based system at 120 °C. In order to further elucidate the effect of modulating agents, we tested formic acid, acetic acid and propionic acid as modulators in this water-based synthesis system. The more modulator was added to the synthesis, the later precipitation of the sample occurred. The influence of the amount of modulator on the crystallinity of the resulting MOF was investigated by powder XRD (Fig. 1).

Without any modulator (0 eq) the reflections are very broad indicating that the particles are either extremely small or that the product is largely amorphous. By increasing the amount of modulator, the reflections become sharper and the full set of reflections develops (10–30 eq of modulator). When the modulating acid is applied at concentrations of 50 eq or more, all reflections are well defined corresponding to highly crystalline materials. The fact that the width of the reflections continues to decrease with increasing amount of modulator indicates that the particles

become larger the higher the amount of modulator is. Values for crystallite dimensions calculated according to Scherrer's equation are given in Table 1 as D_{XRD}.

SEM images taken from samples which were synthesised with different amounts of modulator (in the range of 0–100 eq of formic acid, acetic acid or propionic acid) are shown in Fig. 2. Particle diameter ranges as estimated from visual inspection are provided in Table 1 as D_{SEM}.

With low concentrations of a monocarboxylic acid, large particles with undefined shape and with dimensions of several micrometres were obtained. Although the surface of the particles appeared to be rough, it was not possible to verify whether the particles consisted of smaller nanoparticles with a defined shape due to charging effects occurring in the electron microscope when aiming at higher resolution pictures. Above concentrations of more than 50 eq of modulator, individual nanoparticles with diameters between 20 and 40 nm dominate. The more modulator is added to the synthesis, the larger the particles grow, resulting in non-aggregated and near-spherical nanoparticles with a size of about 50–150 nm, which is in accordance with the findings from the XRD patterns (Fig. 1).

Apart from these general trends, minor differences are observed when comparing the influence of different modulators. Whereas the products of syntheses modulated by acetic or propionic acid appear very similar at all modulator concentrations, the individual particles obtained at modulator concentrations above 30 eq are larger when formic acid is used. In the case of acetic acid and propionic acid, even at a concentration of only 30 eq of the monocarboxylic acid, individual nanoparticles with a size of around 10–25 nm can be presumed (Fig. 2), but no large agglomerates can be ascertained (which were obvious when small amounts of the shorter monocarboxylic acid formic acid were used, or when no modulator at all was used).

Additionally, we investigated the particle size in aqueous suspensions by dynamic light scattering (DLS). All dispersions were filtered by using a 0.8 μm syringe attachment filter to avoid sedimentation and to ensure a stable suspension during the measurement. Only dispersions from products of syntheses batches which contained higher modulator concentrations gave data which meet the quality criteria for a meaningful DLS data evaluation. The hydrodynamic diameters thus calculated are provided as D_{DLS} are Table 1. The data obtained via DLS measurements are in the same range as those calculated with the Scherrer's equation. Thus, individual particles are also present in aqueous dispersions.

In general, by using various amounts of monocarboxylic acid the particle size can be influenced. The higher the amount of modulator is, the larger the particles grow. The effect of the modulator on the particle size appears to be weaker, but similar, for acetic and propionic acid than for formic acid. Interestingly, this allows the synthesis of very small particles: with 30 eq of acetic or propionic acid (but not with formic acid), individual particles with a size around 25 nm can be obtained.

As one of only a few coordination polymers, Zr-*fum* MOF can be synthesised from water with high crystallinity. However, modulation is necessary, as in the synthesis of this compound from the DMF system [8]. In the water-based synthesis, a higher concentration of modulator is necessary to obtain a highly crystalline powder (50 eq formic acid in water compared to only 5 eq in DMF). The water-based synthesis appears very attractive, as the toxic and expensive solvent DMF can be avoided. Comparing the size and shape of the particles obtained from the two solvent systems, at comparable amounts of formic acid the nanoparticles formed in water are smaller than those prepared in DMF. Furthermore, the particles obtained from DMF possess a well-defined octahedral morphology, whereas the nanoparticles from the water-based synthesis are nearly spherical, exhibiting only indications of octahedral faces.
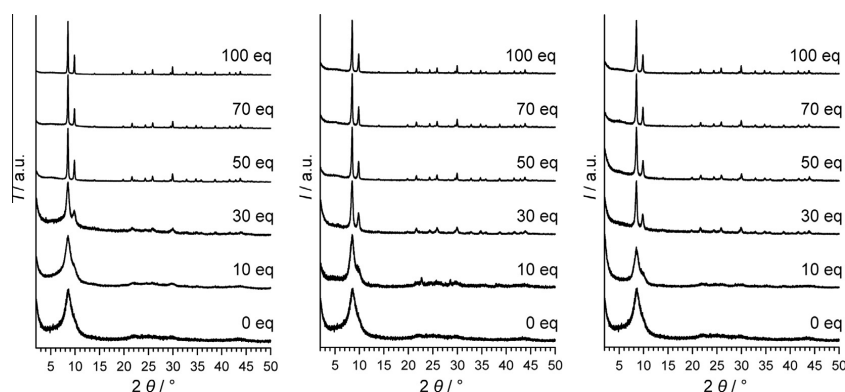
Fig. 1. XRD patterns of synthesis products from water-based syntheses carried out at 120 °C aiming at the formation of Zr-*fum* MOF. Various amounts of a monocarboxylic acid were used as modulator (left: formic acid, middle: acetic acid, right: propionic acid).

Table 1
Diameter in nm of the Zr-fumarate MOF particles synthesised at 120 °C with various amounts of formic acid, acetic acid and propionic acid. Crystallite diameters as calculated using Scherrer's equation based on XRD data are given as D_{XRD}; particle diameter ranges as estimated from SEM pictures are given as D_{SEM}; hydrodynamic diameters of particles in aqueous dispersions as determined by DLS are provided as D_{DLS}.

eq	D_{XRD}			D_{SEM}			D_{DLS}		
	Formic acid	Acetic acid	Propionic acid	Formic acid	Acetic acid	Propionic acid	Formic acid	Acetic acid	Propionic acid
0	_[a]	_[a]	_[a]	_[c]	_[c]	_[c]	_[d]	_[d]	_[d]
10	_[a]	_[a]	_[a]	_[c]	_[c]	_[c]	_[d]	_[d]	_[d]
30	16	25	32	_[c]	10–25	10–25	_[d]	_[d]	20–40 (31)[e]
50	81	65	43	20–80	15–55	10–30	50–80 (72)[e]	50–90 (73)[e]	40–70 (62)[e]
70	_[b]	78	71	30–100	30–70	15–60	90–160 (129)[e]	60–90 (82)[e]	50–80 (69)[e]
100	_[b]	106	77	80–200	30–100	20–80	140–260 (202)[e]	80–120 (109)[e]	70–110 (89)[e]

[a] No distinct reflections visible.
[b] Crystallite sizes were out of scope for determination by Scherrer's equation.
[c] Only large aggregates (1–20 μm) were visible in the SEM pictures.
[d] Determination of D_{DLS} not possible.
[e] Average size given in brackets.

After having discussed the crystallinity and the size and morphology of the particles synthesised with various modulators, we approve that smaller nanoparticles of the Zr-*fum* MOF can be obtained when using a modulator carrying an alkyl chain. Furthermore, with increasing concentration of the modulator, larger particles are obtained. This is in good agreement with the modulation approach published by the group of Kitagawa [3,4] and with observations we have made concerning the modulated synthesis of other Zr-based MOFs [5,7,8]. Investigations on the synthesis of UiO-66 showed that monocarboxylic acids like acetic acid and benzoic acid decelerate the reactions. The delayed formation of the product can be explained by the postulated coordination modulation mechanism in which the monocarboxylic acid molecules compete with the dicarboxylic acids for the coordination at the metal cation. The exchange between modulator and linker in an equilibrium reaction results in longer reaction times with increasing modulator concentration [5]. The decrease in reaction rates affects nucleation as well as crystal growth. Delayed crystal nucleation results in the formation of fewer nuclei per time; fewer nuclei will then grow to larger crystals, albeit in a longer time. The qualitative observations described here have recently been quantified by *in situ* kinetic studies using an energy-dispersive X-ray diffraction set-up confirming a coordination modulation mechanism instead of a deprotonation modulation [19]. In fact, the influence of the modulator formic acid on the pH value plays only a minor role. In the course of earlier investigations we found that the pH value decreased dramatically to pH 1 after the addition of the Zr source (ZrCl$_4$) due to formation of HCl which dissolves in the solution. After addition of formic and fumaric acid, respectively, the pH value remains constant.

3.2. Zr-fumarate MOF synthesised from water at room temperature

Syntheses performed at room temperature revealed that the Zr-fumarate MOF can also be obtained under very mild conditions. In these cases the reaction times were extended to one week to ensure complete formation of the products. As shown in the XRD measurements (Fig. 3), without any modulator no reaction takes place, because all reflections observed belong to the linker fumaric acid which is not dissolved under these conditions.

By increasing the amount of modulator to 10 equivalents of formic acid the reflections of the linker are still present, but additionally a broad reflection at around 8 °2θ appears. As the positions of the two reflections of the Zr-*fum* MOF at lowest 2 theta values agree with the position of this broad reflection, it is indicative of the formation of either very small MOF particles or of an amorphous coordination polymer. At an increased concentration of formic acid (30 eq) the reflections of the Zr-fumarate MOF show up. They become sharper at further increasing this concentration, so that a highly crystalline material could be obtained when using more than 30 equivalents of modulator.

The SEM images taken from samples which were synthesised at room temperature are shown in Fig. 4. In products from syntheses prepared with a low amount of formic acid (10 eq and 30 eq) no individual nanoparticles are present. In the picture of the sample prepared with 10 eq of modulator, a filamentous structure can be
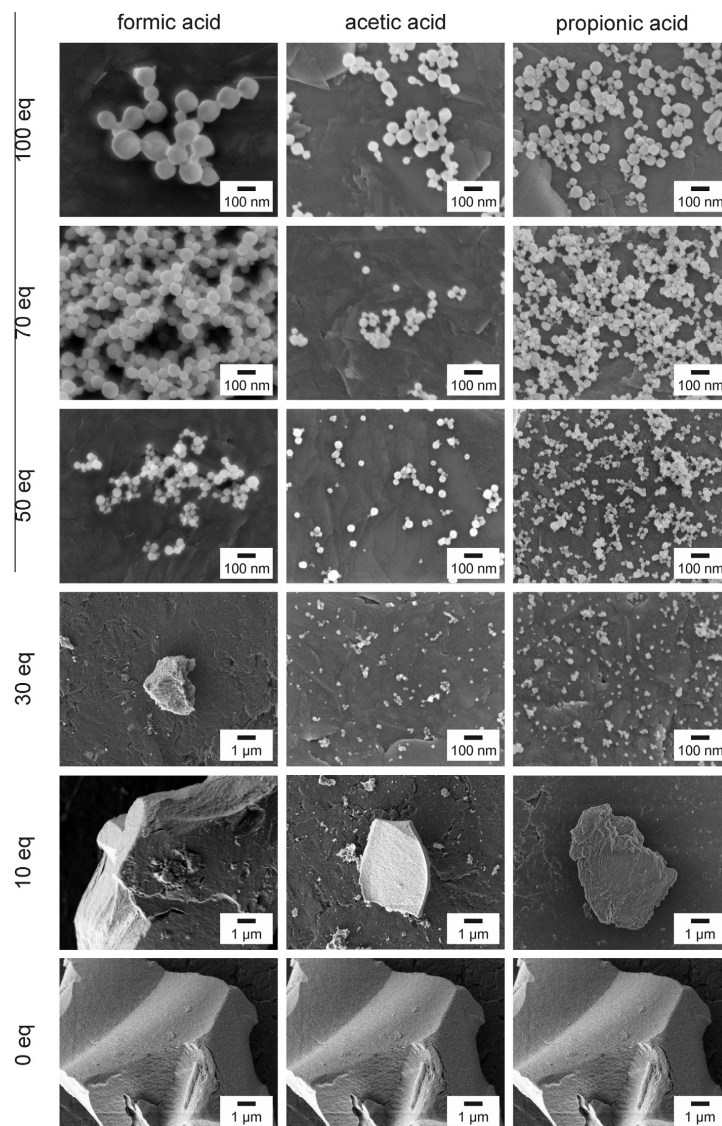
Fig. 2. SEM images of Zr-*fum* MOF particles synthesised at 120 °C with various amounts of one of the modulating agents formic acid, acetic acid or propionic acid, respectively. The amount of modulator is given in molar equivalents with regard to the amount of ZrCl₄ (1 eq).

discerned which could be indicative of a gel phase. In contrast, the SEM of the material prepared with 30 eq shows large aggregates which consist of very small particles with nearly spherical shape. When more than 50 eq of modulator are applied in the synthesis, individual nanoparticles develop, which are larger when 70 eq of formic acid were present in the synthesis. The larger particles are not spherical anymore but show indications of a developing definite morphology. This effect becomes more pronounced when 100 eq of modulator was used in the preparation. The crystallites attain sizes of around 1 μm, but also they start to intergrow and form aggregates and are not present as individual particles

anymore. DLS measurements did not meet the quality criteria for a meaningful DLS data evaluation. Crystallite sizes obtained by applying Scherrer's equation gave diameters of 18 nm and 87 nm, respectively, for samples synthesised with 30 or 50 eq formic acid, which is in good agreement with the sizes of the particles in the corresponding SEM pictures.

3.3. Characterisation

In the following, the thermal and sorption behaviour of the Zr-*fum* MOF will be discussed. For all further investigations, a sample
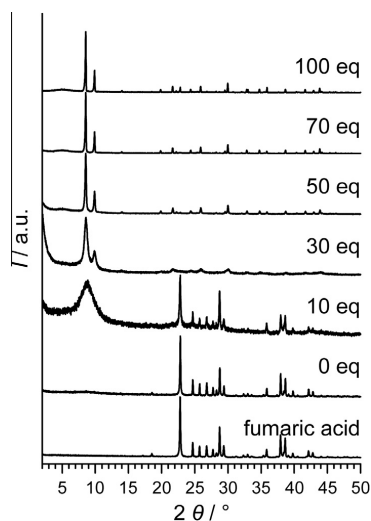
Fig. 3. XRD patterns of Zr-*fum* MOF samples synthesised at room temperature with various amounts of formic acid as modulator. For comparison, the XRD pattern of crystalline fumaric acid is also presented.

synthesised at 120 °C with 70 eq formic acid was used as a standard material. All the samples were further purified via Soxhlet extraction with ethanol.

3.3.1. Thermogravimetric measurements

The thermogravimetric measurements were performed under argon as well as under an argon/oxygen mixture (80% argon, 20% oxygen). As shown in Fig. 5, in both cases the mass loss of the Zr-*fum* MOF takes place in several steps.

Concerning the decomposition under argon, two mass losses are obvious. We assign the first step between 25 °C and 160 °C to the evaporation of guest molecules like ethanol and adsorbed water. In the following, the decomposition of the linker takes place

between 360 °C and 500 °C, which is in good agreement with the thermogravimetric behaviour of pure fumaric acid which decomposes between 200 °C and 400 °C. In contrast, the thermogram measured under a Ar/O₂ mixture reveals three steps of mass loss. The removal of guest molecules takes place in the same way as discussed before, the curves overlapping up to the point where the linker decomposition starts. The latter process, however, occurs in two steps when oxygen is present and leads to a smaller mass of the residue due to the fact that with oxygen, the organic becomes totally combusted whereas under a pure argon atmosphere, carbonisation takes place. The first part of the fumarate linkers decomposes between 350 °C and 450 °C, irrespectively of the atmosphere. However, under the argon/oxygen mixture, another step occurs at around 580 °C which can also be assigned to the decomposition of the linker. In our earlier investigation on Zr-*fum* MOF synthesised from DMF, we have studied this phenomenon by IR spectroscopy and have ascribed this mass loss to the release of carbon dioxide from carbonate ions which are bound to zirconium cations [8]. This idea has now been confirmed by further TG measurements coupled with mass spectrometry (see Supplementary Information, Section A1).

High temperature XRD measurements (Supplementary Material, Section A2) revealed that the crystalline structure is retained until around 300 °C irrespective of the atmosphere applied, which is in good agreement with the results of the thermogravimetric measurements.

3.3.2. Sorption measurements

To characterise the pore system of the Zr-*fum* MOF, sorption investigations were performed with different gases.

For argon sorption measurements, a sample synthesised at 120 °C from water was outgassed in high vacuum for at least 24 h at 120 °C prior to the sorption measurements. The resulting isotherms reveal a microporous pore system corresponding to a typical type I isotherm as classified by IUPAC. After calculating the pore size distribution using NLDFT fitting (Supplementary Material, Section A3), the pore size distribution plot reveals that the Zr-*fum* MOF exhibits micropores in the range of 5–8 Å (Fig. 6).

The BET surface area was calculated to 970 m² g⁻¹ and the total pore volume to 0.49 cm³ g⁻¹. In comparison to a non-extracted sample synthesised in water, no difference in the BET surface area is found (BET-surface: 960 m² g⁻¹). Thus, a Soxhlet-extraction with
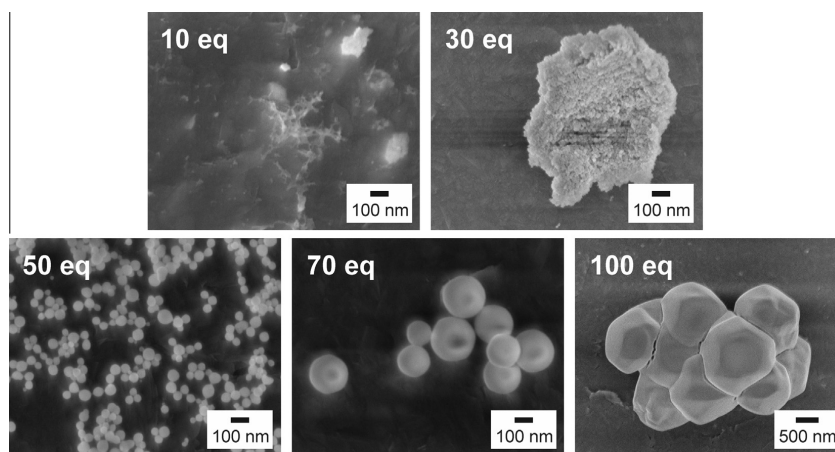

Fig. 4. SEM images of Zr-*fum* MOF products synthesised at room temperature with various amounts of formic acid as modulator (as given in the images).
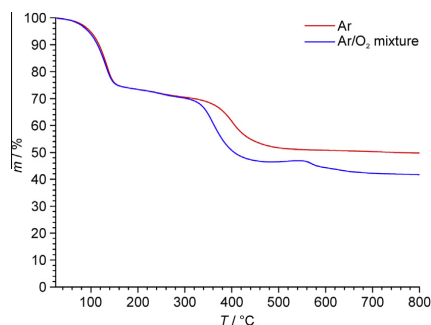
Fig. 5. Thermogravimetric measurements of Zr-*fum* MOF samples synthesised at 120 °C with 70 eq of formic acid as modulator. Measurements were performed under a pure Ar atmosphere and under a mixed Ar/O₂ atmosphere (80% argon, 20% oxygen).

ethanol is apparently not necessary for Zr-*fum* MOF samples synthesised from water, obviously because no guest molecules remain in the porous system after the normal washing process as it is usually carried out after the synthesis. This result is also in good agreement with the value obtained on a sample synthesised from DMF (BET surface area: 1010 m^2 g^{-1}) [8], and with results obtained by Furukawa et al. [10]. However, in the case of the DMF-based synthesis the Soxhlet extraction is necessary, as IR spectra had shown that non-extracted samples still contain large amounts of DMF [8]. When the pore size distribution of Zr-*fum* MOF synthesised from water (Fig. 6, right) is compared to that obtained on a sample which was prepared in DMF and Soxhlet-extracted [8], no significant differences are apparent. Thus, Zr-*fum* MOF samples with similar pore properties can be obtained from the DMF- and the water-based synthesis systems. Using the synthesis from water, however, the additional extraction step to obtain an empty pore system is obsolete, facilitating work-up.

For further characterisation of the pore system, sorption measurements were carried out with methane and carbon dioxide (Fig. 7, top). The results reveal a quite low methane uptake of 0.91 wt% and a comparatively high carbon dioxide uptake of 11.2 wt%. Thus, this material might be interesting for separation processes concerning methane and carbon dioxide. Obviously, the methane molecules are too large to pass the small apertures of the Zr-*fum* MOF pore system (pore limiting diameter = 3.48 Å).

Due to these small pore entrances, the Zr-*fum* MOF seems especially interesting for the sorption of small molecules. Therefore, in addition hydrogen sorption measurements were carried out at 77 K, 87 K and 97 K (Fig. 7, centre). The isotherms show a steep increase at lower pressure leading to a saturation plateau at

standard pressure. Upon increasing the temperature, the slope of the isotherms increase; also, the maximum uptake of hydrogen decreases from 1.20 wt% (77 K) to 0.87 wt% (87 K) to 0.58 wt% (97 K).

From these sorption isotherms measured at different temperatures, the heat of adsorption (Fig. 7, bottom) can be calculated using the Quantachrome Software ASiQwin (version 2.0). By increasing the amount of adsorbed hydrogen the heat of adsorption decreases from 6.9 to 6.4 kJ mol^{-1}, corresponding to an initial adsorption of hydrogen at favoured sorption sites, probably in the small pores near the metal centres of the Zr-fumarate MOF. Further adsorption of hydrogen occurs with a lower heat of adsorption, because the most favoured sites have already been saturated. The average value of 6.7 kJ mol^{-1} is quite high when compared to other metal–organic frameworks like MOF-5 (4.0 kJ mol^{-1}), MIL-53 (5.6 kJ mol^{-1}) and MIL-101 (4.3 kJ mol^{-1}) [20]. This can be ascribed to the presence of very small pores in the Zr-*fum* MOF. Correspondingly, the surface of the pore interior is strongly curved and adsorbed molecules experience van der Waals interaction potentials not only from one wall, but from the whole surrounding. Also, it is known that hydrogen molecules adsorb more strongly near to the inorganic building units than to the organic linkers of MOFs [21–23]; with the large [Zr$_6$O$_4$(OH)$_4$(CO$_2$)$_{12}$] IBU and the very small fumarate linkers the Zr-*fum* MOF has a nearly optimal ratio of inorganic to organic moieties making this material interesting for hydrogen storage.

3.4. Stability tests

The fact that the Zr-*fum* MOF can be synthesised under various conditions from water already shows that this compound is very robust. Also, Furukawa et al. have shown that cyclic water sorption measurements can be performed on this compound [10] and in our own previous work, we had already tested the stability of Zr-*fum* MOF samples synthesised in DMF in physiological sodium chloride solution and phosphate buffered saline (PBS) solution [8], both of importance for biomedical applications. For the water-born Zr-*fum* MOF, the stability against these solutions physiological NaCl and PBS solution was also proved (see Supplementary Material, Section A4). We now extend these investigations to additional stability tests. We have investigated the stability of Zr-*fum* MOF in methanol and ethanol as well as in methanol/water and ethanol/water mixtures. All experiments were carried out for one week during which the powder was stirred in the corresponding solvent at room temperature; for pure ethanol and for the ethanol/water mixture, the experiments were in addition carried out at 80 °C. After the reaction time the powder was collected via centrifugation and dried at room temperature. As no appreciable mass loss could be determined, we can ensure that the powder was not dissolved
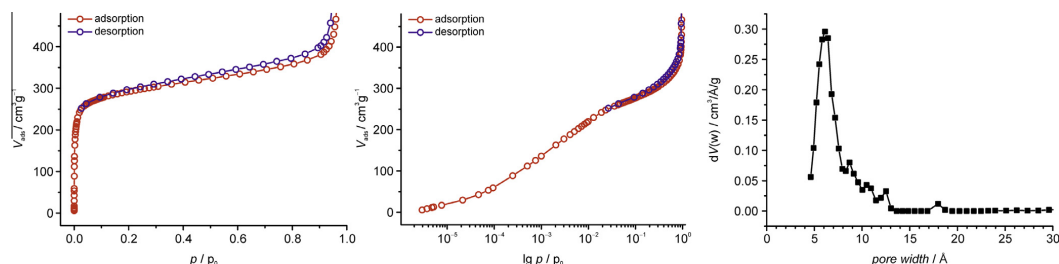

Fig. 6. Argon sorption measurements of a Zr-*fum* MOF sample synthesised at 120 °C with 70 eq of formic acid as modulator. Left: displayed with a linear p/p_0 scale; middle: displayed with a logarithmic p/p_0 scale; right: pore size distribution from the evaluation of these data.
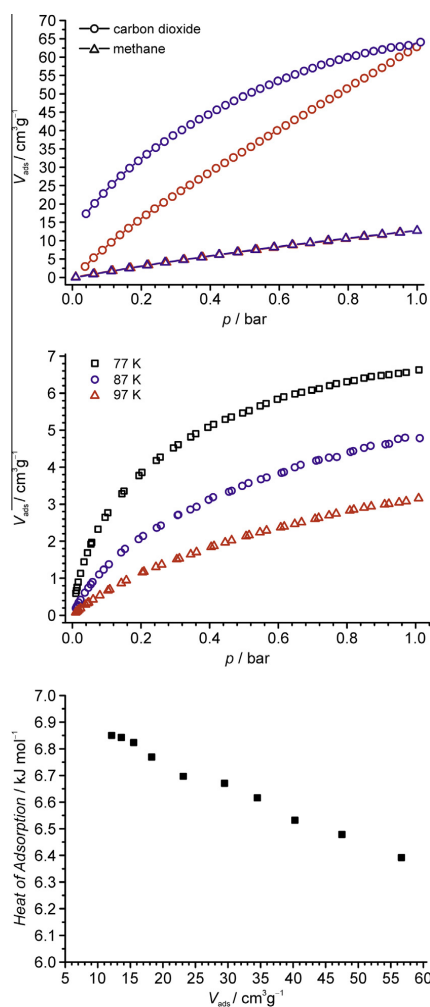
Fig. 7. Sorption behaviour of a Zr-*fum* MOF sample synthesised at 120 °C. Top: Methane sorption and carbon dioxide sorption isotherms (adsorption and desorption are highlighted in red and blue, respectively). Centre: hydrogen sorption isotherms measured at different temperatures. Bottom: heat of adsorption for hydrogen as calculated from the data given in the centre plot. (For interpretation of the references to colour in this figure legend, the reader is referred to the web version of this article.)

Fig. 8. XRD patterns of Zr-*fum* MOF samples after stability tests in various solvents. The samples were synthesised at 120 °C with a modulator concentration of 70 eq formic acid. They were stirred in the various solvents and solvent mixtures at room temperature or, where indicated, at 80 °C.
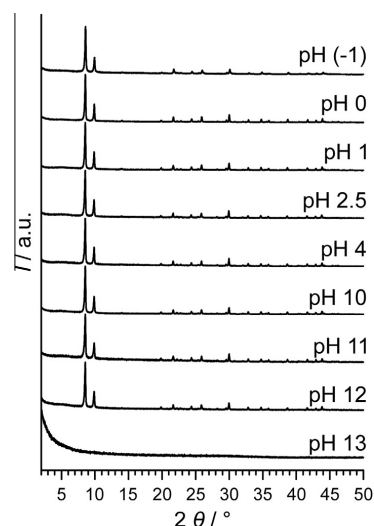
Fig. 9. XRD patterns of Zr-*fum* MOF samples after stability tests at various pH values. The samples were synthesised from water at 120 °C with a modulator concentration of 70 eq formic acid. They were stirred at room temperature and the adjustment of the pH was performed before the MOF sample was added.

to a significant degree in any of the various media. In addition, we analysed the recovered powders by XRD, revealing that the MOFs were structurally still intact (Fig. 8).

Furthermore, we tested the stability of Zr-*fum* MOF at different pH values between −1 and 13. The pH values were adjusted by using hydrochloric acid and sodium hydroxide solutions. Here, no significant loss of the mass of the samples was found after recovering them, except for the samples treated at pH 12 and pH 13. As the XRD patterns show (Fig. 9), the Zr-*fum* MOF structure is maintained from pH 1–12. At pH 13, full destruction of the crystallinity is obvious. The accompanied mass loss of 40–50% concerning the samples treated at high pH values implies that the deconstruction
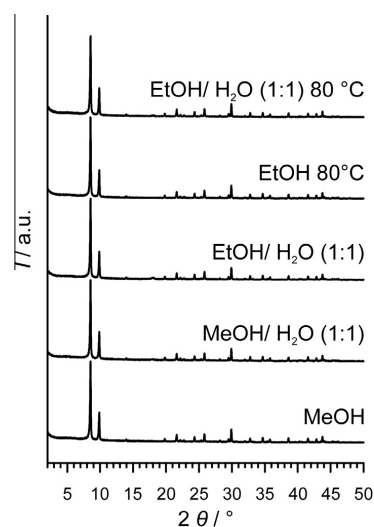
of the Zr-*fum* MOF starts at around a pH of 12. Kandiah and co-workers had reported that UiO-66 as well as its derivatives with tagged linkers also show a very high resistance towards similar chemical treatment [24]. A possible mechanism concerning the destruction of the framework under harsh alkaline conditions was proposed recently by the group of Walton [25]. The alkaline environment causes a structural breakdown presumably via a

nucleophilic attack of hydroxyl groups at the metal centres which might result in the condensation of the IBUs, as it was reported earlier for zirconium hydroxide [26].

4. Conclusions

This paper describes the modulated synthesis of the Zr-fumarate MOF from aqueous systems at 120 °C as well as at room temperature. By applying monocarboxylic acids as modulating agents highly crystalline materials were obtained. Concerning the influence of the chain length of the modulator at 120 °C, smaller particles can be synthesised at equivalent amounts of monocarboxylic acid when using propionic acid in comparison to formic acid. This good control about the particle size is especially interesting for biomedical applications due to the high sensitivity of biological systems to the actual size of nanoparticles. For example, passage of nanoparticles through vessel walls or their uptake by cells are ultimately governed by the particle size.

Samples synthesised with formic acid as modulating agent were further characterised with regard to their sorption and thermal behaviour. Similar to the Zr-*fum* MOF synthesised from DMF, the Zr-*fum* MOF obtained from water exhibits a BET surface area of 970 m^2 g^{-1} and micropores in the range of 5–7 Å. Interestingly, the Zr-*fum* MOF with its small pore entrances shows different sorption behaviour for carbon dioxide and methane. The thermal stability of the Zr-fumarate MOF can be assigned to 300 °C as proven by thermogravimetric analysis and temperature-variable X-ray diffraction. Compared to the synthesis in DMF, the water-based synthesis is advantageous in every respect, because neither the crystallinity nor the porosity of the material is decreased. The reaction conditions are less complex and less time-consuming as the solvent water is non-toxic and no additional purification steps like a Soxhlet-extraction (obligatory to remove DMF from the pores after a synthesis in DMF) is necessary to activate the sample. Furthermore, the Zr-*fum* MOF shows exceptional stability against acidic and alkaline solutions as well as against various solvents and solvent mixtures, even at higher temperatures.

As we have shown in this work, the Zr-*fum* MOF is a porous coordination polymer that can be simply prepared using a benign synthesis procedure. The compound is highly stable and offers many interesting properties, especially for the adsorption of small molecules.

Acknowledgements

Appendix A. Supplementary data

Supplementary data associated with this article can be found, in the online version, at http://dx.doi.org/10.1016/j.micromeso.2014.10.034.

References

[1] J.H. Cavka, S. Jakobsen, U. Olsbye, N. Guillou, C. Lamberti, S. Bordiga, K.P. Lillerud, J. Am. Chem. Soc. 130 (2008) 13850–13851.
[2] L. Valenzano, B. Civalleri, S. Chavan, S. Bordiga, M.H. Nilsen, S. Jakobsen, K.P. Lillerud, C. Lamberti, Chem. Mater. 23 (2011) 1700–1718.
[3] T. Tsuruoka, S. Furukawa, Y. Takashima, K. Yoshida, S. Isoda, S. Kitagawa, Angew. Chem. 121 (2009) 4833–4837. Angew. Chem. Int. Ed. 48 (2009) 4739–4743.
[4] S. Diring, S. Furukawa, Y. Takashima, T. Tsuruoka, S. Kitagawa, Chem. Mater. 22 (2010) 4531–4538.
[5] A. Schaate, P. Roy, A. Godt, J. Lippke, F. Waltz, M. Wiebcke, P. Behrens, Chem. Eur. J. 17 (2011) 6643–6651.
[6] A. Schaate, S. Dühnen, G. Platz, S. Lilienthal, A.M. Schneider, P. Behrens, Eur. J. Inorg. Chem. (2012) 790–796.
[7] A. Schaate, P. Roy, T. Preuße, S.J. Lohmeier, A. Godt, P. Behrens, Chem. Eur. J. 17 (2011) 9320–9325.
[8] G. Wißmann, A. Schaate, S. Lilienthal, I. Bremer, A.M. Schneider, P. Behrens, Microporous Mesoporous Mater. 152 (2012) 64–70.
[9] J. Cravillon, C.A. Schröder, H. Bux, A. Rothkirch, J. Caro, M. Wiebcke, CrystEngComm 14 (2012) 492–498.
[10] H. Furukawa, F. Gándara, Y.-B. Zahng, J. Jiang, W.L. Queen, M.R. Hudson, O.M. Yaghi, J. Am. Chem. Soc. 136 (11) (2014) 4369–4381.
[11] M. Gaab, N. Trukhan, S. Maurer, R. Gummaraju, U. Müller, Microporous Mesoporous Mater. 157 (2012) 131–136.
[12] I. Senkovska, F. Hoffmann, M. Fröba, J. Getzschmann, W. Böhlmann, S. Kaskel, Microporous Mesoporous Mater. 122 (2009) 93–98.
[13] S. Bauer, C. Serre, T. Devic, P. Horcajada, J. Marrot, G. Férey, N. Stock, Inorg. Chem. 47 (2008) 7568–7576.
[14] T. Loiseau, C. Mellot-Draznieks, H. Muguerrra, G. Férey, M. Haouas, F. Taulelle, C.R. Chimie 8 (2005) 765–772.
[15] S.H. Jhung, J.-H. Lee, J.W. Yoon, C. Serre, G. Férey, J.-S. Chang, Adv. Mater. 19 (2007) 121–124.
[16] P. Horcajada, T. Chalati, C. Serre, B. Gillet, C. Sebrie, T. Baati, J.F. Eubank, D. Heurtaux, P. Clayette, C. Kreuz, J.-S. Chang, Y.K. Hwang, V. Marsaud, P.-N. Bories, L. Cynober, S. Gil, G. Férey, P. Couvreur, R. Gref, Nat. Mater. 9 (2010) 172–178.
[17] K.S. Walton, R.Q. Snurr, J. Am. Chem. Soc. 129 (2007) 8552–8556.
[18] Y.-S. Bae, A.O. Yazaydın, R.Q. Snurr, Langmuir 26 (2010) 5475–5483.
[19] G. Zahn, P. Zerner, J. Lippke, F.L. Kempf, S. Lilienthal, C.A. Schröder, A.M. Schneider, P. Behrens, CrystEngComm 16 (2014) 9198–9207.
[20] B. Schmitz, U. Müller, N. Trukhan, M. Schubert, G. Férey, M. Hirscher, ChemPhysChem 9 (2008) 2181–2184.
[21] J.L.C. Rowsell, J. Eckert, O.M. Yaghi, J. Am. Chem. Soc. 127 (2005) 14904–14910.
[22] V.K. Peterson, Y. Liu, C.M. Brown, C.J. Kepert, J. Am. Chem. Soc. 128 (2006) 15578–15579.
[23] K. Sumida, J.-H. Her, M. Dincă, L.J. Murray, J.M. Schloss, C.J. Pierce, B.A. Thompson, S.A. FitzGerald, C.M. Brown, G.R. Long, J. Phys. Chem. C 115 (2011) 8414–8421.
[24] M. Kandiah, M.H. Nilsen, S. Usseglio, S. Jakobsen, U. Olsbye, M. Tilset, C. Larabi, E.A. Quadrelli, F. Bonino, K.P. Lillerud, Chem. Mater. 22 (2010) 6632–6640.
[25] J. DeCoste, G. Peterson, H. Jasuja, T.G. Glover, Y. Huang, K.S. Walton, J. Mater. Chem. A 1 (2013) 5642–5650.
[26] P.D. Southon, J.R. Bartlett, J.L. Woolfrey, B. Ben-Nissan, Chem. Mater. 14 (2002) 4313–4319.

3.3   Insight into the mechanism of modulated syntheses: *In situ* synchrotron diffraction studies on the formation of Zr-fumarate MOF

Gesa Zahn, Philip Zerner, Jann Lippke, Fabian L. Kempf, Sebastian Lilienthal, Christian A. Schröder, Andreas M. Schneider, Peter Behrens

(The first two authors contributed equally to this study.)

The final publication is available at

http://pubs.rsc.org/en/Content/ArticleLanding/2014/CE/C4CE01095G#!divAbstract

Preface

This work describes *in situ* crystallisation studies of the Zr-fumarate MOF from DMF- as well as from water-based systems. For this purpose, energy dispersive X-ray diffraction (EDXRD) measurements were performed at a synchrotron source to benefit from highly intense radiation and fast data collection. The data were evaluated according to the formalisms of GUALTIERI and − for better comparison to other MOF crystallisation behaviours − to AVRAMI-EROFEEV and SHARP-HANCOCK. Concerning the water-based synthesis, addition of formic acid decelerated the reaction rate drastically as expected. In contrast to that, the authors revealed a contradictory behaviour in the DMF-based synthesis. Here, addition of commercially available formic acid resulted in an acceleration of the reaction. Further *in situ* experiments with a varying water content, but constant concentration of modulator unravelled the crucial role of water present in the synthesis. The more water was added to the synthesis, the faster the crystallisation occurred. Thus, the acceleration of the reaction rate in the DMF-based system by increasing the amount of modulator could be traced back to the small amount of water that is present in the commercially available formic acid. This work disclosed the presence of a coordination modulation mechanism in which a monocarboxylic acid competes with the linking dicarboxylate for the coordination sites of the zirconium ions and therefore decelerates the reaction rate. Furthermore, a deprotonation modulation mechanism could be excluded, because in this case addition of a modulator should enhance the crystallisation.

All data were collected at DESY (Deutsches Elektronen-Synchrotron), in Hamburg, Germany at the now closed DORIS III ring at Hasylab. To take advantage of the highly competitive, but limited beamtime JANN LIPPKE, FABIAN L. KEMPF, SEBASTIAN LILIENTHAL and Dr. CHRISTIAN A. SCHRÖDER were involved in the experiments and the data collection. The author of this thesis and PHILIP ZERNER evaluated the data and contributed equally to this publication. Data evaluation was guided by Dr. ANDREAS M. SCHNEIDER. Prof. Dr. PETER BEHRENS initiated and guided this study. The author of this thesis and PHILIP ZERNER wrote the initial manuscript which was refined together with Dr. ANDREAS M. SCHNEIDER and Prof. Dr. PETER BEHRENS.

CrystEngComm

Cite this: *CrystEngComm*, 2014, **16**, 9198

Insight into the mechanism of modulated syntheses: *in situ* synchrotron diffraction studies on the formation of Zr-fumarate MOF†

Gesa Zahn,‡ Philip Zerner,‡ Jann Lippke, Fabian L. Kempf, Sebastian Lilienthal, Christian A. Schröder, Andreas M. Schneider and Peter Behrens*

In this work, the formation of a Zr-based metal–organic framework (MOF), Zr-fumarate MOF (Zr-*fum* MOF), is studied *in situ* by energy-dispersive diffraction. The Zr-*fum* MOF can be synthesised in DMF as well as in water-based synthesis systems. In both cases, its formation requires modulation, *i.e.* a monocarboxylic acid which is used as the modulator has to be added to the synthesis mixture. In general, different mechanisms of modulation are possible, for example, deprotonation of the linker molecule (deprotonation modulation) or coordination modulation (wherein the molecules of the modulator compete with the linker molecules for the coordination sites at the inorganic building units). Independently of the specific mechanism, modulation often improves the reproducibility of the MOF synthesis and the crystallinity of the product and may be used to control crystal size and morphology. This study is the first to investigate the kinetics of modulated MOF syntheses with regard to coordination modulation. According to this concept, the addition of a modulator usually decelerates the reaction. Our kinetic investigations show that this is the case for the formation of Zr-*fum* MOF in the water-based synthesis with formic acid used as a modulator. On the contrary, the addition of formic acid to the DMF-based synthesis results in an accelerating effect. This unexpected effect can be attributed to a small amount of water present in formic acid. Correspondingly, the addition of water to the synthesis mixture also showed an accelerating effect. These investigations emphasise the subtle interplay of the different ingredients in a MOF synthesis. In the case of the Zr-*fum* MOF, both the modulator formic acid and the water content strongly affect the kinetics of crystallisation. Quantitative evaluation of the kinetic data using the Gualtieri equation provides additional insight into the mechanisms of coordination-modulated MOF formation reactions and excludes the idea of deprotonation modulation.

1 Introduction

In recent years, metal–organic frameworks (MOFs) or porous coordination polymers (PCPs) have been the focus of intensive research. The porous network and the associated high surface areas as well as the wide variability in chemical functions have demonstrated MOFs as a novel class of fascinating materials for various applications such as gas storage,[1] separation,[2–4] catalysis,[2–4] sensing,[5] and drug delivery systems.[6,7] Although a large number of MOFs have been synthesised so far,[8] the crystallisation process has rarely been investigated.

Institut für Anorganische Chemie, Leibniz Universität Hannover, Callinstr. 9, 30167 Hannover, Germany. E-mail: Peter.Behrens@acb.uni-hannover.de, Gesa.Wissmann@acb.uni-hannover.de, Philip.Zerner@acb.uni-hannover.de; Fax: +49 511 7623006; Tel: +49 511 7623660, +49 511 76219177, +49 511 7625187
† Electronic supplementary information (ESI) available: Discussion of data evaluation methods, data of additional kinetic analysis, and powder XRD pattern. See DOI: 10.1039/c4ce01095g
‡ These two authors contributed equally to this study.

Correspondingly, details of the reaction and crystallisation mechanisms have remained rather unexplored, and the conditions for the synthesis of a certain MOF are often determined by undirected explorative work. This lack of knowledge also hampers the preparation of MOFs in certain shapes like nanoparticles, single crystals, or thin films, *etc.* as well as the fabrication of composites, although this shape control is often important for applications.

The crystallisation behaviour of MOFs depends strongly on the reaction conditions like temperature, concentration of the reactants and the solvent chosen. Another interesting way to influence the outcome of a MOF synthesis is the application of modulation. In such modulated syntheses, a modulating agent – usually a monocarboxylic acid – is added to the reaction mixture. Previous studies on the synthesis of Zr-based MOFs have shown that modulation enhances the reproducibility of the synthesis and can increase the crystallinity of the products. In some cases, modulation allows control of the shape[11] and the size of the formed crystals,[12]

ranging from nanoparticles to single crystals.[13] It is worth noting that some Zr-based MOFs we have prepared are only accessible when modulation is applied.[9,14,15]

In general, different modulation mechanisms are conceivable. In deprotonation modulation, the modulator enhances the deprotonation of linker molecules (*i.e.* it acts as a base), thus facilitating the attachment of linker molecules to the inorganic building units (IBUs); consequently, the formation of a MOF framework is accelerated. This was shown to be the case in the synthesis of ZIF-8 with formic acid as the modulator.[22] In coordination modulation, the modulator competes with the linker molecules for the coordination sites at the IBUs as proposed in the first applications of modulated syntheses.[11,12] In this way, the formation of amorphous precursors or zirconia gel in the beginning of the reaction is avoided. Nucleation and growth can then occur from dissolved species but proceed at a reduced rate due to the necessary exchange of the coordinated modulator with bridging linker molecules, *i.e.* reaction rates are decreased. Correspondingly, also the number of nuclei formed is small; these can grow to larger crystals, explaining the size control.

As the only prior kinetic study on modulated MOF syntheses[22] revealed a deprotonation modulation mechanism, we have performed the present study on the kinetics of the crystallisation of the Zr-fumarate MOF (Zr-*fum* MOF). This MOF can be synthesised in different solvent systems, namely, in DMF[9] and in water.[10] In both cases, it is necessary to apply the so-called modulation approach; there were indications in these syntheses that a coordination modulation mechanism is operative.[11,12]

In fact, the expected reduction in the reaction rate was observed qualitatively in the synthesis of different Zr-based MOFs.[13,15] In contrast, the crystallisation of the Zr-*fum* MOF from DMF was surprisingly accelerated when the amount of the modulator formic acid was increased.[9] Other experiments by our group on the synthesis of Zr-based MOFs have already shown that the addition of water during modulated synthesis can also influence its outcome.[9,13] Water accelerates the reaction and may even be necessary to obtain a highly crystalline product.[13] In fact, a certain minimal amount of water is absolutely necessary in order to build the inorganic building unit (IBU), as each of the $Zr_6O_4(OH)_4(CO_2)_{12}$ IBUs, which are typical of many Zr-based MOFs, contains four oxo and four hydroxo ligands.

In order to gain further insight into the mechanisms of modulated MOF syntheses, we have investigated the kinetics of the formation of the Zr-*fum* MOF, which can, as already noted above, be synthesised in DMF and in water-based solvent systems. Formic acid was chosen as the modulating agent. The kinetics were studied by *in situ* energy-dispersive X-ray diffraction (EDXRD) employing synchrotron radiation at beamline F3 at HASYLAB facility, DESY (Deutsches Elektronensynchrotron), in Hamburg, Germany.

Quantitative kinetic information is obtained because the intensity of the recorded Bragg reflections is proportional to the amount of solid that exhibits a diffraction phenomenon.[16]

Kinetic evaluations of the so-obtained data are generally performed by applying a certain model. Calculations proposed by Avrami and Erofeev,[17–19] Sharp and Hancock,[20] and Gualtieri[21] are often used to study crystallisation behaviour and growth mechanisms. Here, we have chosen to present kinetic data obtained by the analysis using the Gualtieri method (eqn (1)), which shows that the degree of crystallisation $\alpha(t)$ is dependent on the time t, the fitting parameters a and b, the rate constant of growth k_G and the dimension of growth n.

$$\alpha(t) = \frac{1}{1 + e^{-(t-a)/b}} \left[1 - e^{-(k_G \cdot t)^n} \right] \quad (1)$$

In contrast to the Avrami–Erofeev equation and the Sharp–Hancock evaluation method (which were developed for crystallisation processes in the solid state), the Gualtieri model was constructed to describe solution-mediated transformation reactions (*i.e.* crystallisation of zeolites from aqueous NaOH). It considers both relevant processes, that of nucleation ($1/(1 + \exp(-(t-a)/b))$ term in eqn (1)) and that of crystal growth ($[1 - \exp(-(k_G \cdot t)^n)]$ term), separately. Therefore, this method appears to be especially well suited to describe the crystallisation behaviour of a MOF from a solution. The choice of the preferred evaluation method is discussed in more detail in the ESI† Section S1; there, the results obtained from our data when the Avrami–Erofeev and the Sharp–Hancock methods are used are also given to have better comparison with other kinetic studies on MOF systems.

In the formalism according to Gualtieri, the total number of nuclei (which are of course not directly visible in diffraction experiments) is considered by including the fitting parameters a and b as well as the dimension of growth n and the rate constant of growth k_G.[21] These fitting parameters can define the probability of nucleation P_N, which describes the number of nuclei N present in dependence of the time t (eqn (2)), described by a Gaussian distribution, with a as the position of its maximum and b its variance.

$$P_N = \frac{dN}{dt} = e^{-\frac{(t-a)^2}{2b^2}} \quad (2)$$

Furthermore, the Gualtieri method differentiates between the rate constant of growth k_G and the rate constant of nucleation k_N, which is given as

$$k_N = \frac{1}{a} \quad (3)$$

Our investigation is the first kinetic report to study the coordination modulation synthesis of MOFs. Apart from the study on the formation of a zeolitic-imidazolate framework (ZIF) by Cravillon *et al.* investigating the deprotonation modulation of formate,[22] other studies have so far only concentrated on investigating the crystallisation of HKUST-1,[23] Fe-MIL-53,[23] Mn-MIL-100 (ref. 24) and Al-based MOFs (CAU-1 and CAU-1-(OH)$_2$).[25] There is also a study which is the first to

Paper

focus on the formation of a Zr-based MOF, UiO-66. In this study, no modulator was applied, but hydrochloric acid was used as an additive.[26]

Apart from the directly accessible rate constants, the evaluation methods mentioned above may also provide additional information on the reaction mechanism. For example, Ahnfeldt et al.[25] investigated the kinetics of Al-MOFs like CAU-1 and CAU-1-(OH)$_2$ using conventional and microwave heating. Based on their evaluation of the kinetic data, performed with the Avrami–Erofeev and the Sharp–Hancock formalisms, the authors postulated that the reaction occurs via different crystallisation mechanisms under different heating conditions. Whereas the microwave-heated reaction apparently proceeds via a diffusion-controlled mechanism (Avrami exponent $n_{AE} \approx 0.6$–0.8), conventionally heated reactions seem to proceed via a phase-boundary-controlled reaction (Avrami exponent $n_{AE} \approx 1.0$–1.1). However, the interpretation of the Avrami exponent (for a detailed discussion see the ESI,† Section S1) is not straightforward,[27] and similar Avrami exponents may be obtained as a result of different mechanisms.[28] The investigation of the synthesis of MOF-14 by Millange et al. revealed that this reaction is determined by the nucleation rate because the calculated values for k_N were, in all cases, smaller than values for k_G.[29] In another study by Millange et al., the authors could identify a metastable intermediate in the crystallisation of MIL-53(Fe).[23] Our previous qualitative observations that water might have an accelerating effect[9] are substantiated quantitatively in this publication. The crucial role of the water content was also confirmed recently by Ragon et al. who investigated the crystallisation behaviour of the Zr-based MOF UiO-66, including the addition of hydrochloric acid.[26]

2 Experimental

2.1 Time-resolved in situ X-ray diffraction experiments

Time-resolved in situ X-ray diffraction experiments were performed at the (now closed) beamline F3 at HASYLABs storage ring DORIS III at DESY in Hamburg, Germany. The ring was operated with a positron beam energy of 4.45 GeV. The beamline received white synchrotron X-ray radiation from a bending magnet with a critical energy of 16 keV. A horizontal diffractometer with a heavy load sample stage was installed at the beamline station, equipped with a liquid nitrogen-cooled Ge solid-state detector covering selectable diffraction angles from 0° to 30° 2θ. Collimator diameters were chosen between 200 and 300 μm^2. The detector angle was set to 1.9° or 2.1° 2θ.

Syntheses were carried out in sealed 7 mL Duran® borosilicate glass tubes 1 cm in diameter and equipped with magnetic stir bars. These glass tubes were filled with the reaction mixture and then placed into a circulating oil-heater constructed by the group of Prof. Bensch from the University of Kiel.[30,31] This heater consisted of an aluminium block and was heated by a thermostat via a circular oil flow. Reaction temperatures between 43 °C and 140 °C were chosen. The

measured temperatures had to remain constant for 5 minutes prior to the start of a reaction. The delay time between the moment the reaction vessel was placed in the oven and the opening of the beam shutter was about 1 minute; during that time, a thermocouple indicated that the oil bath had again attained the reaction temperature. The diffraction spectrum covered an energy range from about 10 to 60 keV. The acquisition time for a spectrum was either 30 s, 60 s or 120 s. All reactions delivered the first spectrum after the delay time plus the acquisition time. Reactions were considered complete when the growth of the Bragg reflections of the Zr-fum MOF ended in a distinct saturation level.

Real-time evaluation of the raw data was performed using the programs F3tool and F3tool_extens (versions 0.3k and 0.04, respectively) by André Rothkirch from HASYLAB. The integration was then performed using F3tool by fitting the peaks to obtain the integral intensities of the Zr Kα_1 and Kβ_1 fluorescence lines as well as the 111 and 200 Bragg reflections of the Zr-fum MOF. The intensities of the Bragg reflections were normalised to the mean values of the fluorescence lines, thus accounting for the varying ring current, and then scaled from the mean minimal to the mean maximum intensity to obtain the extent of crystallisation $\alpha(t)$, the so-called crystallisation curves. Induction times t_0 could be obtained directly from the crystallisation curves and are defined as the time when the Bragg peaks could be observed for the first time. Fitting of the crystallisation curves according to the Avrami–Erofeev and Gualtieri equations was performed using the program OriginPro 8.5 by OriginLab, and all fittings according to the Sharp–Hancock model were performed using Microsoft Excel 2007.

2.2 Scanning electron microscopy

Scanning electron microscopy (SEM) images were taken using a JEOL JSM-6700F field-emission instrument with an acceleration voltage of 2 kV and a working distance of 3 mm. All samples were dispersed in ethanol and dropped onto a polished carbon block.

2.3 Synthesis procedures

2.3.1 Synthesis of Zr-fumarate MOF in a water-based system. Zr-fumarate MOF was synthesised in a water-based system by dissolving 48.2 mg of ZrCl$_4$ (0.2 mmol, 1 eq) in 4 mL of H$_2$O (222 mmol, 1074 eq) at room temperature. To investigate the influence of the amount of the modulator, various concentrations of formic acid, 30–150 eq, were added. 72.8 mg of fumaric acid (0.6 mmol, 3 eq) were supplied as the linker. Due to its low water solubility, the fumaric acid was dispersed in the reaction mixture by shaking for approximately 2 min. All experiments were carried out at 43 °C.

2.3.2 Synthesis of Zr-fumarate MOF in a DMF-based system. 24.1 mg of ZrCl$_4$ (0.1 mmol, 1 eq) were dissolved in 4 mL of DMF (52.0 mmol, 500 eq) at room temperature. In order to investigate the temperature dependence of the kinetics of this system, 0.27 mL of formic acid (7.3 mmol, 70 eq) and

CrystEngComm

36.4 mg of fumaric acid (0.3 mmol, 3 eq) were added and mixed until a clear solution was obtained. Reactions were performed at 100 °C, 120 °C, 130 °C and 140 °C.

The influence of the amount of the modulator was tested by adding various concentrations of formic acid, 70–130 eq, and 36.4 mg of fumaric acid (0.3 mmol, 3 eq). The mixture was stirred until a clear solution was obtained. All experiments were carried out at 120 °C.

Furthermore, the influence of the water content in the DMF-based solvent system was examined by adding various amounts of water (0–70 eq) to a reaction mixture containing 24.1 mg of $ZrCl_4$ (0.1 mmol, 1 eq), in 4 mL of DMF (52.0 mmol, 500 eq), 0.27 mL of formic acid (7.3 mmol, 70 eq) and 36.4 mg of fumaric acid (0.3 mmol, 3 eq). These experiments were carried out at 100 °C.

3 Results and discussion

The synthesis in a water-based system was performed by varying the amount of formic acid as the modulator. For synthesis in the DMF-based system, the effects of reaction temperature, the amount of the modulator and the water content were investigated.

In the evaluation of all reactions studied, the intensity evolution of the first intensive 111 Bragg reflection was considered. After a short induction time where no diffracting solid could be detected, the reflections gained intensity until they reached their respective maxima. The ratio of the integrated intensities $I(t)$ and the maximum intensity I_{max} gives the extent of crystallisation $\alpha(t)$:

$$\alpha(t) = \frac{I(t)}{I_{max}} \qquad (4)$$

When $I(t)$ is equivalent to I_{max}, the end of the reaction is reached. Fig. 1 shows a contour plot (Fig. 1a), a 3D view (Fig. 1b), and a crystallisation curve $\alpha(t)$ (Fig. 1c) derived from a typical data set taken during the formation of a Zr-*fum* MOF. Measurements were taken every 2 minutes. For the measurement in Fig. 1, it can be deduced that the induction

time is about 86 min and that the maximum intensity is reached after approximately three and a half hours. In all syntheses, no other crystalline phases except Zr-*fum* MOF were observed and the phase purity of the products was subsequently proved by powder X-ray diffraction (PXRD) measurements (ESI† Section S2).

3.1 Water-based synthesis

To study the crystallisation behaviour of the Zr-*fum* MOF synthesised in the water-based system, reactions were performed at 43 °C. Reactions that were carried out at higher temperatures, *e.g.* at 120 °C, were so fast that no crystallisation curves could be recorded. In these cases the reactions were already finished when the first diffraction patterns were measured around 2 min after the start of the reaction. Thus, the decrease in the reaction temperature to 43 °C was appropriate to obtain evaluable measurement data.

To study the influence of the variation of the modulator concentration in a water-based synthesis, reactions were performed at 43 °C; 70, 100 and 150 eq of formic acid were added. With low concentrations of the modulator, the reaction is very fast; the induction times are approximately 10 and 20 min for 70 and 100 eq of formic acid, respectively. When 150 eq of formic acid are added to the reaction mixture, the induction time increases to 86 min and the plateau corresponding to the end of the crystallisation process is reached much later (Fig. 2). These results support the prevalence of a coordination modulation mechanism instead of deprotonation modulation, as the latter would result in shorter induction times by increasing the amount of the modulator.[22] Furthermore, deprotonation modulation should, in any way, play only a minor role due to the very acidic conditions caused by the hydrolysis of the Zr source. The addition of $ZrCl_4$ decreases the pH value dramatically to around 1 due to the formation of hydrochloric acid; all acids should be protonated to a very high degree under these conditions. Due to the low pH value attained after the addition of the Zr source to the synthesis mixture, no influence of the further addition of the modulating formic acid (or of the linking fumaric acid) on the pH value was found.
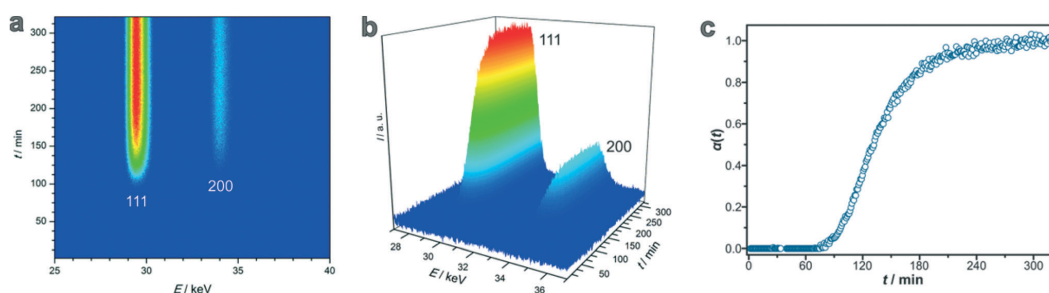

Fig. 1 Examples for the visualisation of time-resolved EDXRD data from Zr-*fum* MOF synthesis ($ZrCl_4$/H_2fum/formic acid/H_2O molar ratios of 1 : 3 : 150 : 1074 at 43 °C). The 111 and 200 Bragg reflections are visible. (a) 2D contour plot; (b) 3D view; (c) crystallisation curve $\alpha(t)$ of the 111 Bragg reflection.
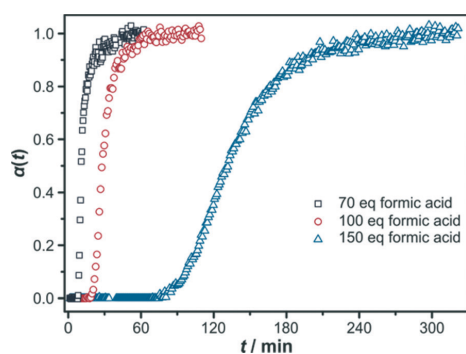
Fig. 2 Extent of crystallisation α plotted against time t. Crystallisation curves measured for syntheses of Zr-*fum* MOF in water-based systems by varying the concentration (x equivalents) of the modulator formic acid x (ZrCl$_4$/H$_2$*fum*/formic acid/water in molar ratios of 1:3:x:1074, 43 °C).

The kinetic data were analysed by applying the Gualtieri method (kinetic data obtained by the evaluation according to the Avrami–Erofeev and the Sharp–Hancock formalisms are presented in the ESI,† Section S1.1). To obtain values of the kinetic parameters, all data of the crystallisation curves were fitted with the Gualtieri equation while keeping n constant at a value of 3, corresponding to three-dimensional growth. This assumption is justified by the cubic crystal system of the Zr-*fum* MOF and the observation that the crystal habit is isometric.[21] An exemplary Gualtieri fitting including the probability of nucleation P_N is shown in Fig. 3; the kinetic parameters obtained for the different reactions are summarised in Table 1.

From these values, it can be concluded that increasing the concentration of the modulator leads to a decrease in the nucleation rate as well as in the growth rate, again substantiating the idea of a coordination modulation mechanism.
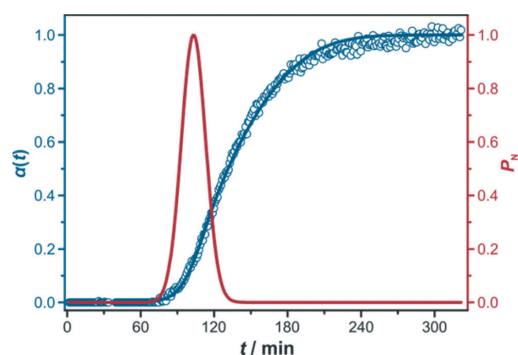

Fig. 3 Extent of crystallisation α plotted against time t (blue circles) and the corresponding Gualtieri fitting (blue curve) as well as the probability for nucleation P_N (red curve). The reaction studied here was carried out at 43 °C with ZrCl$_4$/H$_2$*fum*/formic acid/H$_2$O molar ratios of 1:3:150:1074.

Table 1 Kinetic parameters obtained by fitting of crystallisation curves with the Gualtieri equation. Crystallisation curves were measured for syntheses of Zr-*fum* MOF in water-based systems by varying the concentration (x equivalents) of the modulator formic acid (ZrCl$_4$/H$_2$*fum*/formic acid/water 1:3:x:1074, 43 °C)

x	a/min	b/min	k_G/min^{-1}	k_N/min^{-1}
70	13(5)	3(2)	0.10(7)	0.08(5)
100	19(1)	11(1)	0.038(1)	0.053(1)
150	103(1)	10(1)	0.007(1)	0.009(1)

SEM images of the products collected from the syntheses carried out at the synchrotron facility were obtained. Comparing the morphology of the samples prepared with 70 eq, 100 eq and 150 eq of formic acid (Fig. 4), it can be observed that the particle size increases with increasing amount of the modulator applied.

These results can be explained by the concept of coordination modulation, which states that both nucleation and growth rates are reduced in the presence of a modulator due to the additional equilibrium involving the exchange of modulator molecules coordinated to the metal cations with linkers. The larger the amount of modulator added to the reaction mixture, the smaller is the nucleation rate k_N; therefore, fewer nuclei grow to larger particles, albeit with a decreased growth rate k_G, allowing the formation of a highly crystalline material with well-defined particle morphologies and sizes. These insights into the coordination modulation mechanism regarding the formation of particles are in good agreement with previous qualitative observations on the Zr-*fum* MOF system.[9,10]

3.2 DMF-based synthesis

The Zr-fumarate MOF can also be synthesised in a DMF-based system. By varying the temperature of the reaction, the activation energy can be calculated. Furthermore, the effects of the modulator concentration and of the addition of water on the reaction kinetics were investigated.

3.2.1 Variation of the temperature. Zr-*fum* MOF was synthesised in a temperature range between 100 °C and 140 °C, using the same synthesis batch composition consisting of ZrCl$_4$/H$_2$*fum*/formic acid/DMF in molar ratios of 1:3:70:500. Comparing the time dependence of the extent of crystallisation $\alpha(t)$ at different temperatures (Fig. 5), it is obvious that a higher temperature leads to a faster reaction.

At 100 °C, the reaction takes about 7 hours to reach complete crystallisation, whereas at 140 °C the reaction is completed after only 1 hour. Furthermore, the induction time is significantly decreased by increasing the reaction temperature. The kinetic data were analysed by applying the Gualtieri method (results of Avrami–Erofeev and the Sharp–Hancock evaluations are given in the ESI,† Section S1.2) and are summarised in Table 2.

The calculated k values affirm the previous statement. By increasing the temperature, both k values increase as well. Gualtieri's differentiation between the rate constant of
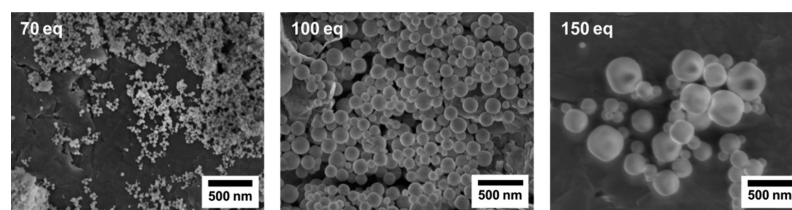
Fig. 4 SEM images of Zr-*fum* MOF samples synthesised with various concentrations of the modulator (as given in the images) in a water-based synthesis at 43 °C (ZrCl$_4$/H$_2$*fum*/formic acid/H$_2$O 1 : 3 : x : 1074).
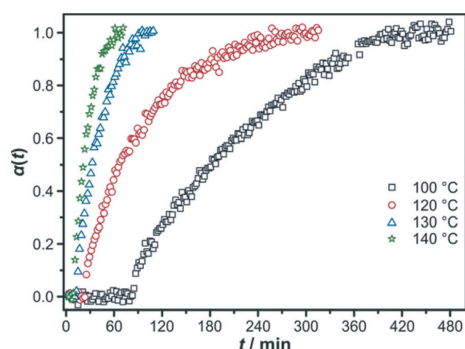

Fig. 5 Extent of crystallisation α plotted against time t. Crystallisation curves measured for syntheses of Zr-*fum* MOF in DMF-based systems by varying the temperature T (ZrCl$_4$/H$_2$*fum*/formic acid/DMF in molar ratios of 1 : 3 : 70 : 500).

Table 2 Kinetic parameters obtained by fitting of crystallisation curves with the Gualtieri equation. Crystallisation curves were measured for syntheses of Zr-*fum* MOF in DMF-based systems by varying the temperature T (ZrCl$_4$/H$_2$*fum*/formic acid/DMF 1 : 3 : 70 : 500)

T/°C	a/min	b/min	k_G/min^{-1}	k_N/min^{-1}
100	183(1)	72(1)	0.010(1)	0.005(1)
120	65(1)	53(1)	0.026(1)	0.015(1)
130	33(1)	17(1)	0.055(2)	0.031(1)
140	21(1)	11(1)	0.074(3)	0.048(1)

growth k_G and the rate constant of nucleation k_N illustrates that the time-defining step in this crystallisation process is the formation of nuclei. The calculation of the rate constants k_G and k_N at different temperatures T offers the opportunity to calculate the activation energies E_A. With the help of the corresponding Arrhenius equations (eqn (5) and (6))

$$k_G = A\,e^{-\frac{E_A(G)}{R \cdot T}} ; k_N = A\,e^{-\frac{E_A(N)}{R \cdot T}} \tag{5}$$

$$\ln k_G = \ln A - \frac{E_A(G)}{RT} ; \ln k_N = \ln A - \frac{E_A(N)}{RT} \tag{6}$$

with the gas constant R and A being the pre-exponential factor, the activation energies of nucleation and growth can

be determined. The corresponding Arrhenius plots are shown in Fig. 6. The slopes of the linear regressions give the activation energies. The values are 71 ± 3 kJ mol^{-1} for E_A(N), the activation energy of nucleation, and 66 ± 6 kJ mol^{-1} for E_A(G), the activation energy of crystal growth.

The calculated activation energies of nucleation and growth thus do not deviate much from each other, both being around 70 kJ mol^{-1}. It is tempting to speculate that both energies reflect the same chemical reaction, namely, the exchange of a modulator ligand on a Zr atom with a bridging linker, a reaction which should not be significantly influenced by the type of entity on which it occurs, *i.e.* on a small forming nucleus or on a large growing crystal.

In general, the observed values are in good agreement with the activation energies observed in the crystallisation of other MOFs, like ZIF-8 (69 kJ mol^{-1} for E_A(N), 72 kJ mol^{-1} for E_A(G))[22] and HKUST-1 (72 kJ mol^{-1} for E_A(N), 64 kJ mol^{-1} for E_A(G)).[29] In the case of Zr-fumarate MOF and HKUST-1 formation, nucleation seems to be the rate-limiting step, whereas in the ZIF-8 system, it is apparently crystal growth. MOF-14 (114 kJ mol^{-1} for E_A(N), 83 kJ mol^{-1} for E_A(G))[29] and Mn-MIL-100 (127 kJ mol^{-1} for E_A(N), 99 kJ mol^{-1} for E_A(G))[24] show somewhat higher activation energies; in these cases, again nucleation seems to limit the reaction rate. A very
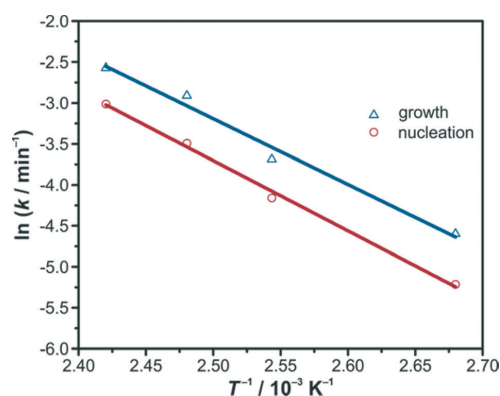

Fig. 6 Arrhenius plots for the temperature-dependent rate constants of growth (blue triangles) and nucleation (red circles) obtained from the Gualtieri evaluation.

recent study demonstrated that for unmodulated syntheses of the Zr-based MOF UiO-66 the activation energies are much lower.[26] Depending on the Zr source used and the amount of hydrochloric acid added to the reaction mixture, the values for $E_A(N)$ vary from 11 kJ mol^{-1} to 39 kJ mol^{-1} and for $E_A(G)$ between 19 kJ mol^{-1} and 46 kJ mol^{-1}; all values indicate that growth is the rate-limiting step. Overall, these results strongly suggest that the formation reactions of different MOFs can deliver variable results and strongly depend on the composition of the reaction mixture; comparisons are therefore difficult.

SEM images (Fig. 7) show that the temperature variation only slightly affects the crystal size of the particles. There appears to be a slight increase in the average particle size with increasing temperature, ranging from *ca.* 100 nm to *ca.* 200 nm. As the amount of modulator is the same in all syntheses, the fact only a slight variation of crystallite size is observed is not unexpected. It is accompanied by the disappearance of smaller particles. The SEM images also show that with increasing temperature, the crystallites tend to exhibit more strongly pronounced faces. All these observations are in line with crystal ripening processes, which proceed faster at higher temperatures due to the increased solubility of the particles. The faces formed are (111) faces, obviously the energetically most favourable ones, as Zr-*fum* MOF crystals typically exhibit octahedral shapes.

3.2.2 Variation of the amount of the modulator. Similarly, reactions were carried out at 120 °C with variation of the amounts of formic acid as the modulator (ZrCl$_4$/H$_2$*fum*/formic acid/DMF 1:3:x:500, 30 ≤ x ≤ 130). Experiments performed with 30 eq and 50 eq of formic acid result in a precipitation of the solid on the glass tube walls and were therefore not considered for further evaluation. Only the reactions with 70 eq, 100 eq and 130 eq of the modulator provided reliable results. The influence of the modulator on the time-dependent extent of crystallisation can be seen in Fig. 8.

The induction time is, in all cases, approximately 20 minutes. Thus, the amount of the modulator does not have an apparent influence on the first precipitation steps in a DMF-based synthesis. This might be an indication of a heterogeneous nucleation process at the glass walls, which is not significantly affected by the modulator. To further rationalise this idea, one has to take into account that the surface chemistry of the glass walls might change by the addition of
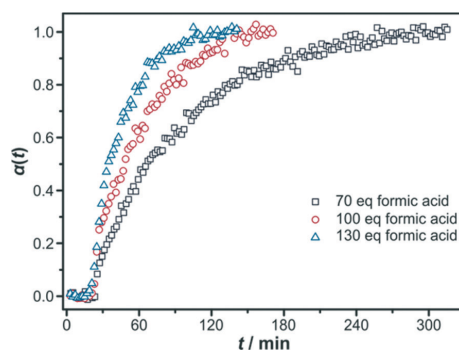

Fig. 8 Extent of crystallisation α plotted against time t. Crystallisation curves measured for syntheses of Zr-*fum* MOF in DMF-based systems by varying the concentration (x equivalents) of the modulator formic acid x (ZrCl$_4$/H$_2$*fum*/formic acid/DMF in molar ratios of 1:3:x:500, 120 °C).

various amounts of the modulator, either by protonation of surface-standing silanol groups or by adsorption of modulator molecules. When only small concentrations of the modulator are present, the glass surface is active and nucleation and crystal growth take place there (as observed when 30 or 50 eq of modulator are added). When the reaction mixture contains 70 eq (or more) of formic acid, nucleation might take place at still active sites on the glass walls; however, crystal growth occurs in the solution.

A surprising fact is observed concerning crystal growth following nucleation: generation of the Zr-*fum* MOF product is faster and ends earlier the more formic acid is added to the reaction mixture; *i.e.* the behaviour contradicts the classical action of a modulator as observed in the water-based system and as rationalised by the coordination modulation concept. In contrast to the water-based synthesis (Section 3.1), where the addition of formic acid decelerated the reaction, the addition of formic acid increases the reaction rates in the DMF-based synthesis. This contradictory behaviour has been described before on a qualitative basis.[9] We ascribe this finding to the accelerating effect of water. Commercially available formic acid contains approximately 2–2.5% of water as the stabiliser. By increasing the amount of this formic acid in the synthesis, the water content is also concomitantly increased,
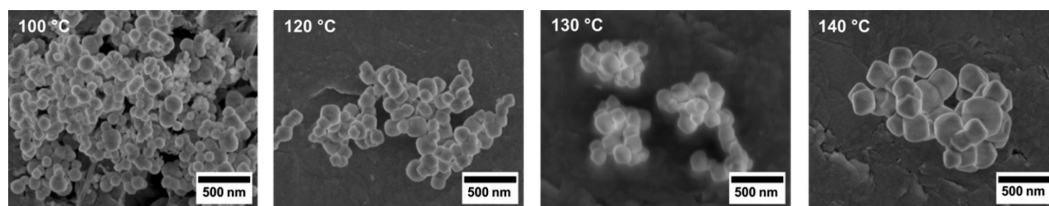

Fig. 7 SEM images of Zr-fumarate MOF synthesised at various temperatures (as given in the images) in a DMF-based synthesis (ZrCl$_4$/H$_2$*fum*/formic acid/DMF 1:3:70:500).

CrystEngComm

explaining the obtained results. The acceleration of the formation of Zr-based MOFs in DMF by the addition of water has been described before[9] and has recently been quantified by kinetic studies on the formation of UiO-66 (ref. 26) in DMF with various amounts of added water but without any modulator. For the formation of the Zr-*fum* MOF in DMF, a similar study is presented in Section 3.2.3, substantiating the mentioned hypothesis that adding formic acid accelerates the reaction due to its water content. In water-based synthesis, the water content of the commercially available formic acid does not play a role because water is present in large excess.

The quantitative results, obtained using the Gualtieri evaluation method, of these kinetic results are shown in Table 3 (for the results from Avrami–Erofeev and Sharp–Hancock evaluations, see the ESI,† Section S1.3). It can be seen that the rate constants only slightly increase by increasing the amount of formic acid x from $k \approx 0.01$–0.02 (70 eq of formic acid) to $k \approx 0.03$–0.04 (130 eq of formic acid). This appears reasonable as this is not an effect of the formic acid itself but of the small amounts of concomitantly added water. The differentiation between k_G and k_N reveals that during the formation of the Zr-fumarate MOF under these conditions, nucleation is probably the rate-determining step.

For this system, the kinetic data show that the decelerating action of the modulator molecules is outshone by the water concomitantly introduced by their addition. The strong sensitivity of the reaction to the presence of small amounts of water is not surprising, as the $ZrCl_4$ precursor molecules have to be hydrolysed in order to be able to form the inorganic building units of the MOF structure. A similar sensitivity to the presence of small amounts of water is observed in, for example, sol–gel processes starting from alcoholates and

being carried out in the corresponding alcohol. That the modulator is working nevertheless, in spite of the contradictory kinetic data, becomes clear upon inspection of the SEM pictures of the formed products. These show that the particle sizes increased with increasing amounts of added formic acid (Fig. 9). Taking this into account, a mechanism emerges where the water introduced generally accelerates the reaction by supplying higher quantities of hydrolysed zirconium species. The construction of the MOF framework, however, is still governed by the intermittent coordination of formic acid molecules to the zirconium ions.

3.2.3 Variation of the water content. To confirm the assumption that water introduced together with the formic acid is responsible for the more rapid formation of the Zr-*fum* MOF with increasing modulator concentration, the influence of the water content on a coordination-modulated synthesis has been investigated independently by *in situ* EDXRD measurements. For this purpose, reactions were carried out in DMF at constant temperature (100 °C) and at a constant modulator concentration ($ZrCl_4/H_2fum$/formic acid/DMF $1:3:70:500$). Additionally, a defined amount of water ($0 \leq x \leq 70$ eq) was added to the reaction mixture to investigate whether the water content influences the reaction rate. As a guideline, the amount of water added with formic acid inevitably corresponds to 3.7 eq of H_2O when the amount of formic acid is 70 eq and is thus very small under these conditions. The recorded crystallisation curves, as depicted in Fig. 10, indeed show a remarkable effect of the water content.

Without any additional water the precipitation of the resulting product starts after approximately 100 min. The reaction is quite sluggish and finishes after 9 hours. By adding only 5 eq of water, the induction time is more than halved, and by increasing the water content to 30 eq or even 70 eq the induction time is reduced dramatically (7 minutes and 3 minutes, respectively), although the modulator is still present in the reaction mixture. Thus, the reaction becomes faster the more water is added. These results can be quantified by analysis with the Gualtieri evaluation (Table 4; for data from Avrami–Erofeev and Sharp–Hancock evaluations see the ESI,† Section S1.4).

All k values strongly increase. By adding 70 eq of water, the rate constants increase by two orders of magnitude compared to synthesis without any additional water. This result

Table 3 Kinetic parameters obtained by fitting of crystallisation curves with the Gualtieri equation. Crystallisation curves were measured for syntheses of Zr-*fum* MOF in DMF-based systems by varying the concentration (x equivalents) of the modulator formic acid ($ZrCl_4/H_2fum$/formic acid/DMF $1:3:x:500$, 120 °C)

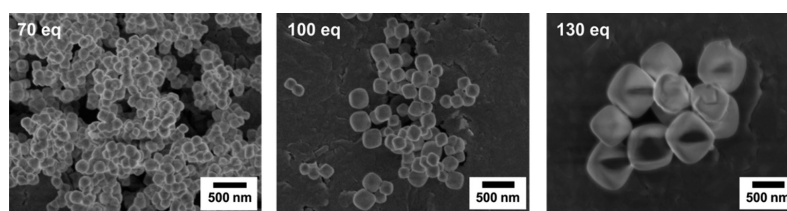| x	a/min	b/min	k_G/min^{-1}	k_N/min^{-1}
70	65(1)	53(1)	0.026(1)	0.015(1)
100	46(1)	28(1)	0.035(1)	0.022(1)
130	32(2)	20(1)	0.036(1)	0.031(2)

Fig. 9 SEM images obtained from Zr-fumarate MOF synthesised with various amounts of formic acid in a DMF-based synthesis ($ZrCl_4/H_2fum$/formic acid/DMF $1:3:x:500$) at 120 °C.
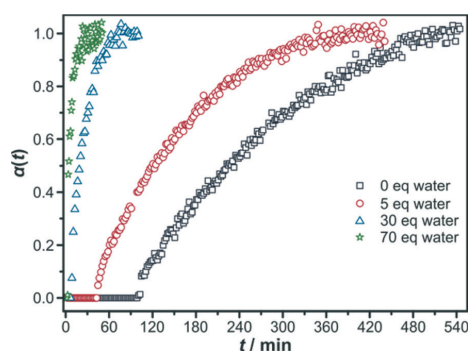
Fig. 10 Extent of crystallisation α plotted against time t. Crystallisation curves measured for syntheses of Zr-*fum* MOF in DMF-based systems by varying the concentration (x equivalents) of the water content (ZrCl$_4$/H$_2$*fum*/formic acid/water/DMF in molar ratios of 1:3:70:x:500, 100 °C).

Table 4 Kinetic parameters obtained by fitting of crystallisation curves with the Gualtieri equation. Crystallisation curves were measured for syntheses of Zr-*fum* MOF in DMF-based systems by varying the concentration (x equivalents) of the water content (ZrCl$_4$/H$_2$*fum*/formic acid/water/DMF 1:3:70:x:500, 100 °C)

x	a/min	b/min	k_G/min^{-1}	k_N/min^{-1}
0	226(1)	89(1)	0.008(1)	0.004(1)
5	123(2)	67(2)	0.016(1)	0.008(1)
30	19(1)	13(1)	0.091(4)	0.053(1)
70	2(1)	6 (1)	0.26(2)	0.5(5)

is confirmed by SEM images (Fig. 11). It is found that the water content strongly influences the particle size as well. The particle size becomes smaller the more water is added to the reaction mixture. Without any additional water, the particle size is around 100 nm, whereas it decreases to around 20 nm when 70 eq of water are used. When the decelerating effect of the modulator is constant, an increase in the water content leads to faster formation of more nuclei. Since the amount of reactants remains constant throughout the experiments, these can grow only to small particles.

All findings concerning the influence of water on the DMF-based modulated synthesis confirm the enormous bearing of water on the crystallisation behaviour. It has become

clear that even small amounts of water as introduced by addition of formic acid to an otherwise water-free synthesis mixture has a notable influence on the reaction rate, as described in Section 3.2.2.

4 Conclusions

In this work we have investigated the crystallisation behaviour of the Zr-fumarate MOF from a water-based as well as in a DMF-based system in modulated synthesis. By applying energy-dispersive diffraction, the formation of the Zr-fumarate MOF was monitored *in situ* revealing a coordination modulation mechanism. Concerning the water-based synthesis, the modulating effect of the formic acid led to a deceleration of the reaction while the induction time increased. The higher the amount of the modulator added to the synthesis mixture, the slower the reaction proceeded. This result is in line with the concept of coordination modulation where the molecules of the modulator compete with the linker molecules for the coordination sites at the metal atoms.

On the contrary, in the DMF-based synthesis, the reaction is accelerated by increasing the amount of formic acid added. This effect can be attributed to the water content of the formic acid which is concomitantly added to the reaction mixture. This low water content of the commercially available formic acid becomes crucial when the reaction is performed in an organic solvent. Investigations concerning the influence of the water content in a DMF-based system proved that water has indeed a strong accelerating effect on the formation of the Zr-fumarate MOF. These findings show that MOF syntheses are very sensitive to the actual composition of the reaction batch and to the reaction conditions.

Quantitative evaluation of the measured data according to the Gualtieri equation[21] gives further insight into the mechanism of modulated reactions. It implies that in most cases the nucleation process is the rate-limiting mechanism, as $k_N < k_G$. When induction times are insensitive to the variation of the reaction conditions, as is the case in the synthesis of Zr-*fum* MOF in DMF-based systems by varying the modulator concentration, this can be an indication of heterogeneous nucleation, which is indeed directly observed in this system at a small modulator concentration (crystallisation on the glass walls of the container). The finding that the activation energies for nucleation and growth are very similar, as
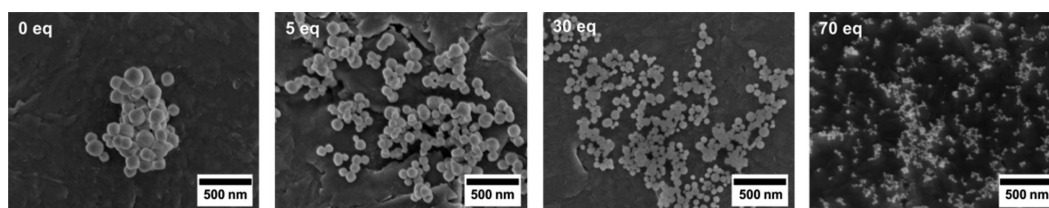

Fig. 11 SEM images obtained from Zr-fumarate MOF synthesised with various amounts of water x added to a DMF-based synthesis (ZrCl$_4$/H$_2$*fum*/formic acid/water/DMF 1:3:70:x:500, 100 °C).

CrystEngComm Paper

observed in the study of the reaction in the DMF-based system at variable temperatures, might be due to a coincidence, but does fit well to the concept of coordination modulation, which implies that nucleation and growth proceed *via* exchange of modulator molecules to linkers. A corresponding temperature-variable study on the reaction taking place in water would be very interesting.

Clearly, more kinetic studies on the formation of MOFs are necessary. Unfortunately, timely access to corresponding high-level experiments at synchrotron beamlines is difficult.

Finally, our investigations suggest that the Gualtieri equation appears to be well suited for the evaluation of kinetic data from reactions where a solid is formed from a liquid solution.

Acknowledgements

Notes and references

1 M. Eddaoudi, J. Kim, N. Rosi, D. Vodak, J. Wachter, M. O'Keeffe and O. M. Yaghi, *Science*, 2002, **295**, 469.

2 S. T. Meek, J. A. Greathouse and M. D. Allendorf, *Adv. Mater.*, 2011, **23**, 249.

3 H.-L. Jiang and Q. Xu, *Chem. Commun.*, 2011, **47**, 3351.

4 A. U. Czaja, N. Trukhan and U. Müller, *Chem. Soc. Rev.*, 2009, **38**, 1284.

5 S. Achmann, G. Hagen, J. Kita, I. M. Malkowsky, C. Kiener and R. Moos, *Sensors*, 2009, **9**, 1574.

6 S. Keskin and S. Kızılel, *Ind. Eng. Chem. Res.*, 2011, **50**, 1799.

7 P. Horcajada, R. Gref, T. Baati, P. K. Allan, G. Maurin, P. Couvreur, G. Férey, R. E. Morris and C. Serre, *Chem. Rev.*, 2012, **112**, 1232.

8 H. Furukawa, K. E. Cordova, M. O'Keeffe and O. M. Yaghi, *Science*, 2013, **341**, 974.

9 G. Wißmann, A. Schaate, S. Lilienthal, I. Bremer, A. M. Schneider and P. Behrens, *Microporous Mesoporous Mater.*, 2012, **152**, 64.

10 G. Wißmann, H. A. Schulze, J. Lippke, S. König, U. Sazama, M. Fröba and P. Behrens, *Microporous Mesoporous Mater.*, submitted.

11 T. Tsuruoka, S. Furukawa, Y. Takashima, K. Yoshida, S. Isoda and S. Kitagawa, *Angew. Chem.*, 2009, **121**, 4833 (*Angew. Chem., Int. Ed.*, 2009, **48**, 4739).

12 S. Diring, S. Furukawa, Y. Takashima, T. Tsuruoka and S. Kitagawa, *Chem. Mater.*, 2010, **22**, 4531.

13 A. Schaate, P. Roy, A. Godt, J. Lippke, F. Waltz, M. Wiebcke and P. Behrens, *Chem. – Eur. J.*, 2011, **17**, 6643.

14 A. Schaate, P. Roy, T. Preuße, S. J. Lohmeier, A. Godt and P. Behrens, *Chem. – Eur. J.*, 2011, **17**, 9320.

15 A. Schaate, S. Dühnen, G. Platz, S. Lilienthal, A. M. Schneider and P. Behrens, *Eur. J. Inorg. Chem.*, 2012, 790.

16 R. I. Walton and D. O'Hare, *Chem. Commun.*, 2000, 2283.

17 M. Avrami, *J. Chem. Phys.*, 1939, **7**, 1103.

18 M. Avrami, *J. Chem. Phys.*, 1940, **8**, 212.

19 M. Avrami, *J. Chem. Phys.*, 1941, **9**, 177.

20 J. D. Hancock and J. H. Sharp, *J. Am. Ceram. Soc.*, 1972, **55**, 74.

21 A. F. Gualtieri, *Phys. Chem. Miner.*, 2001, **2**, 719.

22 J. Cravillon, C. A. Schröder, H. Bux, A. Rothkirch, J. Caro and M. Wiebcke, *CrystEngComm*, 2012, **14**, 492.

23 F. Millange, M. I. Medina, N. Guillou, G. Férey, K. M. Golden and R. I. Walton, *Angew. Chem., Int. Ed.*, 2010, **49**, 763.

24 H. Reinsch and N. Stock, *CrystEngComm*, 2013, **15**, 544.

25 T. Ahnfeldt, J. Moellmer, V. Guillerm, R. Staudt, C. Serre and N. Stock, *Chem. – Eur. J.*, 2011, **17**, 6462.

26 F. Ragon, P. Horcajada, H. Chevreau, Y. K. Hwang, U. Lee, S. R. Miller, T. Devic, J. Chang and C. Serre, *Inorg. Chem.*, 2014, **53**, 2491.

27 E. E. Finney and R. G. Finke, *Chem. Mater.*, 2009, **21**, 4692.

28 T. Pradell, D. Crespo, N. Clavaguera and M. T. Clavaguera-Mora, *J. Phys.: Condens. Matter*, 1998, **10**, 3833.

29 F. Millange, R. El Osta, M. E. Medina and R. I. Walton, *CrystEngComm*, 2011, **13**, 103.

30 L. Engelke, M. Schaefer, M. Schnur and W. Bensch, *Chem. Mater.*, 2001, **13**, 1383.

31 N. Pienack, C. Näther and W. Bensch, *Eur. J. Inorg. Chem.*, 2009, 937.

4   Conclusion and Outlook

This work deals with the synthesis and characterisation of a new Zr-based MOF with fumarate as linker. The aim of this work was the development of a porous, highly crystalline and stable material that might be interesting for biomedical applications. To achieve a well-adjusted drug delivery system, several characteristics have to be considered. The toxicity of the compound and its components, the particle size, the nature of the porous system as well as the stability of the particles have to be tailored according to the desired application. Zr-based MOFs appeared as promising candidates as their exceptional thermal and chemical stability was reported earlier. The chosen linker, fumaric acid, is a biologically occurring molecule that appears as a side product in the KREBS cycle and should therefore not cause any toxic reaction in the human body. Also, the liberation of small amounts of Zr^{4+} ions is obviously tolerated by the human body, as zirconium dioxide and zirconium phosphate are well-established as biomaterials.

In the first part of this thesis, the synthesis of the Zr-fumarate MOF is reported. Zr-based MOFs like UiO-66 and UiO-67 could be successfully synthesised from organic solvents like dimethylformamide (DMF). For that reason, first attempts were carried in a DMF-based system resulting in an amorphous product. Inspired by the work of KITAGAWA and SCHAATE,[3,4,5] the modulation method was applied: By the addition of a monocarboxylic acid as a modulator to the reaction mixture, a highly crystalline material was obtained. According to the coordination modulation approach, a monocarboxylic acid can coordinate to intermediately formed metal clusters, but as it is not able to act as a bridging molecule between the metal nodes, the modulator molecules have to be exchanged in an equilibrium reaction with the linker species. Due to this deceleration of MOF formation, fewer nuclei are formed and crystal growth occurs more regulated, leading to a highly crystalline material. Furthermore, the modulator influences the degree of aggregation and the particle size. Only small amounts of modulator result in particles that are small and strongly intergrown. By increasing the modulator concentration, individual particles with an octahedral shape develop that are larger in size. For other Zr-based MOFs the coordination modulation

[3] Diring, S.; Furukawa, S.; Takashima, Y.; Tsuruoka, T.; Kitagawa, S. *Chem. Mater.* **2010**, *22*, 4531−4538.

[4] Tsuruoka, T.; Furukawa, S.; Takashima, Y.; Yoshida, K.; Isoda, S.; Kitagawa, S. *Angew. Chem. Int. Ed.* **2009**, *48*, 4739−4743.

[5] Schaate, A.; Roy, P.; Godt, A.; Lippke, J.; Waltz, F.; Wiebcke, M.; Behrens, P. *Chem. Eur. J.* **2011**, *17*, 6643−6651.

approach even opened the possibility to obtain single crystals, e.g. of amino-functionalised UiO-68 and Zr-*abdc* MOF. Unfortunately, in the synthesis of Zr-*fum* MOF, further increase of the modulator concentration did not result in the formation of single crystals. The structure was therefore determined from powder X-ray diffraction data revealing a cubic primitive space group *Pn*−3 with a defined orientational arrangement of the kinked fumarate linkers. Recently, FURUKAWA *et al.* substantiated our results by performing a single-crystal analysis with the help of synchrotron radiation. By using $ZrOCl_2 \cdot 8H_2O$ as zirconium source and formic acid as modulator they obtained Zr-*fum* MOF single crystals (renamed to MOF-801-SC) with a diameter of around 20 μm.[6]

The pore system of the Zr-fumarate MOF was investigated by argon sorption measurements. According to these measurements, micropores with diameters of 5 and 7 Å, respectively, and a BET surface area of around $1000\ m^2 \cdot g^{-1}$ were calculated so that an encapsulation of drugs in the porous network appears possible. In addition to a good thermal stability up to 400 °C, Zr-fumarate MOF also shows a good chemical stability against aqueous solutions. This is especially important for the application as a drug delivery system as a premature destruction of the framework is unfavoured.

The stability of the Zr-*fum* MOF incited us to test the synthesis of Zr-fumarate MOF from a water-based synthesis system, thus avoiding the toxic solvent DMF. The water-based synthesis is described in the second part of this work. Again by applying the modulation method, the Zr-fumarate MOF can be synthesised. The influence of formic acid, acetic acid and propionic acid as modulators was tested. The particle size is decreased when acetic or propionic acid are used as modulating agents. An increased particle size can be obtained when the reaction is carried out at room temperature with formic acid as modulator. Zr-*fum* MOF can thus be synthesised under very mild reaction conditions and the particle size can be varied by the choice of the monocarboxylic acid, its concentration and the reaction temperature. Synthesis under such mild reaction conditions as well as control of the particle size are not granted, making this material particularly interesting for biomedical applications. Stability tests performed in various physiological solutions, in different organic

---

[6] Furukawa, H.; Gándara, F.; Zhang, Y.-B.; Jiang, J.; Queen, W. L.; Hudson, M. R.; Yaghi, O. M. *J. Am. Chem. Soc.* **2014**, *136*, 4369–4381.

solvents or solvent mixtures and in aqueous acidic and alkaline solutions confirmed the retention of the structure.

One challenge might be the incorporation of a drug into the microporous framework as well as its release, as drug molecules might be too large to penetrate the pores. Apart from the idea of incorporating active agents inside the pores or loading the outer surface area of particles or, possibly, of coatings with larger biomolecules, the small pores might also offer the opportunity for the delivery of small gaseous bioactive molecules like NO. From another point of view, the small pores could also be used for gas storage or separation. The sorption behaviour with regard to carbon dioxide and methane has shown that, presumably due to the pore limiting diameter of 3.48 Å, the amount of adsorbed carbon dioxide was much higher than the low methane uptake. Thus, Zr-fumarate MOF might also be interesting for gas separation. Furthermore, the group of YAGHI performed water sorption measurements with the Zr-fumarate MOF (MOF-801), recently.[6] Their investigations revealed a much higher water uptake for Zr-*fum* MOF powder samples (MOF-801-P, 28 wt% at $p/p_0 = 0.9$) in comparison to Zr-*fum* MOF single crystals (MOF-801-SC, 36 wt% at $p/p_0 = 0.9$). Probably, these differences can be assigned to missing linker defects in the powder sample. Temperature-dependent measurements have shown that Zr-*fum* MOF might also be a promising candidate for the application as thermal batteries.

The third part of this work focuses on the influence of the modulator on the crystallisation processes in the water- as well as in the DMF-based synthesis. Using synchrotron radiation and energy-dispersive X-ray diffraction (EDXRD) the crystallisation of Zr-fumarate MOF could be observed *in situ*. Concerning the water-based synthesis, addition of formic acid decelerated the reaction rate. It can be concluded that the modulator coordinates to the zirconium and competes with the linker for the coordination site. The only former kinetic study of a modulated reaction by CRAVILLON *et al.* showed another effect.[7] In that case, the addition of formate ions accelerated the formation of the metal-organic framework ZIF-8. In this case, it was assumed that the formate ions deprotonate the linker molecules, resulting in a faster formation of the framework. In general, the question whether modulation occurs via a deprotonation modulation or a coordination modulation mechanism can

[7] Cravillon, J.; Schröder, C.A.; Bux, H.; Rothkirch, A.; Caro, J.; Wiebcke, M. *CrystEngComm* **2012**, *14*, 492–498.

thus be answered by performing *in situ* EDXRD measurements. As in the case of the formation of the Zr-*fum* MOF, the addition of formic acid decelerated the reaction in the water-based synthesis, a coordination modulation could be confirmed. Nonetheless, in a DMF-based synthesis the addition of formic acid results in an acceleration of the reaction. This acceleration was attributed to a small amount of water present in the commercially available formic acid. To proof this assumption, syntheses with an unchanged modulator concentration, but varying water content were carried out in DMF. As a result, a strong influence of additionally added water could be observed. For that reason, the acceleration of the reaction rate by increasing the amount of added formic acid is not surprising as the amount of water is increased concomitantly. On the contrary, in the water-based synthesis the water content of the formic acid plays only a minor role, as water is present in excess and the modulation effect dominates the crystallisation behaviour. In general, syntheses performed in water were completed by far earlier in comparison to the syntheses carried out in DMF. The reaction in DMF was also investigated with regard to the influence of the temperature. This allowed the calculation of activation energies for nucleation and growth. Interestingly, these were quite similar, indicating that the basic reactions of nucleation and growth are similar, consisting for example in the exchange of a modulator against a linking molecule, occurring either on a forming nucleus or on a growing particle. Such a temperature-dependent investigation was not possible for the water-based synthesis, which, when carried out at temperatures notably higher than ca. 40 °C, was so fast that the influence of the temperature was not measurable. Lower temperatures could not be accessed due to limitations of the experimental set-up at the synchrotron and the lack of beamtime.

After having synthesised and characterised the Zr-*fum* MOF in detail, first toxicity experiments were performed in cooperation with the Ludwig-Maximilians-Universität in Munich (AG MEINERS and AG VOLLMAR) as well as with the Hannover Medical School (AG HAASTERT-TALINI and AG STIESCH). The great advantage that Zr-fumarate MOF can be synthesised in various particle sizes from a non-toxic water-based synthesis offered the possibility for a particle size-dependent study with several cell types. All tested cells − including lung macrophages, lung epithelial cells, SCHWANN cells and gingival fibroblasts − showed good cell viability in a wide concentration range nearly independent of the particle size. Only at higher MOF concentrations above 200 µg·mL^{-1} some cells show a decreased metabolic

activity. As the toxicity of MOFs has been rarely investigated until today these investigations substantiate that Zr-fumarate MOF might be a promising candidate for biomedical applications. Nevertheless, further cell culture tests are necessary to find out whether Zr-*fum* MOF is cytotoxic with regard to other cell lines or is able to penetrate the cell membrane. If this is the case, the material becomes especially interesting for anticancer therapy, because an anticancer drug might then be delivered to the cell. For that purpose, it would be of advantage to label the MOF particle with a fluorescent dye so that they can be visualised during *in vitro* tests. For further investigation the incorporation of drugs will also be an important issue. As already mentioned, Zr-fumarate MOF exhibits quite small pores with a limited pore opening so that the application of longer linkers like muconic acid should be considered for bio-friendly Zr-based MOFs as well. As the Zr-*fum* MOF can be synthesised under very mild reaction conditions, the drug might also be encapsulated during the MOF crystallisation process with the delivery taking place caused by degradation in the human body. Apart from the synthesis of Zr-fumarate MOF as nanoparticles for the preparation of stable suspensions that can be injected, also film formation might offer advantages, for example as implant coatings. Finally, *in vivo* tests of the material will be inevitable.

5   Supplementary Information

5.1   Modulated Synthesis of Zr-fumarate MOF (Supplementary Material)

Supplementary Material

Modulated Synthesis of Zr-fumarate MOF

Gesa Wißmann, Andreas Schaate, Sebastian Lilienthal, Imke Bremer, Andreas M. Schneider, Peter Behrens

Table A1. Indexing of the X-ray powder diffraction pattern of Zr-*fum* MOF synthesised with 30 equivalents of modulator.

N	2θ (obs)	H	K	L	2θ (calc)	obs-calc	Int.	d (obs)	d (calc)
1	8.5288	1	1	1	8.5448	-0.0161	100.0	10.35911	10.33976
2	9.8503	2	0	0	9.8698	-0.0195	38.0	8.97220	8.95449
3	13.9644	2	2	0	13.9754	-0.0110	2.9	6.33675	6.33178
4	19.8121	4	0	0	19.8138	-0.0017	4.5	4.47763	4.47725
5	21.6132	3	3	1	21.6120	0.0012	9.1	4.10838	4.10860
6	22.1783	4	2	0	22.1805	-0.0022	3.3	4.00496	4.00457
7	22.7303	4	2	1	22.7355	-0.0052	2.5	3.90893	3.90806
8	24.3302	4	2	2	24.3284	0.0018	6.3	3.65539	3.65566
9	25.3402	4	3	1	25.3380	0.0022	2.3	3.51194	3.51224
10	25.8287	3	3	3	25.8289	-0.0002	9.8	3.44661	3.44659
11	28.1654	4	4	0	28.1642	0.0012	2.2	3.16576	3.16589
12	29.4929	5	3	1	29.4834	0.0095	4.0	3.02621	3.02717
13	29.9122	6	0	0	29.9113	0.0009	16.6	2.98474	2.98483
14	30.7427	6	1	1	30.7509	-0.0082	1.4	2.90598	2.90522
15	31.9732	6	2	1	31.9729	0.0003	1.9	2.79689	2.79691
16	32.7638	5	3	3	32.7649	-0.0011	5.4	2.73118	2.73109
17	34.6741	4	4	4	34.6744	-0.0003	5.6	2.58496	2.58494
18	35.7728	5	5	1	35.7771	-0.0043	3.9	2.50805	2.50776
19	38.5853	5	5	3	38.5837	0.0016	5.3	2.33146	2.33155
20	40.2560	8	0	0	40.2531	0.0029	1.6	2.23847	2.23862

Table A2. Metric of the unit cell and table of atomic coordinates of the structural

model of Zr–*fum* MOF as obtained by structural modelling.

Cubic crystal system, space group *P*-3*n* (No. 201)
$a = b = c = 17.909$ Å, $V = 5744$ Å^3
$\alpha = \beta = \gamma = 90.0$ °

symbol	element	x / a	y / b	z / c
O1	O	0.66425	0.27385	0.9548
O2	O	0.87028	0.25685	0.93686
O3	O	0.77331	0.36957	0.9371
O4	O	0.75915	0.16374	0.95501
O5	O	0.83158	0.31899	0.80795
C6	C	0.59165	0.27636	0.93835
C7	C	0.93878	0.24856	0.90848
Zr8	Zr	0.76152	0.26135	0.88368
C9	C	0.53831	0.28103	0.00421
C10	C	0.00446	0.24819	0.96178
O11	O	0.81986	0.18014	0.81986
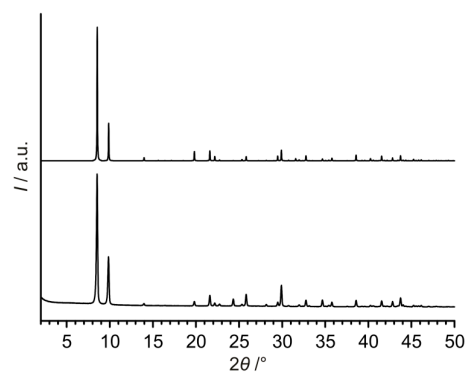
Figure A1. Experimental PXRD pattern of Zr-*fum* MOF (bottom) in comparison to a simulated pattern (top) of an extended structural model of the MOF containing guest species. To represent the electron density of included guest species, chloride anions were placed in the centers of the octahedral and tetrahedral pores of the structure. Especially the experimentally detected reflection at ca. 14° 2θ is only found in the simulated powder pattern of a structural model containing guest species.
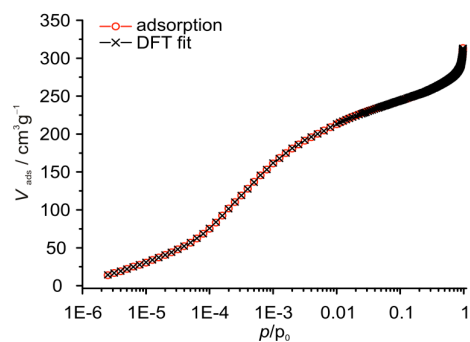

Figure A2. NL-DFT fit of the Ar sorption isotherm of Zr-*fum* MOF synthesised with 30 equivalents of modulator.

5.2   A Water-Born Zr-Based Porous Coordination Polymer: Modulated Synthesis of Zr-fumarate MOF (Supplementary Material)

Supplementary material

A Water-Born Zr-Based Porous Coordination Polymer:
Modulated Synthesis of Zr-fumarate MOF

Gesa Zahn,[a] Hendrik Albert Schulze,[a] Jann Lippke,[a] Sandra König,[b] Uta

Sazama,[b] Michael Fröba,[b] Peter Behrens[a]

[a] *Leibniz Universität Hannover, Institut für Anorganische Chemie, Callinstr. 9,*
30167 Hannover, Germany;
also at the ZFM - Center for Solid-State Chemistry and New Materials
[b] *Universität Hamburg, Institut für Anorganische und Angewandte Chemie,*
Martin-Luther-King-Platz 6, 20146 Hamburg, Germany

A1   Thermogravimetric analysis

Thermogravimetric analysis (TGA) measurements coupled with mass spectrometry analysis were performed using a Netzsch STA 449 F3 Jupiter® silmultane TG analyzer and a Netzsch QMS 403C Aëolos® Quadrupole mass spectrometer. The samples were heated in alumina crucibles up to 800 °C under pure argon or under an argon/oxygen mixture (80:20) as flushing gas.

Thermogravimetric measurements coupled with mass spectrometry show signals of mass-to-charge ratios of 12, 17, 18, 28 and 44 (Figure A1.1).
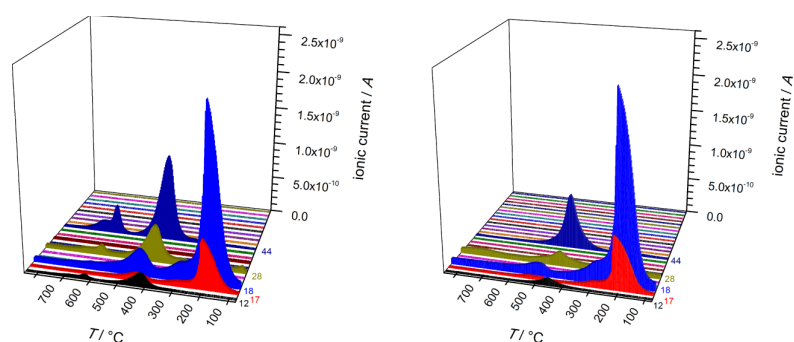
Figure A1.1. Ionic currents measured during thermogravimetric analysis of a Zr-*fum* sample (synthesised at 120 °C with 70 eq of formic acid). Measurements were performed under an Ar/O_2 mixture (80:20) (left) or under pure argon (right).

At low temperatures between 25 °C and 200 °C, signals with a mass-to-charge ratio of 17 and 18 dominate the spectra, characteristic of the fragments OH and H_2O, respectively, resulting from occluded water, alcohols or carboxylic acids. During the decomposition of the linker between 350 °C and 450 °C,

further signals referring to C^+ fragments (m/z 12), CO fragments (m/z 28) and CO$_2$ fragments (m/z 44) are present. These signals can be ascribed to the fragmentation of the fumaric acid. Only signals related to the fragment CO$_2$ (m/z 44) persist during the final decomposition between 580–600 °C. As proposed earlier [8], this fact can best be explained by carbonate ions, resulting from the decomposition of the fumarate linkers, being coordinated to Zr cations or Zr-oxo clusters. At high temperatures, carbon dioxide is expelled (Figure A1.2, left), leaving behind zirconium dioxide as the final product of the combustion. A similar effect cannot be measured during the decomposition under argon atmosphere; no mass loss occurs at 580 °C and the mass spectrum shows only a negligibly small ionic current for m/z = 44 (CO$_2$) (Figure A1.2, right). Due to the non-oxidizing atmosphere, no carbonate ions can be formed and consequently, no carbon dioxide can be released, resulting finally in a higher residual mass in the thermogravimetric measurements.
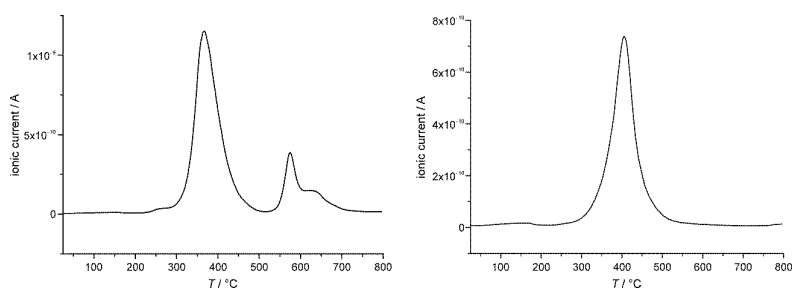
Figure A1.2. Ionic current measured during thermogravimetric analysis for m/z = 44 (CO$_2$) in mass spectra of a Zr-*fum* MOF sample (synthesised at 120 °C with 70 eq of formic acid as modulator). Measurements were performed under an Ar/O$_2$ mixture (80:20) (left) or under pure argon (right).
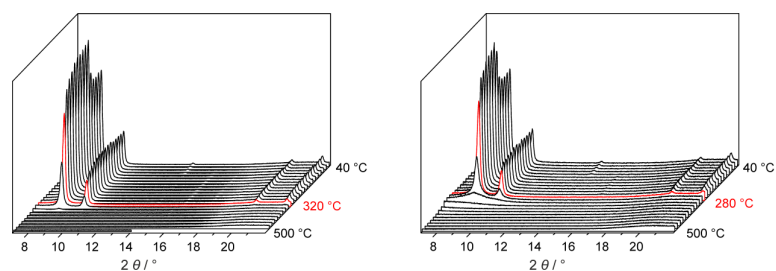
3

A2   High temperature X-ray diffraction

Figure A2. High temperature XRD measurements of a Zr-*fum* MOF sample synthesised in a DMF-based reaction at 120 °C with 30 eq of formic acid (left) and synthesised in a water-based synthesis at 120 °C with 70 eq of formic acid (right).
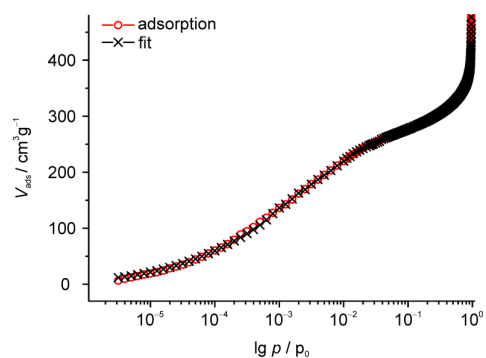
A3   Sorption behaviour

Figure A3. NLDFT fit of the argon sorption isotherm of a Zr-*fum* MOF sample synthesised at 120 °C with 70 eq of formic acid. The resulting pore size distribution is shown in Fig. 6 of the article.

A4   Stability tests
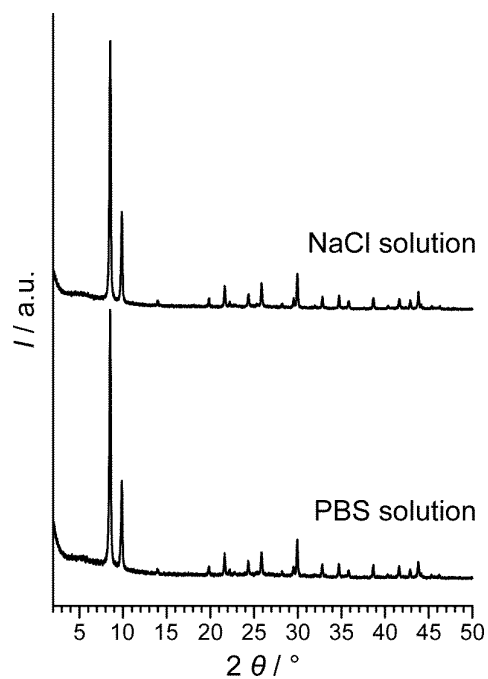
Figure A4. XRD patterns of Zr-*fum* MOF samples after stability tests in physiological sodium chloride (NaCl) and phosphor buffered saline (PBS) solution. The samples were synthesised from water at 120 °C with a modulator concentration of 70 eq formic acid and stirred in the various solutions at room temperature.

5.3 Insight into the mechanism of modulated syntheses: *In situ* synchrotron diffraction studies on the formation of Zr-fumarate MOF (Supplementary Material)

Supplementary Information

Insight into the mechanism of modulated syntheses:

In situ synchrotron diffraction studies on the formation of Zr-fumarate MOF

Gesa Zahn,* Philip Zerner,* Jann Lippke, Fabian L. Kempf, Sebastian Lilienthal, Christian A. Schröder, Andreas M. Schneider, Peter Behrens

Institut für Anorganische Chemie, Leibniz Universität Hannover, Callinstr. 9, 30167 Hannover, Germany; also at the ZFM - Center for Solid-State Chemistry and New Materials, Leibniz Universität Hannover

* These two authors contributed equally to this study

Contents

S1   Data evaluation with the Avrami-Erofeev and Sharp-Hancock formalisms

For a long time, the Avrami-Erofeev equation (equation S1)[1,2,3,4] or its linearized equivalent, the Sharp-Hancock formalism (equation S2)[5] have been preferred in publications dealing with the evaluation of kinetic data concerning the formation of a solid from a liquid or from another solid (e.g. glass crystallisation). This is also true for the porous solids, as, *e.g.*, silicium-aluminium phosphates like SAPO-34[6], gallium oxyfluorophosphates like ULM-3 and ULM-4[7], layered manganese thioantimonates[8] several MOFs or ZIFs,[9,10,11,12] and also the Zr-based UiO-66 and its derivatives.[13]

$$\alpha(t) = 1 - e^{-(k \cdot t)^{n_{AE}}}$$
(S1)

$$ln\left[-ln(1-\alpha)\right] = n_{AE} \cdot \ln(k) + n_{AE} \cdot ln(t - t_0)$$
(S2)

$\alpha(t)$:   *degree of crystallisation*
t: *time*
k: *overall rate constan*
n_{AE}:   *Avrami exponent*

Concerning the crystallisation of layered manganese thioantimonates, Engelke *et al*. showed that two crystallisation mechanisms occur during the synthesis of $Mn_2Sb_2S_5 \cdot DAP$ (DAP=1,3-diaminopropane). With increasing temperature the mechanism changes from a phase-boundary-controlled reaction (Avrami exponent $n_{AE} \approx 1$ for $\alpha < 0.75$ at 130 °C) to a diffusion-controlled reaction (Avrami exponent $n_{AE} \approx 0.5$ for $\alpha > 0.75$ at 130 °C). Furthermore, the presence of two crystalline intermediates could be detected at lower temperatures. These are transformed to the final product after a short period of time in a temperature range of 105-130 °C. Ahnfeldt *et al.*[9] investigated the kinetics of Al-MOFs like CAU-1 and CAU-1-(OH)$_2$ using conventional and microwave heating. In general, the reaction and induction times are shortened when the temperature is increased.[14] Apart from the fact that the microwave heating resulted in increased synthesis rates and thus in smaller particles, the kinetic evaluation according to Avrami-Erofeev and Sharp-Hancock revealed different crystallisation mechanisms comparing the microwave heating with conventional heating. Whereas the microwave-heated reaction shows a diffusion-controlled mechanism (Avrami exponent $n_{AE} \approx 0.6$-0.8), the conventional heating rather led to a

phase-boundary-controlled reaction (Avrami exponent $n_{AE} \approx$ 1.0-1.1). The activation energy was calculated to 131-136 kJ irrespective of the heat source.[9]

A classical nucleation-growth kinetic was also found by Millange *et al.* in a time-resolved *in situ* diffraction study of HKUST-1.[11] In the quite fast formation of HKUST-1, no induction time is detectable and the Avrami-Erofeev and Sharp-Hancock evaluation revealed that the reaction is controlled by the formation of new nucleation sites (Avrami exponent $n_{AE} \approx$ 1.5). They further revealed that the crystallisation of MIL-53(Fe) occurs via a metastable intermediate, the lifetime of which can be prolonged by decreasing the reaction temperature.

Another MOF of the MIL family, Mn-MIL-100, does not show any intermediate formation. Instead, the kinetic results indicate a two-stage reaction process with two different reaction mechanisms. At the beginning of the reaction, the crystallisation is nucleation-controlled with the Avrami exponent $n_{AE} \approx$ 2 but changes to $n_{AE} \approx$ 1 as the reaction proceeds.[12] Recently, Ragon *et al*. investigated the crystallisation behaviour of the Zr-MOF UiO-66 and found out that the addition of both water and hydrochloric acid leads to faster crystallisation rates.[13] Since they discovered that only the presence of water seems to be the cause for this acceleration, these results are in good agreement with this work and our previous observations.[15]

Although the traditional Avrami-Erofeev-based mode of evaluation is well-established, the procedure proposed by Gualtieri in 2001 is becoming more and more popular. Millange *et al.* used this evaluation and pointed out that the Avrami-Erofeev method shows severe limitation since it had been developed for a specific solid-solid reaction. They emphasise that the fitting parameters are not applicable for heterogeneous crystallisation of a solid from a liquid. For that reason, the Gualtieri evaluation was applied for the investigation of the crystallisation of MOF-14. It was discovered that this reaction is nucleation rate-determined, because the calculated values for k_N were in all cases smaller than k_G.[16]

A combined evaluation using Avrami-Erofeev and Sharp-Hancock as well as the Gualtieri model was applied by Cravillon *et al.*[10] In this work the formate-modulated synthesis of ZIF-8 was investigated by using time-resolved *in situ* X-ray diffraction. On the one hand, the results of the Avrami-Erofeev and Sharp-Hancock evaluation revealed that the modulated synthesis of ZIF-8 is rate-limited by a phase-boundary reaction (Avrami exponent $n_{AE} \approx$ 1.0-1.3). On the other hand, by applying the Gualtieri evaluation, k_N was in all cases smaller than k_G, so that the calculations resulted in a nucleation-controlled

reaction rate. This work illustrates the divergence of the different models and demands a sensitive judgement concerning the evaluation of kinetic data on the formation of a solid.

Given the uncertainties in the interpretation of kinetic data obtained with the Avrami-based evaluation, especially with regard to the meaning of different Avrami exponents n_{AE}[17] and to the fact that this equation was originally compiled for the description of a solid-solid crystallisation,[1,2,3] we preferred to present our results as obtained by the evaluation using the Gualtieri equation.[18] The fact that this equation contains two different terms for nucleation and crystal growth fits well to the investigated reactions. In fact, it allows us in some cases to obtain a deeper interpretation of the kinetic data, for example when it is found that the activation energies for nucleation and growth are very similar, indicating that the same basic process is concerned in the corresponding rate-determining steps.

In contrast, the evaluation methods according to Avrami-Erofeev as well as to Sharp and Hancock (effectively a linearization of the Avrami-Erofeev equation) do not contain separate terms for the nucleation and growth. However, in order to be able to compare our kinetic investigations to studies of MOF formation reactions where the data were evaluated by applying the Avrami-Erofeev and Sharp-Hancock equations, we here present the results of the analysis of our data when these formalisms are used.

S1.1 Variation of the modulator concentration in the water-based synthesis
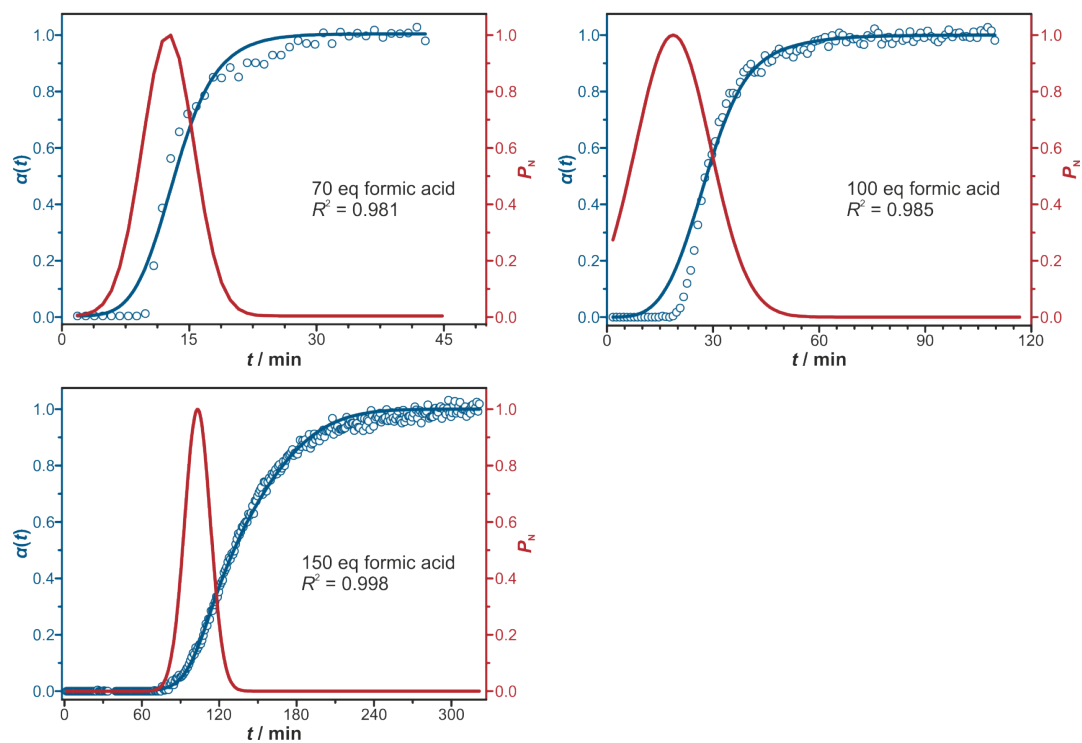
water, 43 °C, *x* eq modulator

Figure S1. Extent of crystallisation α plotted against time t (blue circles) and the corresponding Gualtieri fitting (blue curve) as well as the probability for nucleation P_N (red curve) for varied amounts of modulator in water. The reactions studied here were carried out at 43 °C with molar ratios $ZrCl_4/H_2fum$/formic acid/H_2O of 1:3:*x*:1074.
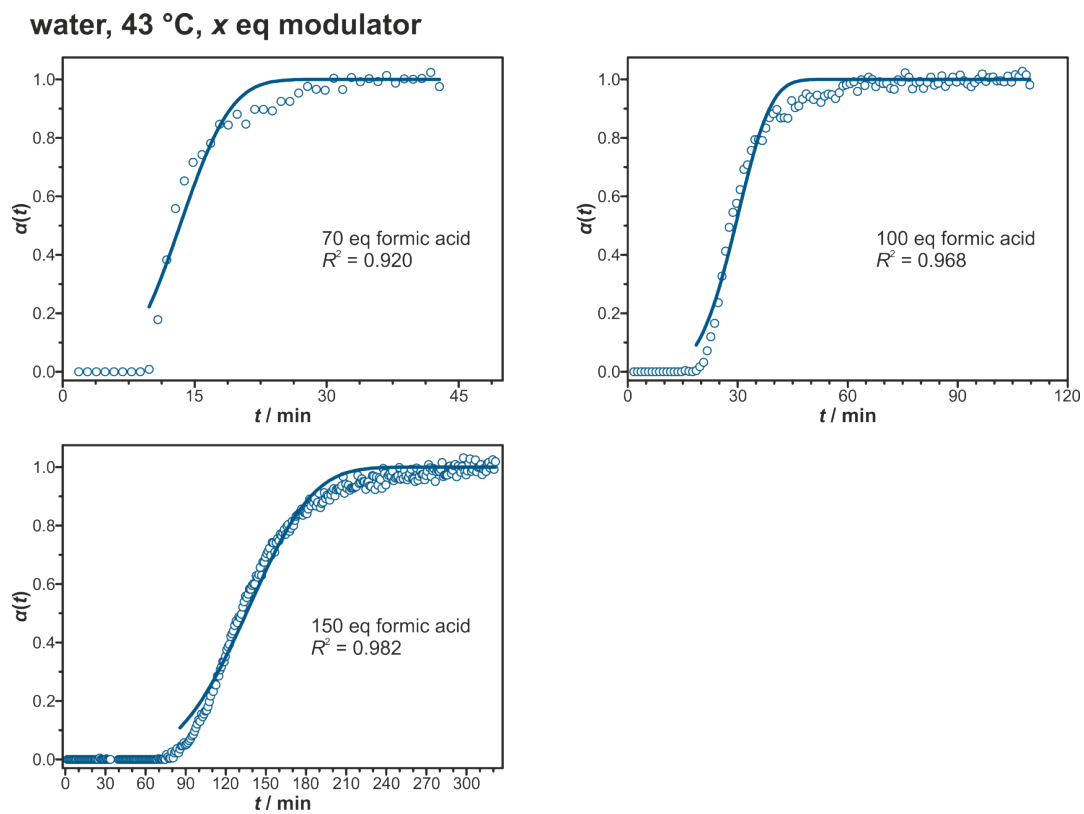
water, 43 °C, *x* eq modulator

Figure S2. Extent of crystallisation α plotted against time t (blue circles) and the corresponding Avrami-Erofeev fitting (blue curve) for varied amounts of modulator in water. The reactions studied here were carried out at 43 °C with molar ratios $ZrCl_4/H_2fum$/formic acid/H_2O of 1:3:*x*:1074.
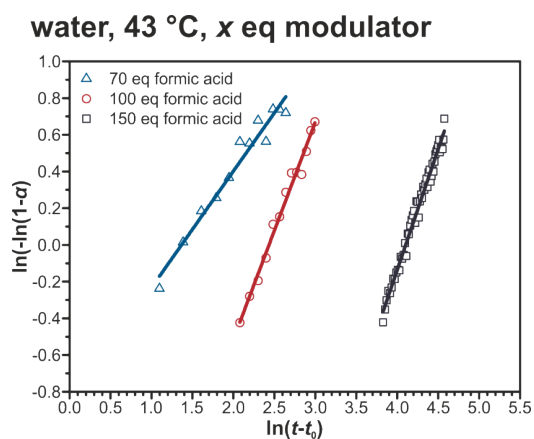
water, 43 °C, *x* eq modulator

Figure S3. Sharp-Hancock plots for varied amounts of modulator in water. The reactions studied here were carried out at 43 °C with molar ratios $ZrCl_4/H_2fum$/formic acid/H_2O of 1:3:*x*:1074.

Table S1. Kinetic parameters obtained by fitting of the crystallisation curves with the Avrami-Erofeev and Sharp-Hancock equation. Crystallisation curves were measured for syntheses of Zr-*fum* MOF in water-based systems under variation of the concentration (*x* equivalents) of the modulator formic acid (ZrCl$_4$/H$_2$*fum*/formic acid/water 1:3:*x*:1074, 43 °C).

x	n_{AE}	k_{AE} / min^{-1}	n_{SH}	k_{SH} / min^{-1}
70	3.3(4)	0.067(1)	0.79(5)	0.242(1)
100	4.4(2)	0.031(1)	1.40(5)	0.088(1)
150	3.9(1)	0.007(1)	1.45(1)	0.017(1)

S1.2 Variation of the temperature in the DMF-based synthesis

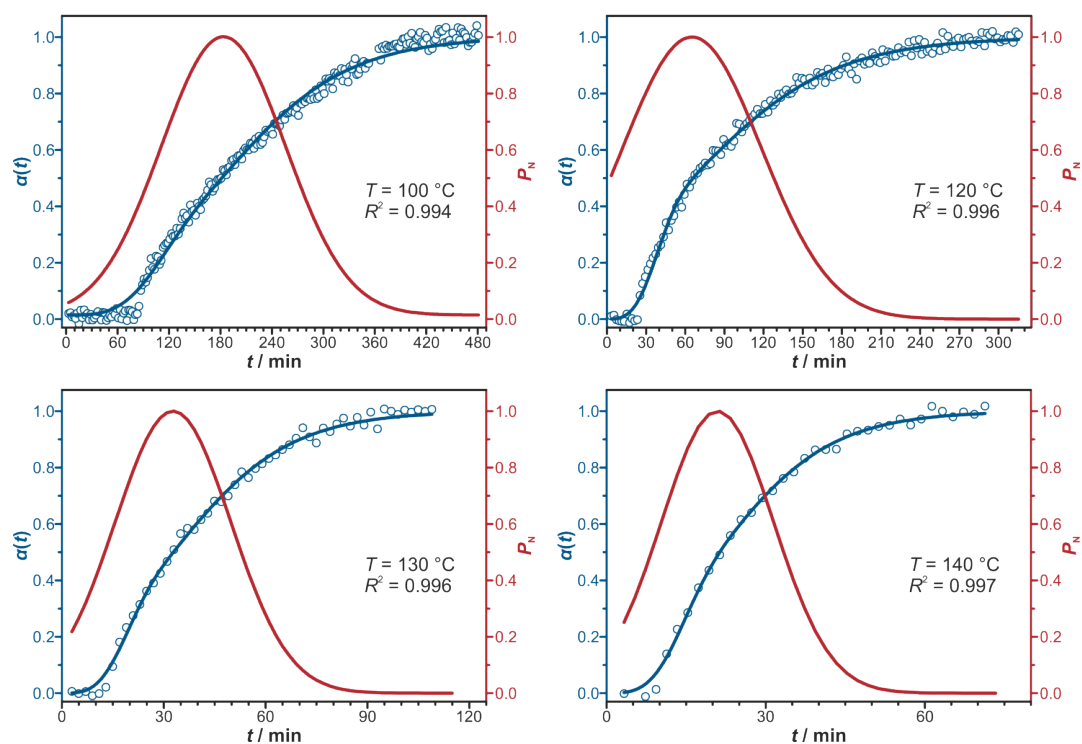**DMF, *x* °C, 70 eq modulator**

Figure S4. Extent of crystallisation *α* plotted against time *t* (blue circles) and the corresponding Gualtieri fitting (blue curve) as well as the probability for nucleation P_N (red curve) for varied temperatures. The reactions studied here were carried out in DMF with molar ratios ZrCl$_4$/H$_2$*fum*/formic acid/DMF of 1:3:70:500.
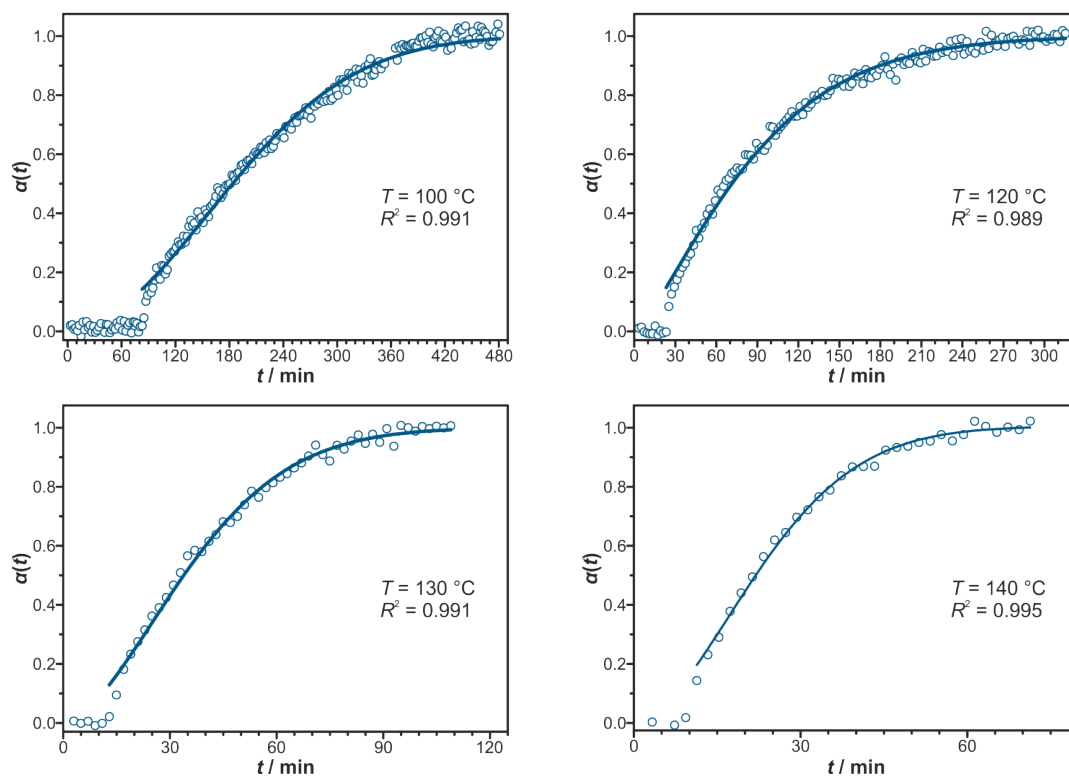
DMF, *x* °C, 70 eq modulator

Figure S5. Extent of crystallisation *α* plotted against time *t* (blue circles) and the corresponding Avrami-Erofeev fitting (blue curve) for varied temperatures. The reactions studied here were carried out in DMF with molar ratios $ZrCl_4$/H_2fum/formic acid/DMF of 1:3:70:500.
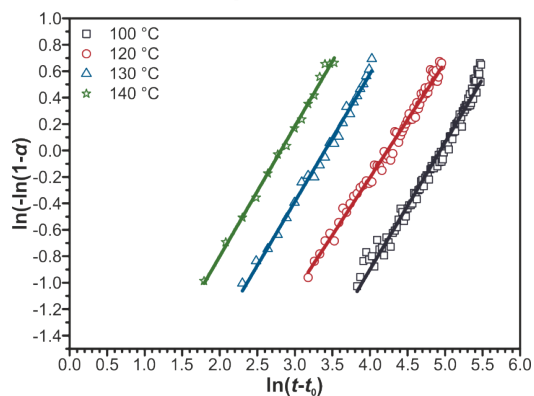
DMF, *x* °C, 70 eq modulator

Figure S6. Sharp-Hancock plots for varied temperatures. The reactions studied here were carried out in DMF with molar ratios $ZrCl_4$/H_2fum/formic acid/DMF of 1:3:70:500.

Table S2. Kinetic parameters obtained by fitting of the crystallisation curves with the Avrami-Erofeev and Sharp-Hancock equation. Crystallisation curves were measured for syntheses of Zr-*fum* MOF in DMF-based systems under variation of the temperature T (ZrCl$_4$/H$_2$*fum*/formic acid /DMF 1:3:70:500).

T/ °C	n_{AE}	k_{AE} / min^{-1}	n_{SH}	k_{SH} / min^{-1}
100	1.99(2)	0.0045(1)	1.04(2)	0.0075(1)
120	1.30(2)	0.0106(1)	0.88(1)	0.0150(1)
130	1.68(4)	0.0237(2)	1.03(2)	0.0361(1)
140	1.77(4)	0.0368(3)	1.06(2)	0.0590(1)

Table S3. Activation energies obtained from the Arrhenius evaluation of temperature-variable rate constants as obtained by applying the Avrami-Erofeev and the Sharp-Hancock fitting.

Avrami-Erofeev	*Sharp-Hancock*
E_A/ kJ·mol^{-1}	E_A/ kJ·mol^{-1}
69 ± 7	67 ± 10

S1.3 Variation of the amount of modulator in the DMF-based synthesis

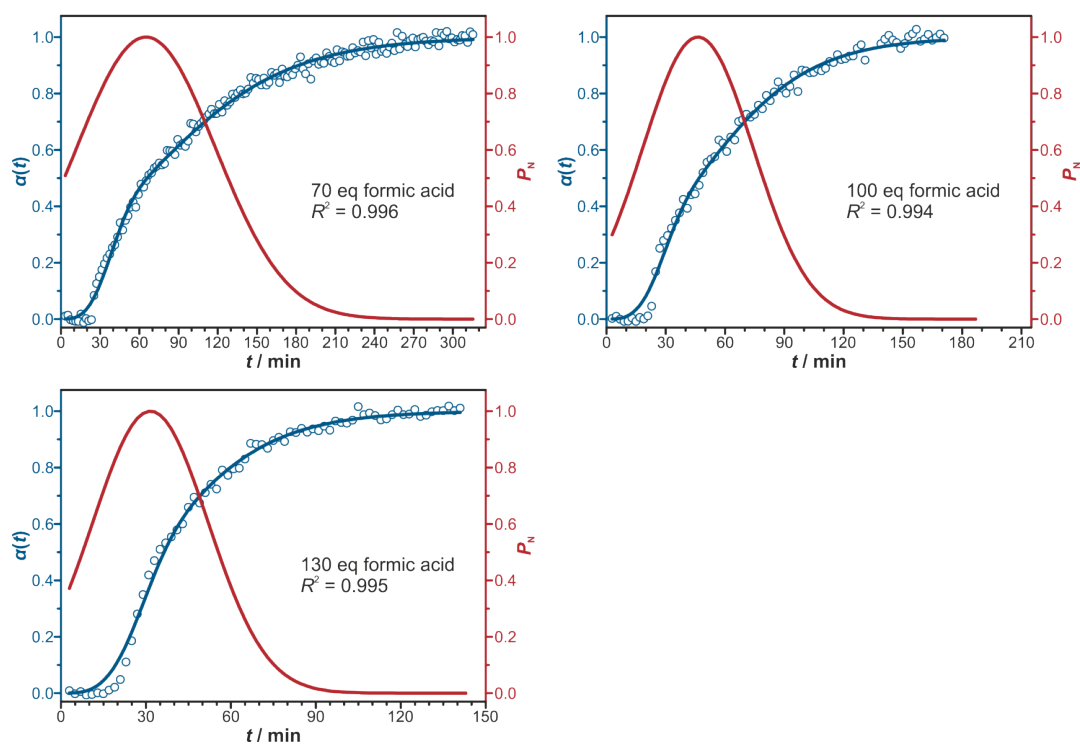**DMF, 120 °C, *x* eq modulator**

Figure S7. Extent of crystallisation *α* plotted against time *t* (blue circles) and the corresponding Gualtieri fitting (blue curve) as well as the probability for nucleation P_N (red curve) for varied amounts of modulator in DMF. The reactions studied here were carried out at 120 °C with molar ratios ZrCl$_4$/H$_2$*fum*/formic acid/DMF of 1:3:*x*:500.
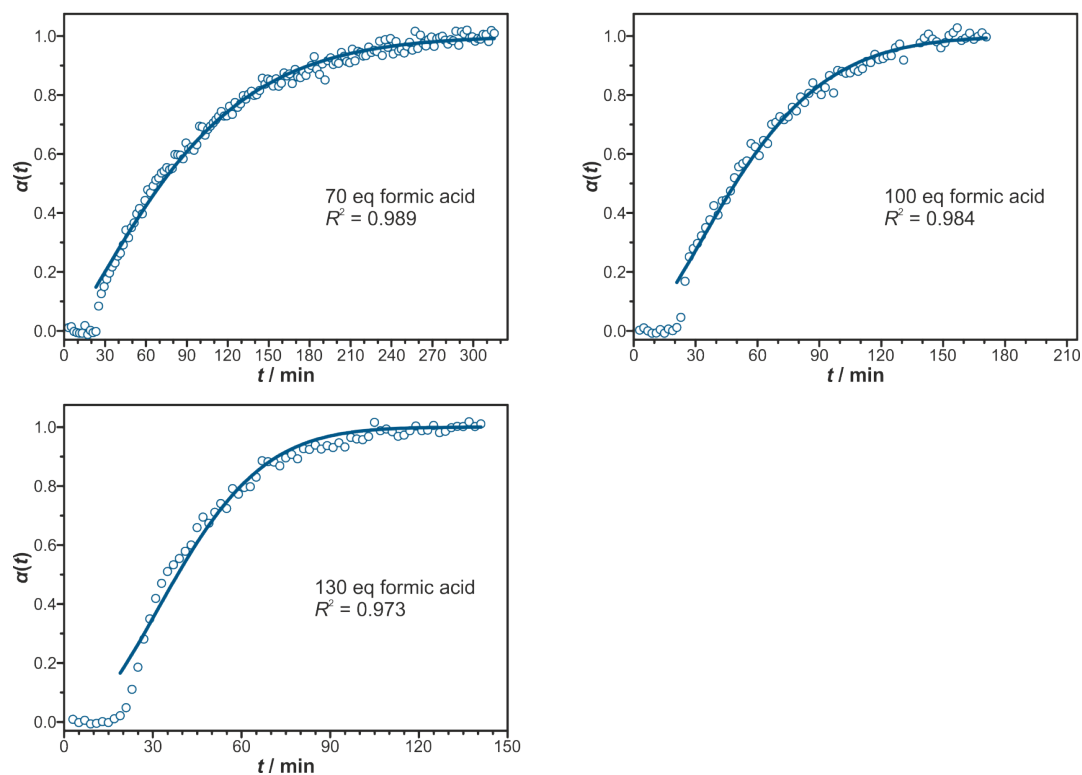
DMF, 120 °C, *x* eq modulator

Figure S8. Extent of crystallisation *α* plotted against time *t* (blue circles) and the corresponding Avrami-Erofeev fitting (blue curve) for varied amounts of modulator in DMF. The reactions studied here were carried out at 120 °C with molar ratios $ZrCl_4$/H_2*fum*/formic acid/DMF of 1:3:*x*:500.
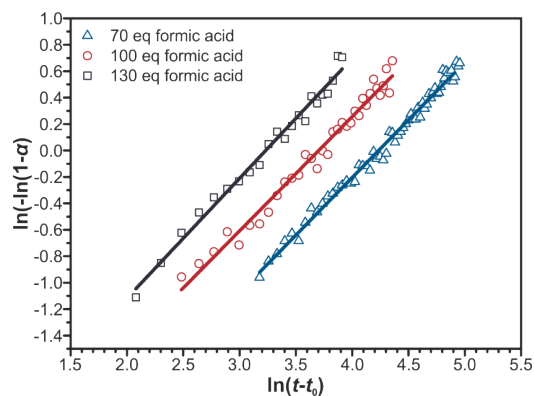
DMF, 120 °C, *x* eq modulator

Figure S9. Sharp-Hancock plots for varied amounts of modulator in DMF. The reactions studied here were carried out at 120 °C with molar ratios $ZrCl_4$/H_2*fum*/formic acid/DMF of 1:3:*x*:500.

Table S4. Kinetic parameters obtained by fitting of the crystallisation curves with the Avrami-Erofeev and Sharp-Hancock equation. Crystallisation curves were measured for syntheses of Zr-*fum* MOF in DMF-based systems under variation of the concentration (*x* equivalents) of the modulator formic acid (ZrCl$_4$/H$_2$*fum*/formic acid /DMF 1:3:*x*:500, 120 °C).

x	n_{AE}	k_{AE} / min^{-1}	n_{SH}	k_{SH} / min^{-1}
70	1.30(2)	0.0106(1)	0.88(1)	0.0150(1)
100	1.57(4)	0.0161(2)	0.90(2)	0.0259(1)
130	1.90(8)	0.0215(3)	0.93(3)	0.0407(1)

S1.4 Variation of the water content in the DMF-based synthesis
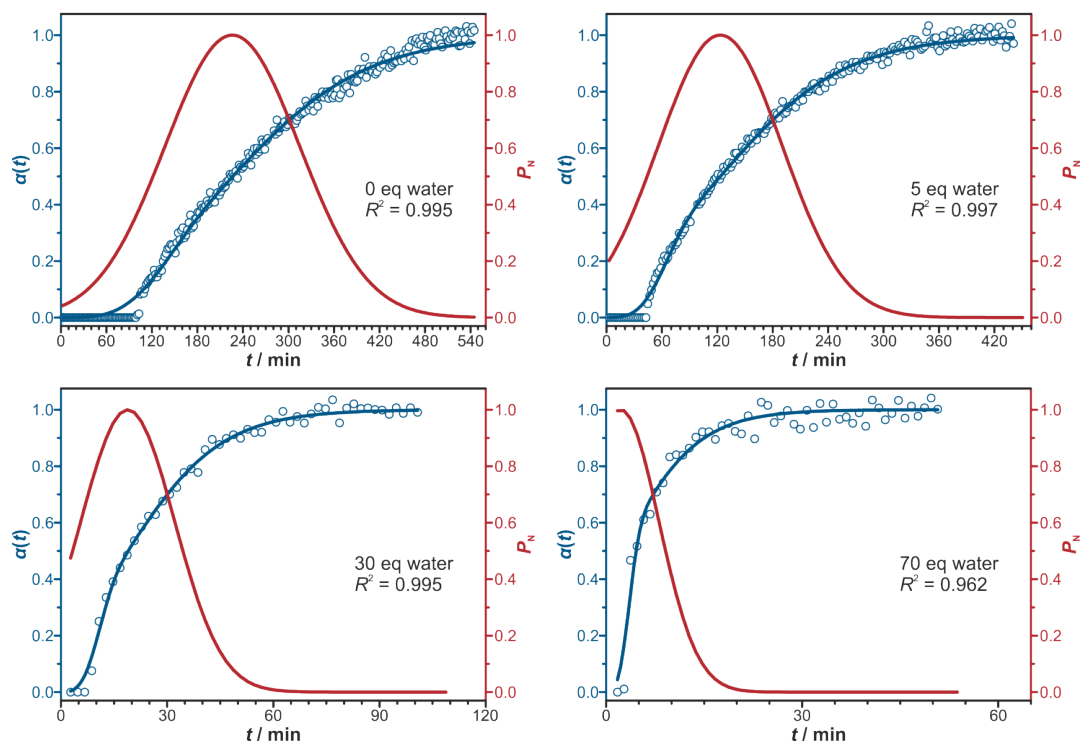
DMF, 100 °C, 70 eq modulator, *x* eq water

Figure S10. Extent of crystallisation *α* plotted against time *t* (blue circles) and the corresponding Gualtieri fitting (blue curve) as well as the probability for nucleation P_N (red curve) for varied amounts of water in DMF. The reactions studied here were carried out at 100 °C with molar ratios ZrCl$_4$/H$_2$*fum*/formic acid/water/DMF of 1:3:70:*x*:500.

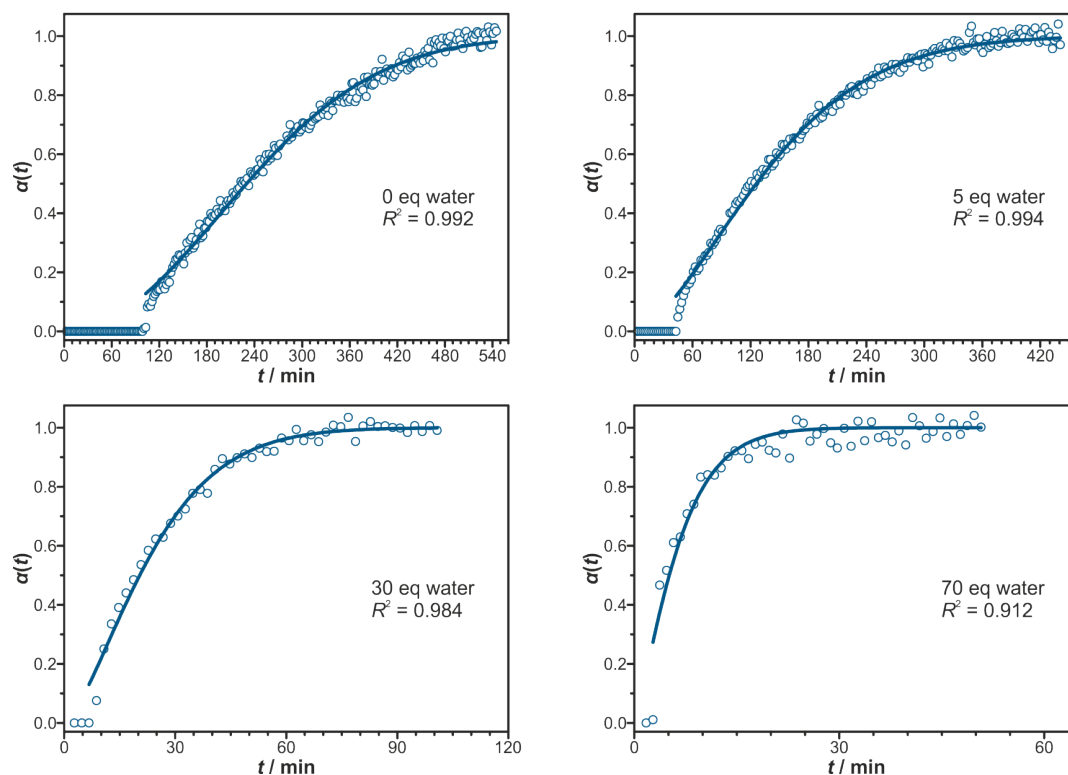**DMF, 100 °C, 70 eq modulator, *x* eq water**

Figure S11. Extent of crystallisation *α* plotted against time *t* (blue circles) and the corresponding Avrami-Erofeev fitting (blue curve) for varied amounts of water in DMF. The reactions studied here were carried out at 100 °C with molar ratios $ZrCl_4$/H_2fum/formic acid/water/DMF of 1:3:70:*x*:500.
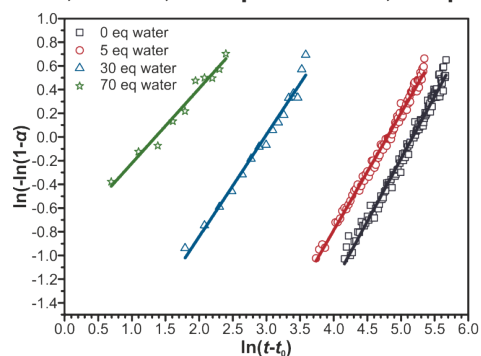
DMF, 100 °C, 70 eq modulator, *x* eq water

Figure S12. Sharp-Hancock plots for varied amounts of water in DMF. The reactions studied here were carried out at 100 °C with molar ratios $ZrCl_4$/H_2fum/formic acid/water/DMF of 1:3:70:*x*:500.

Table S5. Kinetic parameters obtained by fitting of the crystallisation curves with the Avrami-Erofeev and Sharp-Hancock equation. Crystallisation curves were measured for syntheses of Zr-*fum* MOF in DMF-based systems under variation of the concentration (*x* equivalents) of water (ZrCl$_4$/H$_2$*fum*/formic acid/water/DMF 1:3:70:*x*:500, 100 °C).

x	n_{AE}	k_{AE} / min^{-1}	n_{SH}	k_{SH} / min^{-1}
0	2.02(2)	0.0036(1)	1.09(1)	0.0060(1)
5	1.57(2)	0.0063(1)	1.01(1)	0.0089(1)
30	1.44(5)	0.0380(6)	0.84(2)	0.0541(1)
70	1.2(1)	0.145(5)	0.68(4)	0.2893(1)

S2   *Powder X-ray diffraction (PXRD) patterns*

Powder X-ray diffraction (PXRD) patterns were measured on the products after the reactions using a Stoe StadiP diffractometer working in transmission mode and operated with Ge(111)-monochromatized CuK$_{\alpha 1}$ radiation (λ = 1.54060 Å). An exemplary PXRD pattern of a Zr-*fum* MOF sample that was collected after the reaction is shown in Figure S13.
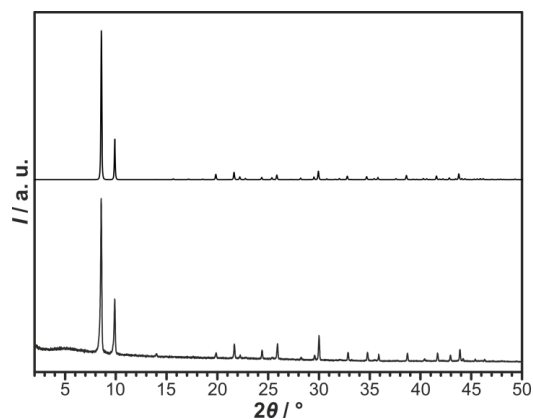

Figure S13. Simulated PXRD pattern for the Zr-*fum* MOF[15] (top) and PXRD pattern of a Zr-*fum* MOF sample after the reaction during which its formation was studied (bottom, molar ratios ZrCl$_4$/H$_2$*fum*/formic acid/H$_2$O of 1:3:150:1074 at 43 °C).

Literature

1   M. Avrami, *J. Chem. Phys.*, 1939, **7**, 1103.

2   M. Avrami, *J. Chem. Phys.*, 1940, **8**, 212.

3   M. Avrami, *J. Chem. Phys.*, 1941, **9**, 177.

4   The original Avrami-Erofeev equation was formulated as $\alpha(t) = 1 - e^{-k \cdot t^n}$, i.e. without brackets around the term $-k \cdot t$. However, in today´s application, the form given as in equation S1 is preferred. Therefore, for better comparison, this form of the equation is also used here. The original formulation was given by Erofeev (B. V. Erofeev, *Dokl. Akad. Nauk SSSR*, 1946, **52**, 511, cited after ref. 17, supporting information). In addition, Khanna and Taylor found that only the modified equation provides meaningful data on reaction rates and activation energies (Y. P. Khanna and T. J. Taylor, *Polym. Eng. Sci.*, 1988, **28**, 1042).

5   J. D. Hancock and J.H. Sharp, *J. Am. Ceram. Soc.*, 1972, **55**, 74.

6   Ø. B. Vistad, D. E. Akporiaye and K. P. Lillerud, *J. Phys. Chem. B*, 2001, **105**, 12437.

7   R. I. Walton, T. Loiseau, D. O'Hare and G. Férey, *Chem. Mater.*, 1999, **11**, 3201.

8   L. Engelke, M. Schaefer, M. Schnur and W. Bensch, *Chem. Mater.*, 2001, **13**, 1383.

9   T. Ahnfeldt, J. Moellmer,V. Guillerm, R. Staudt, C. Serre and N. Stock, *Chem. Eur. J.*, 2011, **17**, 6462.

10   J. Cravillon, C. A. Schröder, H. Bux, A. Rothkirch, J. Caro and M. Wiebcke, *CrystEngComm*, 2012, **14**, 492.

11   F. Millange, M. I. Medina, N. Guillou, G. Férey, K. M. Golden, R. I. Walton and *Angew. Chem. Int. Ed.*, 2010, **49**, 763.

12   H. Reinsch and N. Stock, *CrystEngComm*, 2013, **15**, 544.

13   F. Ragon, P. Horcajada, H. Chevreau, Y. K. Hwang, U. Lee, S. R. Miller, T. Devic, J. Chang and C. Serre, *Inorg. Chem.*, 2014, **53**, 2491.

14   P. Norby and J. C. Hanson, *Catal. Today*, 1998, **39**, 301.

15   G. Wißmann, A. Schaate, S. Lilienthal, I. Bremer, A. M. Schneider and P. Behrens, *Microporous Mesoporous Mater.*, 2012, **152**, 64.

16   F. Millange, R. El Osta, M. E. Medina and R. I. Walton, *CrystEngComm*, 2011, **13**, 103.

17   E. E. Finney and R. G. Finke, *Chem. Mater.*, 2009, **21**, 4692.

18   A. F. Gualtieri, *Phys. Chem. Miner.*, 2001, **2**, 719.

6   Curriculum Vitae

	Gesa Zahn, geb. Wißmann
Date of birth	May 25, 1986
Place of birth	Celle
Nationality	German
09/2010 - 10/2014	Dissertation at the Institute for Inorganic Chemistry, Gottfried Wilhelm Leibniz Universität Hannover in the group of Prof. Dr. Peter Behrens Title: "Synthesis and Characterisation of Zr-fumarate MOF - a Promising Candidate for Biomedical Applications"
02/2010 - 08/2010	Diploma work at the Institute for Inorganic Chemistry, Gottfried Wilhelm Leibniz Universität Hannover in the group of Prof. Dr. Peter Behrens Title: "Herstellung von nanoskaligen Apatitpartikeln durch Umwandlung von Monetit"
10/2005 - 08/2010	Study of chemistry at the Universität Hannover (Diploma)
06/2005	Abitur (A-Levels) at the Hermann-Billung Gymnasium (grammar school) in Celle

7   List of Publications

Articles

Title: "Evolution of the Morphologies of Zinc Oxide Mesocrystals Under the Influence of Natural Polysaccharides"

Florian Waltz, Gesa Wißmann, Jann Lippke, Andreas M. Schneider, Hans-Christoph Schwarz, Armin Feldhoff, Stefanie Eiden, Peter Behrens, Cryst. Growth Des. **2012**, *12*, 3066−3075.

Title: "Modulated synthesis of Zr-fumarate MOF"

Gesa Wißmann, Andreas Schaate, Sebastian Lilienthal, Imke Bremer, Andreas M. Schneider, Peter Behrens, *Microporous Mesoporous Mater.* **2012**, *152*, 64−70.

Title: "The Phosphate Source Influences Gene Expression and Quality of Mineralization during *In Vitro* Osteogenic Differentiation of Human Mesenchymal Stem Cells"

Luisa M. Schäck, Sandra Noack, Ramona Winkler, Gesa Wißmann, Peter Behrens, Mathias Wellmann, Michael Jagodzinski, Christian Krettek, Andrea Hoffmann, *PLoS ONE 8* **2013**, *6*, e65943.

Title: "Insight into the mechanism of modulated syntheses: *In situ* synchrotron diffraction studies on the formation of Zr-fumarate MOF"

Gesa Zahn, Philip Zerner, Jann Lippke, Fabian L. Kempf, Sebastian Lilienthal, Christian A. Schröder, Andreas M. Schneider, Peter Behrens, *CrystEngComm* **2014**, *16*, 9198−9207.

Title: "A Water-Born Zr-Based Porous Coordination Polymer: Modulated Synthesis of Zr-fumarate MOF"

Gesa Zahn, Hendrik Albert Schulze, Jann Lippke, Sandra König, Uta Sazama, Michael Fröba, Peter Behrens, *Microporous Mesoporous Mater.* **2015**, *203*, 186–194.

Talks at Conferences

24. Deutsche Zeolith-Tagung, Magdeburg, Germany, March 2012
Title: "Modulated Synthesis of Zr-fumarate MOF"
Gesa Wißmann, Andreas Schaate, Sebastian Lilienthal, Imke Bremer, Andreas M. Schneider, Peter Behrens.

Final MACADEMIA project meeting and workshop, Brussels, Belgium, June 2013
Title: "Modulated synthesis of the Zr-fumarate MOF from a water-based system"
Gesa Wißmann, Philip Zerner, Jann Lippke, Sebastian Lilienthal, Fabian Kempf, Andreas M. Schneider, Peter Behrens.

LNQE Nanoday 2014, Hannover, Germany, October 2014
Title: "Understanding adsorption in Zr-organic frameworks: A computational study"
Sebastian Lilienthal, Jann Lippke, Gesa Zahn, Andreas M. Schneider, Peter Behrens, Tobias von Zons, Thomas Preuße, Adelheid Godt.

Poster Presentations

Ringberg Symposium "Molecular Bionics - From Biomineralization to Functional Materials", Tegernsee/Rottach-Egern, Germany, October 2010
Title: "Calcium phosphates for the fabrication of biocompatible nacre-like composites"
Gesa Wißmann, Britta Hering, Sajjad Waraich, Henning Menzel, Peter Behrens.

DGBM 2010, Jahrestagung der Deutschen Gesellschaft für Biomaterialien e.V., Heilbad Heiligenstadt, Germany, November 2010
Title: "Synthesis of Nacre-Like Composites with Calcium Phosphate Nanoparticles"
Gesa Wißmann, Britta Hering, Sajjad Waraich, Henning Menzel, Peter Behrens.

Hybrid Materials 2011, Strasbourg, France, March 2011
Title: "Synthesis of Calcium Phosphate Platelets for the Fabrication of Biocompatible Nacre-Like Composites"
Gesa Wißmann, Britta Hering, Sajjad Waraich, Henning Menzel, Peter Behrens.

LNQE Nanoday 2011, Hannover, Germany, September 2011

Title: "Synthesis of Calcium Phosphate Platelets for the Fabrication of Biocompatible Nacre-Like Composites"

Gesa Wißmann, Britta Hering, Sajjad Waraich, Henning Menzel, Peter Behrens.

MOF 2012, Edinburgh, Great Britain, September 2012

Title: "A Water-Born Zr-Based Porous Coordination Polymer: Modulated Synthesis of Zr-fumarate MOF"

Gesa Wißmann, Andreas Schaate, Sebastian Lilienthal, Imke Bremer, Andreas M. Schneider, Peter Behrens.

Kolloquium Innovative Implantate, Sonderforschungsbereich 599 "Zukunftsfähige bioresorbierbare und permanente Implantate aus metallischen und keramischen Werkstoffen", Hannover, Germany, November 2012

Title: "Calcium phosphates for biomedical application"

Gesa Wißmann, Peter Behrens.

European XFEL Users' Meeting 2013, DESY Photon Science Users' Meeting, January 2013

Title: "Modulated synthesis of Zr-based MOFs: Time-resolved *in situ* X-ray diffraction studies"

Philip Zerner, Gesa Wißmann, Jann Lippke, Christian A. Schröder, Fabian Kempf, Sebastian Lilienthal, Peter Behrens.

25. Deutsche Zeolith-Tagung, Hamburg, Germany, March 2013

Title: "A Water-Born Zr-Based Porous Coordination Polymer: Modulated Synthesis of Zr-fumarate MOF"

Gesa Wißmann, Hendrik A. Schulze, Sebastian Lilienthal, Andreas M. Schneider, Peter Behrens.

25. Deutsche Zeolith-Tagung, Hamburg, Germany, March 2013

Title: "Modulated synthesis of Zr-based MOFs: Time-resolved *in situ* X-ray diffraction studies"

Philip Zerner, Gesa Wißmann, Jann Lippke, Christian A. Schröder, Fabian Kempf, Sebastian Lilienthal, Peter Behrens.

3rd Workshop ENMIX (European Nanoporous Materials Institute of Excellence) Hannover, Germany, March 2013

Title: "A Highly Robust Porous Coordination Synthesized from Water: Zr-fumarate MOF"

Gesa Wißmann, Hendrik A. Schulze, Sebastian Lilienthal, Andreas M. Schneider, Peter Behrens.

8th International Mesostructured Materials Symposium, Awaji Island, Japan, May 2013

Title: "Modulation Effects in the Synthesis of MOFs"

Peter Behrens, Gesa Wißmann, Jann Lippke, Philip Zerner, Imke Bremer, Sebastian Lilienthal, Fabian Kempf, Andreas M. Schneider.

International MOF Symposium Dresden, Germany, September 2013

Title: "A Water-Born Zr-Based Porous Coordination Polymer: Modulated Synthesis of Zr-fumarate MOF"

Gesa Wißmann, Hendrik A. Schulze, Sebastian Lilienthal, Andreas M. Schneider, Peter Behrens.

International MOF Symposium Dresden, Germany, September 2013

Title: "Modulated synthesis of Zr-*fum* MOF: Time-resolved *in situ* X-ray diffraction studies"

Philip Zerner, Gesa Wißmann, Jann Lippke, Christian A. Schröder, Fabian Kempf, Sebastian Lilienthal, Peter Behrens.

LNQE Nanoday 2013, Hannover, Germany, October 2013

Title: "A Water-Born Zr-Based Porous Coordination Polymer: Modulated Synthesis of Zr-fumarate MOF"

Gesa Wißmann, Hendrik A. Schulze, Sebastian Lilienthal, Andreas M. Schneider, Peter Behrens.

26. Deutsche Zeolith-Tagung, Paderborn, Germany, February 2014

Title: "Particle size control of Zr-based metal-organic frameworks by applying the modulation approach"

Gesa Wißmann, Hendrik A. Schulze, Andreas Schaate, Jann Lippke, Philip Zerner, Peter Behrens.

26. Deutsche Zeolith-Tagung, Paderborn, Germany, February 2014

Title: "Zr-MOF/Graphite Oxide Composite Materials"

Philip Zerner, Janina Willkomm, Thomas S. Asche, Gesa Wißmann, Hans-Christoph Schwarz, Peter Behrens.

MOF 2014, Kobe, Japan, September 2014

Title: "Zr-MOF/Graphite Oxide Composite Materials: Synthesis and Properties"

Philip Zerner, Janina Willkomm, Thomas S. Asche, Gesa Zahn, Peter Behrens.